4

Experimental Methods in Chaotic Vibrations

Perfect logic and faultless deduction make a pleasant theoretical structure, but it may be right or wrong: The experimenter is the only one to decide, and he is always right.
L. Brillouin, *Scientific Uncertainty and Information*, 1964

4.1 INTRODUCTION: EXPERIMENTAL GOALS

A review of physical systems that exhibit chaotic vibrations was presented in Chapter 3. In this chapter, we discuss some of the experimental techniques that have been used successfully to observe and characterize chaotic vibrations and strange attractors. To a great extent, these techniques are specific to the physical medium, for example, rigid body, elastic solid, fluid, or reacting medium. However, many of those measurements which are unique to chaotic phenomenon, such as Poincaré maps or Lyapunov exponents, are applicable to a wide spectrum of problems.

A diagram outlining the major components of an experiment is shown in Figure 4-1. In this example, the vibrating object is an elastic beam with either nonlinear boundary conditions or multiple equilibrium positions. Also, the source of the vibration is an electromagnetic shaker. In the case of an autonomous system, such as the Rayleigh–Benard convection cell, the source of instability is a prescribed temperature difference across the cell, and the nonlinearities reside in the convective terms in the acceleration of each fluid element.

The other major elements include *transducers* to convert physical variables into electronic voltages, a *data acquisition* and storage system, *graphical display* (such as an oscilloscope), and data analysis computer.

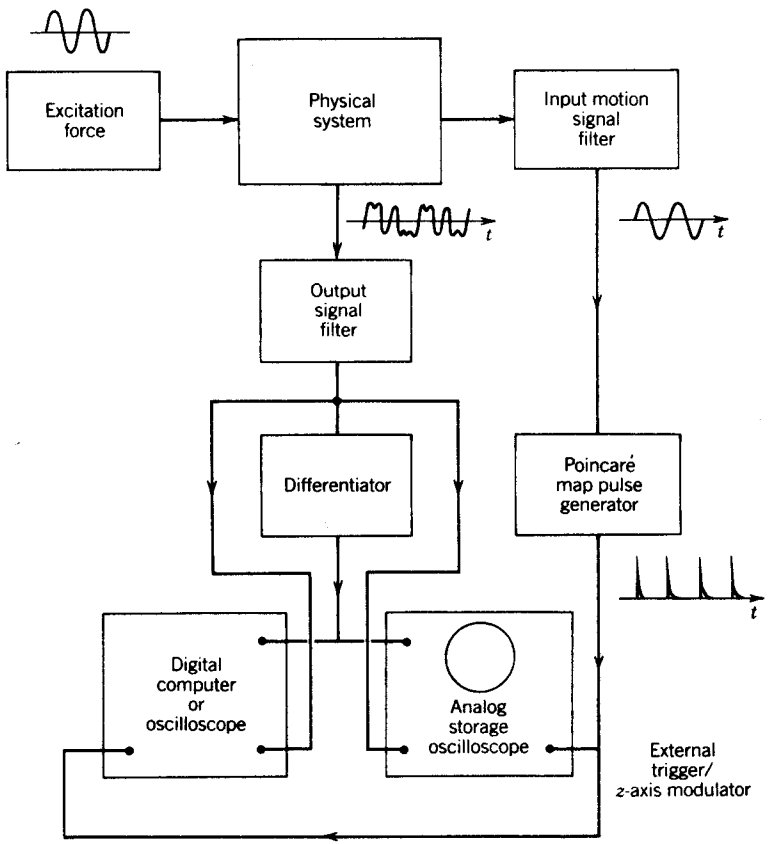

Figure 4-1 Diagram showing components of an experimental system to measure the Poincaré map of a chaotic physical system.

The techniques that must be mastered for experiments in chaotic vibrations depend to some extent on the goals that one sets up for the experimental study. These goals could include the following:

1. Establish existence of chaotic vibration in a particular physical system.
2. Determine critical parameters for bifurcations.
3. Determine criterion for chaos.
4. Map out chaotic regimes.
5. Measure qualitative features of chaotic attractor, for example, Poincaré maps.

6. Measure quantitative properties of attractor, for example, Fourier spectrum, Lyapunov exponent, probability density function, fractal dimension.

4.2 NONLINEAR ELEMENTS IN DYNAMICAL SYSTEMS

The phenomena of chaotic vibrations cannot occur if the system is linear. Thus, in performing experiments in chaotic dynamics, one should understand the nature of the nonlinearities in the system. To refresh one's memory, a linear system is one in which the principle of superposition is valid. Thus, if $x_1(t)$ and $x_2(t)$ are each possible motions of a given system, then the system is linear if the sum $c_1x_1(t) + c_2x_2(t)$ is also a possible motion. Another form of the superposition principle is more easily described in mathematical terms. Suppose the dynamics of a given system can be modeled by a set of differential or integral equations of the form

$$\mathbf{L}[\mathbf{X}] = \mathbf{f}(t) \tag{4-2.1}$$

and $\mathbf{X} = (x_1, x_2, \ldots, x_k(t), \ldots, x_n)$ represents a set of independent dynamical variables that describe the system. Suppose the system is forced by two different input functions $\mathbf{f}_1(t)$ and $\mathbf{f}_2(t)$, with outputs $\mathbf{X}_1(t)$ and $\mathbf{X}_2(t)$. If the system is linear, the effect of two simultaneous inputs can easily be found:

$$\mathbf{L}[c_1\mathbf{X}_1 + c_2\mathbf{X}_2] = c_1\mathbf{f}_1(t) + c_2\mathbf{f}_2(t) \tag{4-2.2}$$

The only way that this property can hold is for the terms in the differential equation (4-2.1) to be to the first power $\mathbf{X}_1$ or $\dot{\mathbf{X}}_1$, and so on: hence the term *linear* system. Nonlinear systems involve the unknown functions in forms other than to the first power, that is, $x^2, x^3, \sin x, x^a, 1/(x^2 + b)$, or similar forms for the derivatives or integrals of the function, that is, $\dot{x}^2, [\int x\,dt]^2$.

Experimental nonlinearities can be created in many ways, some of them quite subtle. In mechanical or electromagnetic systems, nonlinearities can occur in the following forms:

(a) Nonlinear material or constitutive properties (stress versus strain, voltage versus current)
(b) Nonlinear acceleration or kinematic terms (e.g., centripetal or Coriolis acceleration terms)
(c) Nonlinear body forces
(d) Geometric nonlinearities

(a) Material Nonlinearities

Examples of material nonlinearities in mechanical and electrical systems include the following

Solid Materials. Nonlinear stress versus strain: (1) elastic (e.g., rubber) and (2) inelastic (e.g., steel beyond the yield point, plasticity, creep).

Magnetic Materials. Nonlinear magnetic field intensity **H** versus flux density **B**

$$\mathbf{B} = \mathbf{f}(\mathbf{H})$$

(e.g., ferromagnetic material iron, nickel, cobalt—hysteretic in nature).

Dielectric Materials. Nonlinear electric displacement **D** versus electric field intensity **E**

$$\mathbf{D} = \mathbf{f}(\mathbf{E})$$

(e.g., ferroelectric materials).

Electric Circuit Elements. Nonlinear voltage versus current

$$V = f(I)$$

(e.g., Zener and tunnel diodes, nonlinear resistors, field effect transistors (FET), metal oxide semiconductors (MOSFET)). Nonlinear voltage versus charge

$$V = g(Q)$$

(e.g., capacitors). Other material nonlinearities include nonlinear optical materials (e.g., lasers), heat flux–temperature gradient properties, nonlinear viscosity properties in fluids, voltage–current relations in electric arcs, and dry friction.

(b) Kinematic Nonlinearities

This type of nonlinearity occurs in fluid mechanics in the Navier–Stokes equations where the acceleration term includes a nonlinear velocity operator

$$v\frac{\partial v}{\partial x} \quad \text{or} \quad \mathbf{v} \cdot \nabla \mathbf{v}$$

which represents convective effects.

In particle dynamics, one often uses local coordinate systems to describe motion relative to some inertial reference frame. When the local frame rotates with angular velocity $\boldsymbol{\Omega}$ relative to the large frame, the absolute acceleration is given by

$$\mathbf{A} = \mathbf{a} + \mathbf{A}_0 + \dot{\boldsymbol{\Omega}} \times \boldsymbol{\rho} + \boldsymbol{\Omega} \times \boldsymbol{\Omega} \times \boldsymbol{\rho} + 2\boldsymbol{\Omega} \times \mathbf{v} \tag{4-2.3}$$

where $\mathbf{A}_0$ is the acceleration of the origin of the small frame relative to the reference, and $\boldsymbol{\rho}$ and $\mathbf{v}$ are the local position vector and velocity, respectively, of the particle. The last two terms are called the centripetal and Coriolis acceleration terms. The last three terms are *nonlinear* in the variables $\boldsymbol{\rho}$, $\mathbf{v}$, $\boldsymbol{\Omega}$.

For a rigid body in pure rotation, nonlinear terms appear in Euler's equations for the rotation dynamics:

$$\begin{aligned} M_x &= I_x\frac{d\omega_x}{dt} - (I_z - I_y)\omega_y\omega_z \\ M_y &= I_y\frac{d\omega_y}{dt} - (I_x - I_z)\omega_z\omega_x \\ M_z &= I_z\frac{d\omega_z}{dt} - (I_y - I_x)\omega_x\omega_y \end{aligned} \tag{4-2.4}$$

where (M_x, M_y, M_z) are applied force moments and (I_x, I_y, I_z) are principal second moments of mass about the center of mass.

(c) Nonlinear Body Forces

Electromagnetic forces are represented as follows:

Currents	$F = \alpha I_1 I_2$ or βIB
Magnetization	$\mathbf{F} = \mathbf{M} \cdot \nabla \mathbf{B}$
Moving media	$\mathbf{F} = q\mathbf{v} \times \mathbf{B}$

(Here I is current, $\mathbf{B}$ is the magnetic field, $\mathbf{M}$ is the magnetization, q represents charge, and $\mathbf{v}$ is the velocity of a moving charge.)

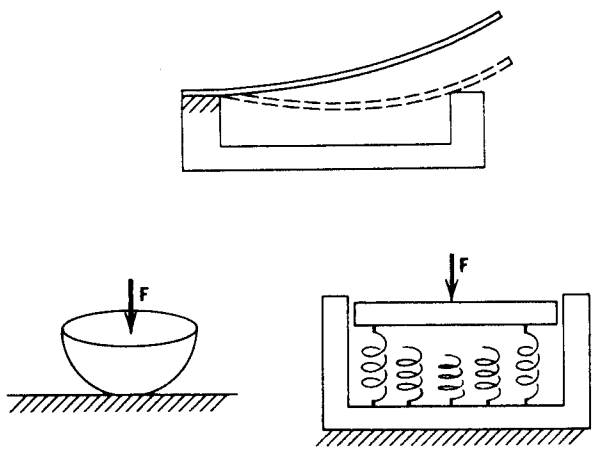

Figure 4-2 Examples of mechanical systems with geometric nonlinearities.

(d) Geometric Nonlinearities

Geometric nonlinearities in mechanics involve materials with linear stress–strain behavior but the geometry changes with deformation. One example is shown in Figure 4-2 where the constraint on the tip displacement of the cantilever depends on the displacement.

Another classic example is the contact of two smooth elastic bodies (called a Hertz contact). The force–displacement law for curved surfaces follows a nonlinear power law

$$F = c\delta^{3/2}$$

where δ is the relative approach of the two bodies.

Another classic example of a geometric nonlinearity is the elastica shown in Figure 4-3. In this problem, the material is linearly elastic but the large deformations produce a nonlinear force–displacement or moment–angle relation of the form

$$M = A\kappa$$

$$\kappa = \frac{u''}{\left[1 + (u')^2\right]^{3/2}}$$

where M is the bending moment, κ is the curvature of the neutral axis of the beam, and $u(x)$ is the transverse displacement of the beam. This

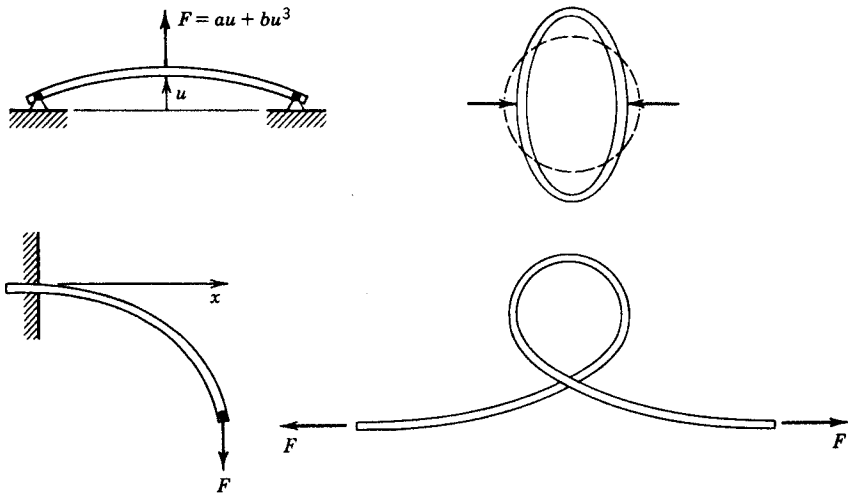

Figure 4-3 Examples of geometric nonlinearities in elastic structures.

problem is an interesting one for study of chaotic vibrations since the elastica can exhibit multiple equilibrium solutions (see Chapter 2). Cylindrical and spherical shells also exhibit geometric elastic nonlinearities (e.g., see Evensen, 1967).

4.3 EXPERIMENTAL CONTROLS

First and foremost, the experimenter in chaotic vibrations should have control over noise, both mechanical and electronic. If one is to establish chaotic behavior for a deterministic system, the noise inputs to the system must be minimized.

For example, mechanical experiments such as vibration of structures or autonomous fluid convection problems should be isolated from external laboratory or building vibrations. This can be accomplished by using a large-mass table with low-frequency air bearings. A low-cost solution is to work at night when building noise is at a minimum.

Second, one should build in the ability to control significant physical parameters in the experiments, such as forcing amplitude or temperature gradient. This is especially important if one wishes to observe bifurcation sequences such as period-doubling phenomena. Where possible, one should use continuous element controls and avoid devices with incremental or step

changes in the parameters. In some problems, there is more than one dynamic motion for the same parameters. Thus, control over the initial state variables may also be important.

Control of the number of degrees of freedom is another consideration. For example, if one wishes to observe low-frequency oscillations of a structure, care should be taken to make sure other vibration modes are not excited. Other extraneous vibration modes can creep into the experiment from the boundary conditions that support or clamp the structure. This may call for securing the structure to a large-mass base.

Another factor is the number of significant figures required for accurate measurement. For example, to plot Poincaré maps from digitally sampled data, an 8 bit system may not be sensitive enough and one may have to go with 12 bit electronics or better. In some of our experiments on Poincaré maps, we have obtained better results from analog devices, such as a good analog storage oscilloscope, than an 8 bit digital oscilloscope especially as regards resolution of fine fractal structure in the maps.

Frequency Bandwidth

Most experiments in fluid, solid, or reacting systems may be viewed as infinite-dimensional continua. However, one often tries to develop a mathematical model with a few degrees of freedom to explain the major features of the chaotic or turbulent motions of the system. This is usually done by making measurements at a few spatial locations in the continuous system and by limiting the frequency bandwidth over which one observes the chaos. This is especially important if velocity measurements for phase plane plots are to be made from deformation histories. Electronic differentiation will amplify higher-frequency signals, which may not be of interest in the experiment. Thus, extremely good electronic filters are often required, especially ones that have little or no phase shift in the frequency band of interest.

4.4 PHASE SPACE MEASUREMENTS

It was pointed out in Chapter 2 that chaotic dynamics are most easily unraveled and understood when viewed from a phase space perspective. In particle dynamics, this means a space with coordinates composed of the position and velocity for each independent degree of freedom. In forced problems, time becomes another dimension. Thus, the periodic forcing of a two-degree-of-freedom oscillator with generalized positions $(q_1(t), q_2(t))$ has a phase space representation with coordinates $(q_1, \dot{q}_1, q_2, \dot{q}_2, \omega t)$, where ω is the forcing frequency.

If one measures displacement $q(t)$, a differentiation circuit is required. If velocity is measured, the phase space may be spanned by $(v, \int v\,dt)$, which calls for an integrator circuit. As noted above, in building integrator or differentiator circuits, care should be taken that the phase as well as the amplitude is not distorted within the frequency band of interest.

In electronic or electrical circuit problems, the current and voltage can be used as state variables. In fluid convection problems, temperature and velocity variables are important.

Pseudo-Phase-Space Measurements

In many experiments, one has access to only one measured variable $\{x(t_1), x(t_2), \dots\}$ (where t_1 and t_2 are sampling times, not to be confused with Poincaré maps). When the time increment is uniform, that is, $t_2 = t_1 + \tau$ and so on, a pseudo-phase-space plot can be made using $x(t)$ and its past (or future) values:

$(x(t), x(t-\tau))$, or $(x(t), x(t+\tau))$ two-dimensional phase space

$(x(t), x(t-\tau), x(t-2\tau))$ three-dimensional phase space

One can show that a closed trajectory in a phase space in $(x, \dot{x})$ variables will be closed in the $(x(t), x(t-\tau))$ variables (one must connect the points when the system is digitally sampled) as shown in Figure 4-4. Likewise, chaotic trajectories in $(x, \dot{x})$ look chaotic in $(x(t), x(t-\tau))$ variables. The plots can be carried out after the experiment by a computer or one may perform on-line pseudo-phase-plane plots using a sample and hold circuit.

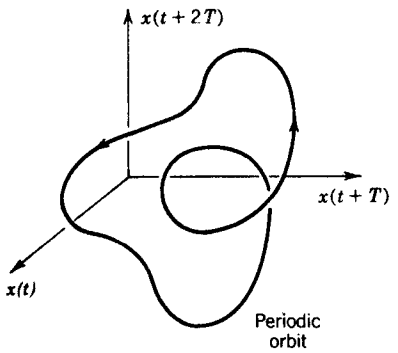

Figure 4-4 Periodic trajectory of a third-order dynamical system using pseudo-phase-space coordinates.

The one difficulty with pseudo-phase-space variables is taking a Poincaré map. For example, when there is a natural time scale, such as in forced periodic motion of a system with frequency ω, the sample time τ is usually chosen much smaller than the driving period; that is, $\tau \ll 2\pi/\omega \equiv T$. If τ is not an integer fraction of T, Poincaré maps may lose some of the fine fractal structure.

4.5 BIFURCATION DIAGRAMS

As discussed in Chapter 2, one of the signs of impending chaotic behavior in dynamical systems is a series of changes in the nature of the periodic motions as some parameter is varied. Typically, in a single-degree-of-freedom oscillator, as the control parameter approaches a critical value for chaotic motion, subharmonic oscillations appear. In the now classic "logistic equation," a series of period 2 oscillations appear [Eq. (1-3.6)]. The phenomenon of sudden change in the motion as a parameter is varied is called a *bifurcation*. A sample experimental bifurcation diagram is shown in Figure 4-5. Such diagrams can be obtained experimentally by time sampling the motion as in a Poincaré map and displaying the output on an oscilloscope as shown in Figure 4-5. Here the value of the control parameter, for example, a forcing amplitude or frequency, is plotted on the horizontal axis and the time-sampled values of the motion are plotted on the vertical axis. This diagram actually represents a series of experiments, where each value of the control parameter is an experiment. When the control parameter can be varied automatically, such as by a computer and digital-to-analog device, the diagram can be obtained quite rapidly. Care must be taken, however, to make sure transients have died out after each change in the control parameter.

In the bifurcation diagram of Figure 4-5, the continuous horizontal lines represent periodic motions of various subharmonics. The values in the dashed line areas represent chaotic regions. The boundary between chaotic and periodic motions can clearly be seen in this diagram.

When this is automated, one must be careful not to mistake a quasiperiodic motion for a chaotic motion. A phase plane Poincaré map is still very useful for distinguishing between quasiperiodic and chaotic motions.

4.6 EXPERIMENTAL POINCARÉ MAPS

Poincaré maps are one of the principal ways of recognizing chaotic vibrations in low-degree-of-freedom problems (see Table 2-2). We recall that the dynamics of a one-degree-of-freedom forced mechanical oscillator or

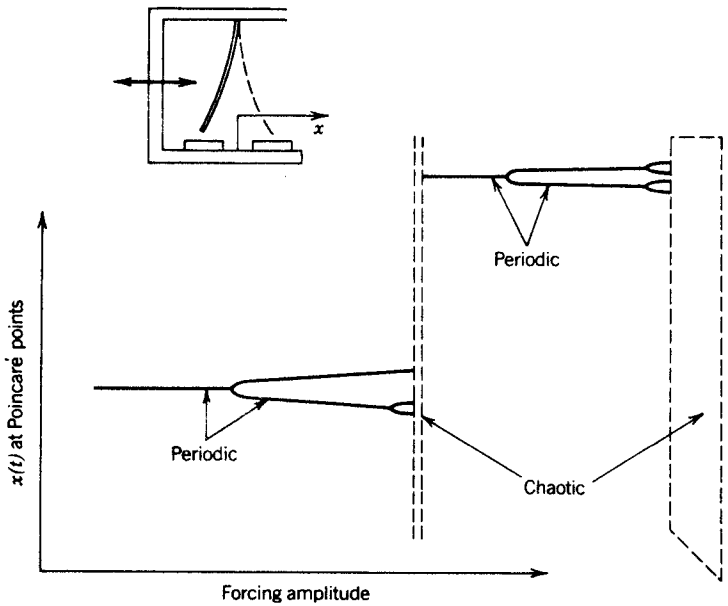

Figure 4-5 Experimental bifurcation diagram for the vibration of a buckled beam: Poincaré map samples of bending displacement versus amplitude of forcing vibration.

L–R–C circuit may be described in a three-dimensional phase space. Thus, if $x(t)$ is the displacement, $(x, \dot{x}, \omega t)$ represents a point in a cylindrical phase space where $\phi = \omega t$ represents the phase of the periodic forcing function. A Poincaré map for this problem consists of digitally sampled points in this three-dimensional space, for example, $(x(t_n), \dot{x}(t_n), \omega t_n = 2\pi n)$. As discussed in Chapter 2, this map can be thought of as slicing a torus (see Figure 4-6).

Experimentally this can be done in several ways. If one has a storage oscilloscope, the Poincaré map is obtained by intensifying the image on the screen at a certain phase of the forcing voltage (sometimes called *z-axis modulation*) (Figure 4-1). In our laboratory, we were able to generate a 5–10 V pulse of 1–2 μs duration when the forcing function reached a certain phase:

$$\omega t_n = \phi_0 + 2\pi n \tag{4-6.1}$$

This pulse was then used to intensify a phase plane image, $(x(t), \dot{x}(t))$, using two vertical amplifiers as in Figure 4-7.

One can also use a digital oscilloscope in an external sampling rate mode with the same narrow pulse signal used for the analog oscilloscope. A

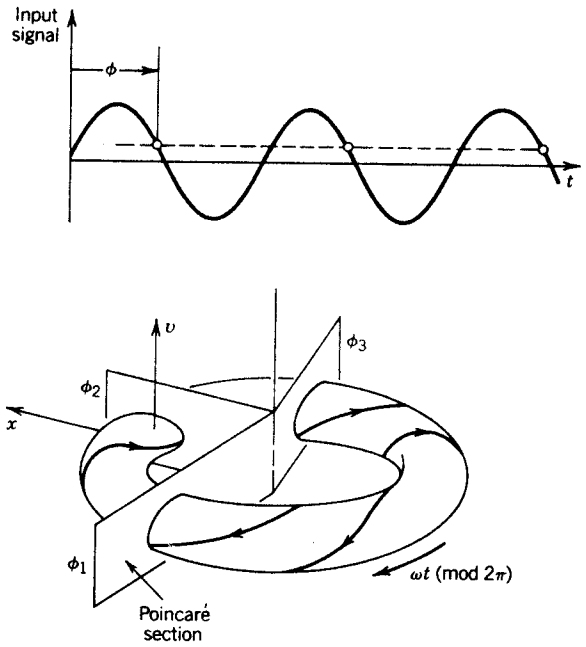

Figure 4-6 *Top*: Poincaré map sampling times at constant phase of forcing function. *Bottom*: Geometric interpretation of Poincaré sections in the three-dimensional phase space.

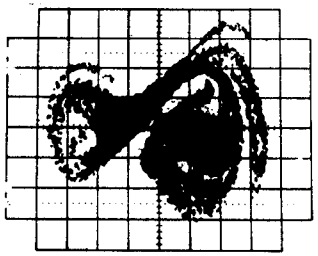

Figure 4-7 Example of an experimental Poincaré map for periodic forcing of a buckled beam.

similar technique can be employed using an analog-to-digital (A-D) signal converter by storing the sampled data in a computer for display at a later time. The important point here is that the sampling trigger signal must be exactly synchronous with the forcing function.

Poincaré Maps—Change of Phase. As noted in Chapter 2, chaotic phase plane trajectories can often be unraveled using the Poincaré map by taking

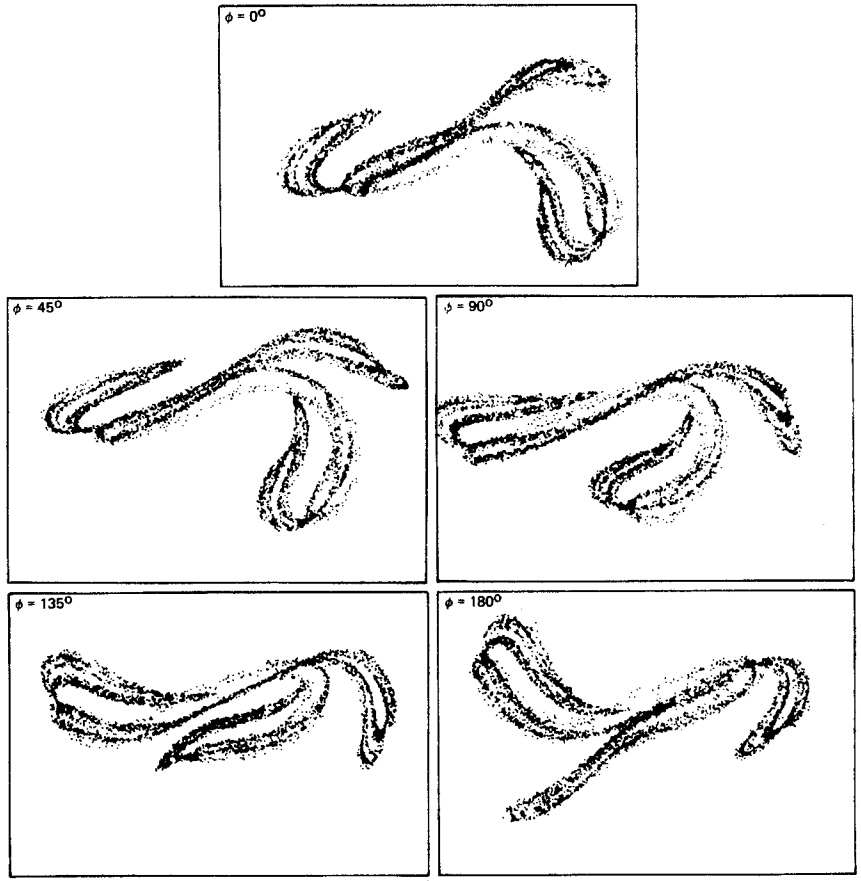

Figure 4-8 Poincaré maps of a chaotic attractor for a buckled beam for different phases of the forcing function.

a set of pictures for different phases ϕ_0 in Eq. (4-6.1) (see Figure 4-8). This is tantamount to sweeping the Poincaré plane in Figure 4-6. While one Poincaré map can be used to expose the fractal nature of the attractor, a complete set of maps varying ϕ_0 from 0 to 2π is sometimes needed to obtain a complete picture of the attractor on which the motion is riding.

A series of pictures of various cross sections of a chaotic torus motion in a three-dimensional phase space is shown in Figure 4-8. Note the symmetry in the $\varphi = 0°$ and $180°$ maps for the special case of the buckled beam (Figure 4-5).

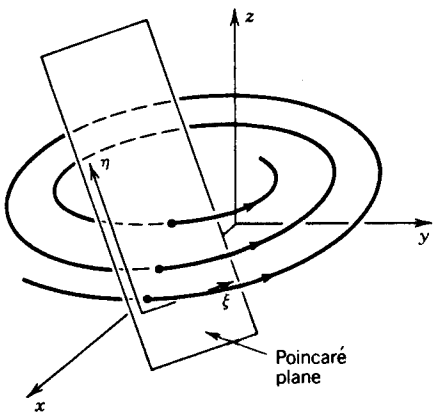

Figure 4-11 General Poincaré surface of section in phase space for the motion of a third-order dynamical system.

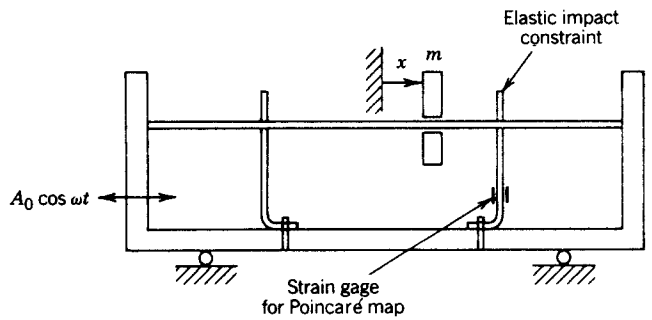

Figure 4-12 Sketch of experimental setup for a position triggered Poincaré section.

An example of the experimental technique to obtain a (v_n, ϕ_n) Poincaré map is shown in Figure 4-12. When the mass hits the position constraint, a sharp signal is obtained from a strain gauge or accelerometer. This sharp signal can be used to trigger a data storage device (such as a storage or digital oscilloscope) to store the value of the velocity of the particle. (In the case shown in Figure 4-12, a linear variable differential transformer —LVDT—is used to measure position, and this signal is electronically differentiated to get the velocity.) To obtain the phase ϕ_n modulo 2π, we generate a periodic ramp signal in phase with the driving signal where the minimum value of zero corresponds to $\phi = 0$, and the maximum voltage of the ramp corresponds to the phase $\phi = 2\pi$. The impact-generated sharp spike voltage is used to trigger the data storage device and store the value of the ramp voltage along with the velocity signal before or after impact. A

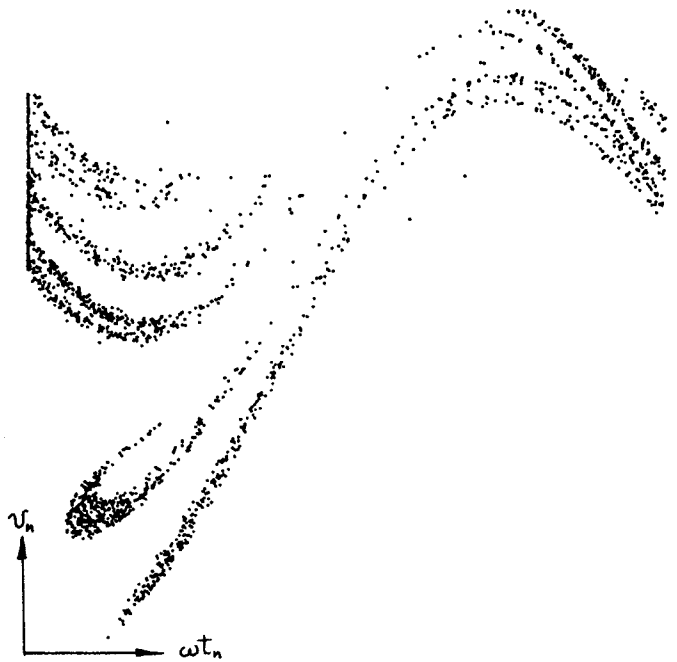

Figure 4-13 Position triggered Poincaré map for an oscillating mass with impact constraints (Figure 4-12).

Poincaré map for a mass bouncing between two elastic walls using this (v_n, ϕ_n) technique is shown in Figure 4-13.

Another example of this kind of Poincaré map is shown in Figure 4-14 for the chaotic vibrations of a motor. In this problem, the motor has a nonlinear torque–angle relation created by a dc current in one of the stator poles, and the permanent magnet rotor is driven by a sinusoidal torque created by an ac current in an adjacent coil. The equation of motion for this problem is

$$J\ddot{\theta} + \gamma\dot{\theta} + \kappa \sin\theta = F_0 \cos\theta \cos\omega t \qquad (4\text{-}6.4)$$

To obtain a Poincaré map, we choose a plane in the three-dimensional space $(\theta, \dot{\theta}, \omega t)$, where $\theta = 0$ (Figure 4-14). This is done experimentally by using a slit in a thin disk attached to the rotor and using a light-emitting diode and detector to generate a voltage pulse every time the rotor passes through $\theta = 0$ (see Figure 4-14). This pulse is then used to sample the velocity and measure the time. The data can be displayed directly on a

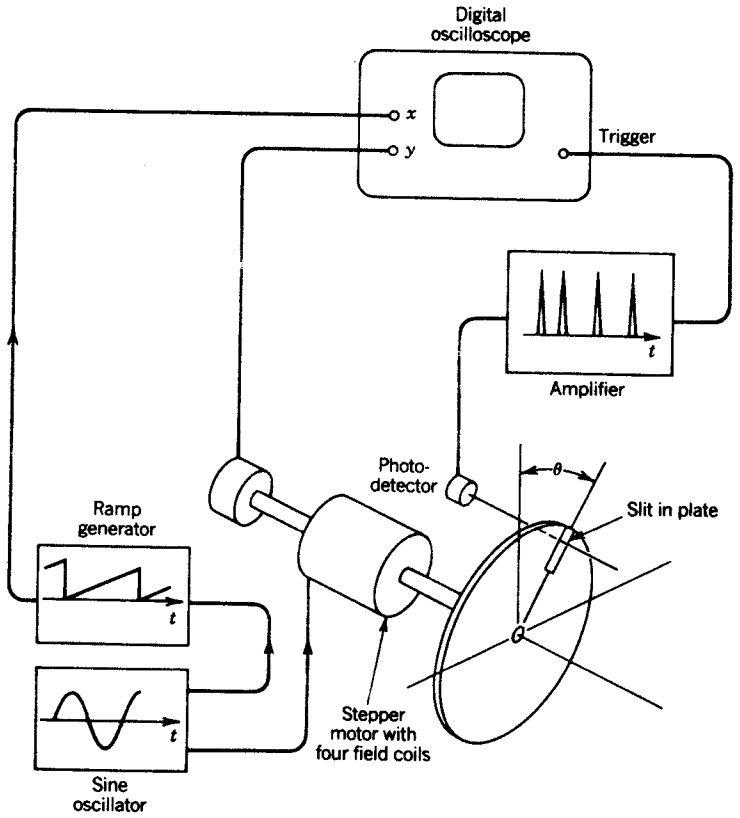

Figure 4-14 Diagram of experimental apparatus to obtain position triggered Poincaré maps for a periodically forced rotor with a nonlinear torque–angle relation.

storage oscilloscope or, using a computer, can be replotted in polar coordinates as shown in Figure 4-15.

Another variation of the method of Poincaré sections is to sample data when some variable attains a *peak* value. This has been used by Bryant and Jeffries (1984b) of the University of California–Berkeley. They examine the dynamics of a circuit with a nonlinear hysteretic iron core inductor shown in Figure 4-16. (The nonlinear properties are related to the ferromagnetic material in the inductor.) They sample the current in the inductor $I_L(t)$ as well as the driving voltage $V_s(t)$, when $V_L = 0$. This is tantamount to measuring the *peak* value of the flux in the inductor φ. This is because $V_L = -\dot{\varphi}$, where φ is the magnetic flux in the inductor, and $\varphi = \hat{\varphi}(I)$, so

Figure 4-15 Position triggered Poincaré map for chaos in a nonlinear rotor (see Figure 4-14).

that when $\dot{\varphi} = 0$, the flux is at a maximum or minimum. The Poincaré map is then a collection of pairs of points (V_{sn}, I_{Ln}) which can be displayed on a storage or digital oscilloscope.

Construction of One-Dimensional Maps from Multidimensional Attractors

There are a number of physical and numerical examples where the attracting set appears to have a sheetlike behavior in some three-dimensional phase space as illustrated in Figure 4-17. [The Lorenz equations (1-3.9) are such an example.] This often means that a Poincaré section, obtained by measuring the sequence of points that pierce a plane transverse to the attractor, will appear as a set of points along some one-dimensional line. This suggests that if one could parameterize these points along the line by a

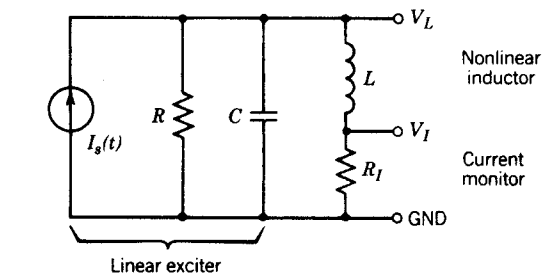

(a)

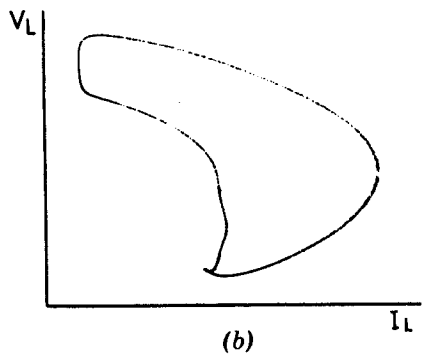

(b)

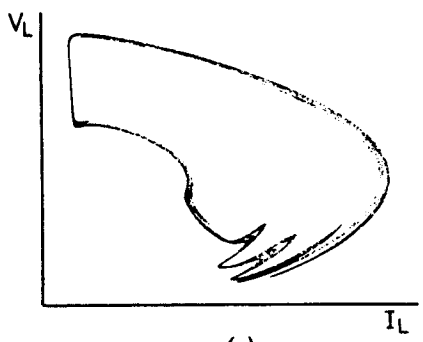

(c)

Figure 4-16 Peak amplitude-generated Poincaré maps for a circuit with nonlinear inductance [from Bryant and Jeffries (1984) with permission of The American Physical Society, copyright 1984].

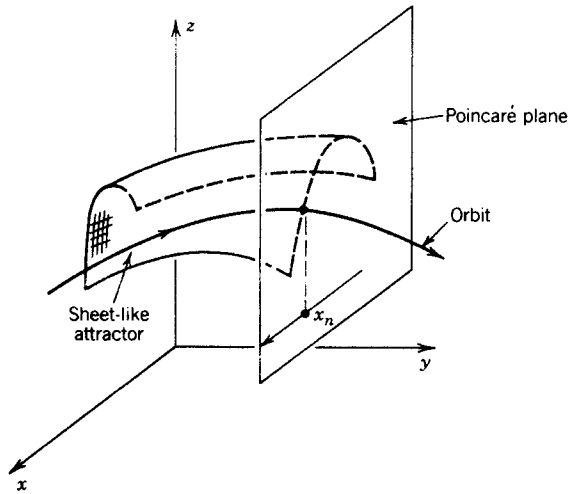

Figure 4-17 Construction of a one-dimensional return map in a three-dimensional phase space.

variable x, it would be possible that a function exists that relates x_{n+1} and x_n:

$$x_{n+1} = f(x_n)$$

The function (called a return map) may be found by simply plotting x_{n+1} versus x_n. One example is the experiments of Shaw (1984) on the dripping faucet shown in Figure 3-39 or the nonlinear circuit in Figure 3-32. (See also Simoyi et al., 1982). The existence of such a function $f(x)$ implies that the mathematical results for one-dimensional maps, such as period doubling and Feigenbaum scaling, may be applicable to the more complex physical problem in explaining, predicting, or organizing experimental observations.

For some problems, the function $f(x)$, when it exists, appears to cross itself or is tangled. This may suggest that the mapping function can be untangled by plotting the dynamics in a higher dimensional embedding space using three successive values of the Poincaré sampled data $[x(t_n), x(t_{n+1})$, and $x(t_{n+2})]$. The three-dimensional nature of the relationship can sometimes be perceived by changing the projection of the three-dimensional curve onto the plane of a graphics computer monitor. This may suggest a special two-dimensional map of the form

$$x_{n+2} = f(x_{n+1}, x_n)$$

or

$$x_{n+1} = f(x_n, y_n)$$
$$y_{n+1} = Ax_n$$

This form is similar to the Henon map (1-3.8). This method has been used successfully by Van Buskirk and Jeffries (1985) in their study of circuits with p–n junctions and by Brorson et al. (1983) who studied a sinusoidally driven resistor–inductor circuit with a varactor diode.

Double Poincaré Maps

So far we have only talked of Poincaré maps for third-order systems, such as a single degree of freedom with external forcing. But what about higher-order systems with motion in a four- or five-dimensional phase space? For example, a two-degree-of-freedom autonomous aeroelastic problem would have motion in a four-dimensional phase space (x_1, v_1, x_2, v_2), or if $x_1 \equiv x$, $(x(t), x(t-\tau), x(t-2\tau), x(t-3\tau))$. A Poincaré map triggered on one of the state variables would result in a set of points in a three-dimensional space. The fractal nature of this map, if it exists, might not be evident in three dimensions and certainly not if one projects this three-dimensional map onto a plane in two of the remaining variables.

A technique to observe the fractal nature of a three-dimensional Poincaré map of a fourth-order system has been developed in our laboratory which we call a *double Poincaré section* (see Figure 4-18). This technique enables one to slice a finite-width section of the three-dimensional map in order to uncover fractal properties of the attractor and hence determine if it is "strange." (See Moon and Holmes, 1985.)

We illustrate this technique with an example derived from the forced motion of a buckled beam. In this case, we examine a system with two incommensurate driving frequencies. The mathematical model[1] has the form

$$\begin{aligned} \dot{x} &= y \\ \dot{y} &= -\gamma y + F(x) + f_1 \cos\theta_1 + f_2 \cos(\theta_2 - \phi_0) \\ \dot{\theta}_1 &= \omega_1 \\ \dot{\theta}_2 &= \omega_2 \end{aligned} \qquad (4\text{-}6.5)$$

[1] In multidimensional dynamical systems, such as fluid-thermal problems, one important route to chaos is the occurrence of two limit cycle oscillations (Hopf bifurcations) resulting in quasiperiodic motion. This route to chaos was discussed in Chapter 2. The dynamics of this motion have been modeled by flow on a torus and the resulting Poincaré sections become closed circular arcs. Despite the importance of quasiperiodic oscillation to chaotic dynamics, very little has been done in other systems aside from fluids. Thus, we decided to explore quasiperiodic oscillations in a nonlinear structure such as a buckled beam.

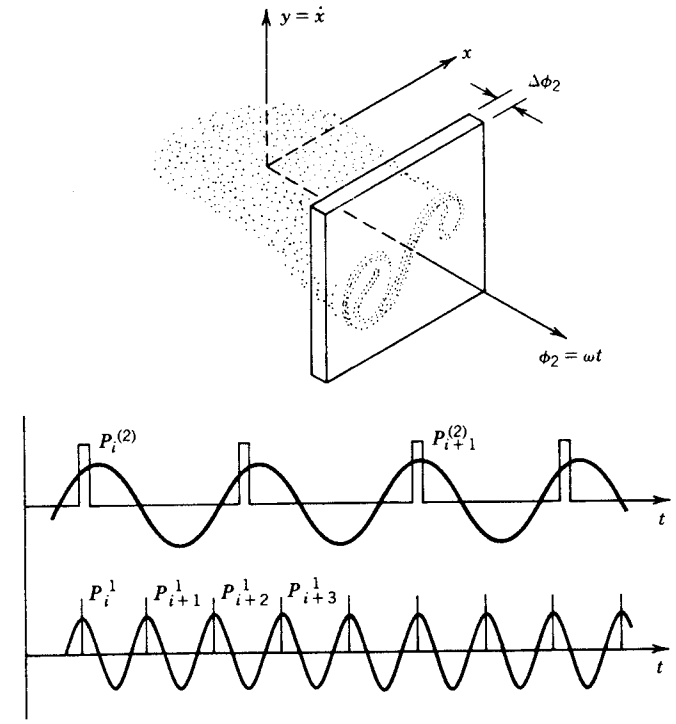

Figure 4-18 *Top*: Single Poincaré map dynamical system; finite width slice of second Poincaré section. *Bottom*: Poincaré sampling voltages for a second-order oscillator with two harmonic driving functions.

The experimental apparatus for a double Poincaré section is shown in Figure 4-19. The driving signals were produced by identical signal generators and were added electronically. The resulting quasiperiodic signal was then sent to a power amplifier which drove the electromagnetic shaker.

The first Poincaré map was generated by a 1 μs trigger pulse synchronous with one of the harmonic signals. The Poincaré map (x_n, v_n) using one trigger results in a fuzzy picture with no structure, as shown in Figure 4-20*a*. To obtain the second Poincaré section, we trigger on the second phase of the driving signal. However, if the pulse width is too narrow, the probability of finding points coincident with the first trigger is very small. Thus, we set the second pulse width 1000 times the first, at 1 ms. The second pulse width represents less than 1% of the second frequency phase of 2π. The (x, v) points were only stored when the first pulse was *coincident* with the second, as shown in Figure 4-18. This was accomplished using a

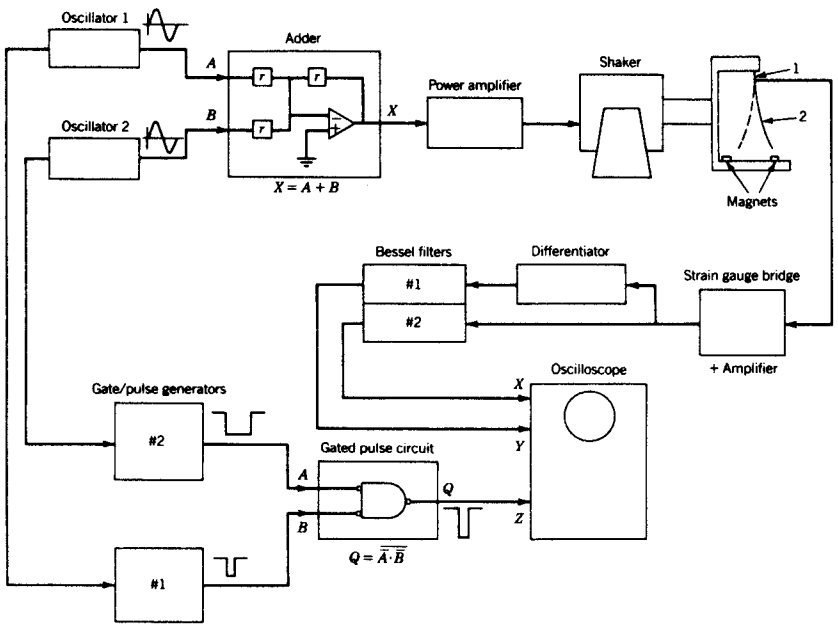

Figure 4-19 Sketch of experimental apparatus to obtain Poincaré map for an oscillator with two driving frequencies [from Moon and Holmes (1985) with permission of Elsevier Science Publishers, copyright 1985]. Note: Strain gauges—1; steel beam—2.

digital circuit with a logical NAND gate. Because of the infrequency of the simultaneity of both events, a map of 4000 points took more than 10 h compared to 8–10 min to obtain a conventional Poincaré map for driving frequencies less than 10 Hz.

The experimental results using this technique are shown in Figure 4-20 which compares a single with a double Poincaré map for the two-frequency forced problem. The single map is fuzzy while the double section reveals a fractal-like structure characteristic of a strange attractor.

One can of course generalize this technique to five- or higher-dimensional phase space problems. However, the probability of three or more simultaneous events will be very small unless the frequency is order of magnitudes higher than 1–10 Hz. Such higher-dimensional maps may be useful in nonlinear circuit problems.

This technique can be used in numerical simulation and has been employed by Lorenz (1984) to examine a strange attractor in a fourth-order system of ordinary differential equations. Kostelich and Yorke (1985) have also employed this method to study the dynamics of a kicked or pulsed

Figure 4-20 (*a*) Single Poincaré map of a nonlinear oscillator with two driving frequencies.

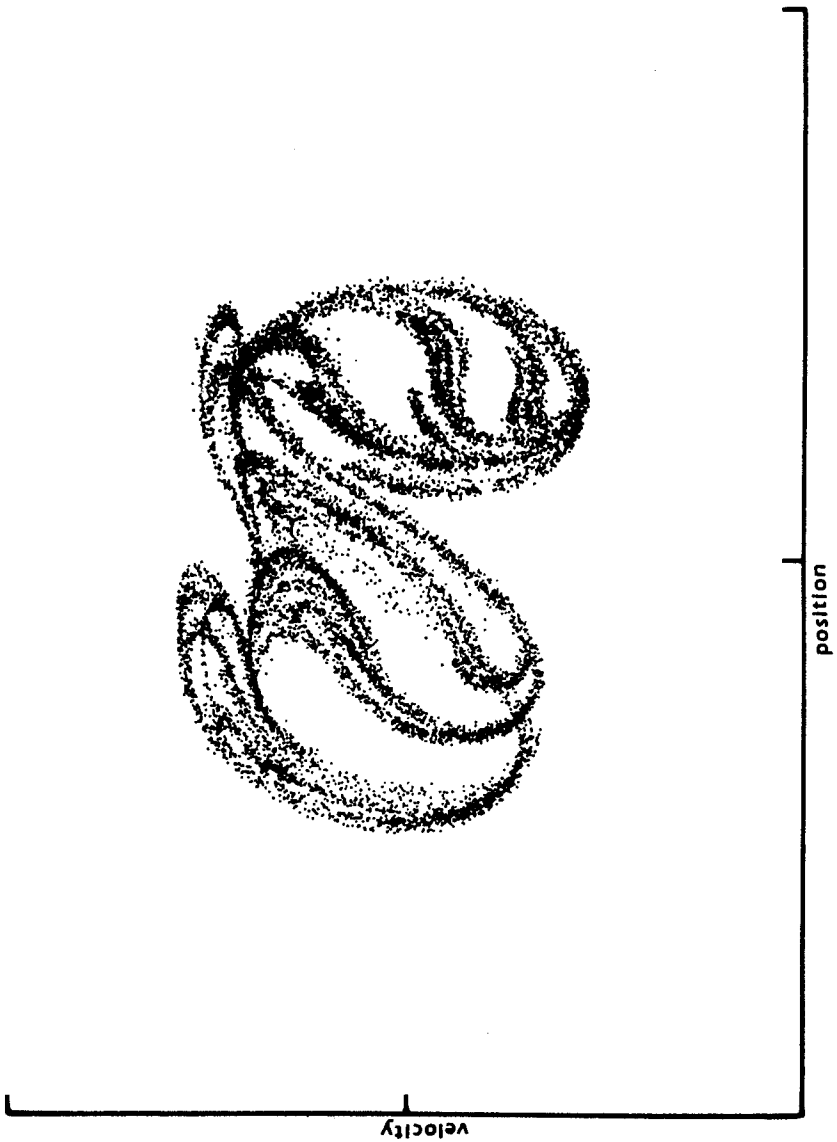

Figure 4-20 (*b*) Double Poincaré map showing fractal structure characteristic of a strange attractor.

double rotor. They call the method "Lorenz cross sections" (see also Kostelich et al., 1987).

4.7 QUANTITATIVE MEASURES OF CHAOTIC VIBRATIONS

Poincaré maps and phase plane portraits, when they can be obtained, can often provide graphic evidence for chaotic behavior and the fractal properties of strange attractors. However, quantitative measures of chaotic dynamics are also important and in many cases are the only hard evidence for chaos. The latter is especially true for systems with extreme frequencies 10^6–10^9 (as in laser systems) in which Poincaré maps may be difficult or impossible to capture. In addition, there are systems with many degrees of freedom where the Poincaré map will not reveal the fractal structure of the attractor section on double or multiple Poincaré maps) or the damping is so low that the Poincaré map shows no structure but looks like a cloud of points.

At this time in the development of the field there are three principal measures of chaos and another of emerging importance:

(a) Fourier distribution of frequency spectra
(b) Fractal dimension of chaotic attractor
(c) Lyapunov exponents
(d) Invariant probability distribution of attractor

It should be pointed out that while phase plane pictures and Poincaré maps can be obtained directly from electronic laboratory equipment, the above measures of chaos require a computer to analyze the data, with the possible exception of the frequency spectrum measurement. Electronic spectrum analyzers can be obtained but they are often expensive, and one might be better off investing in a laboratory micro or minicomputer that has the capability to perform other data analyses besides Fourier transforms.

If one is to analyze the data from chaotic motions digitally, then usually an *analog-to-digital converter* will be required as well as some means of storing the data. For example, the digitized data can be stored in a buffer in the electronic A-D device and then transmitted directly or over phone lines to a computer. Another option is a *digital oscilloscope* which performs the A-D conversion, displays the data graphically on the oscilloscope, and stores the data on a floppy disk. The latter method is often limited to eight 4000 bit records.

Finally, if one has the funds, one can store the output from the A-D converter directly onto a hard disk for direct transfer to a laboratory computer.

(a) Frequency Spectra—FFT

This is by far the most popular measure because the idea of decomposing a nonperiodic signal into a set of sinusoidal or harmonic signals is widely known among scientists and engineers. The assumption made in this method is that the periodic or nonperiodic signal can be represented as a synthesis of sine or cosine signals

$$f(t) = \frac{1}{2\pi}\int_{\Gamma} F(\omega)e^{i\omega t}\,d\omega \tag{4-7.1}$$

where $e^{i\omega t} = \cos \omega t + i \sin \omega t$.

Since $F(\omega)$ is often complex, the absolute value $|F(\omega)|$ is used in graphical displays. In practice, one uses an electronic device or computer to calculate $|F(\omega)|$ from input data from the experiment while varying some parameter in the experiment (see Chapter 2, Routes to Chaos). When the motion is periodic or quasiperiodic, $|F(\omega)|$ shows a set of narrow spikes or lines indicating that the signal can be represented by a discrete set of harmonic functions $\{e^{\pm i\omega_k t}\}$, where $k = 1, 2, \ldots$. Near the onset of chaos, however, a continuous distribution of frequency appears, as shown in Figure 4-21*a*, and in the fully chaotic regime, the continuous spectrum may dominate the discrete spikes.

In general, the function $F(\omega)$ is a complex function of ω and to represent certain classes of signals $f(t)$, the integration (4-7.1) must be carried out along a path Γ in the complex ω plane. Numerical calculation of $F(\omega)$, given $f(t)$, can often be very time consuming even on a fast computer. However, most modern spectrum analyzers use a discrete version of (4-7.1) along with an efficient algorithm called the fast Fourier transform (FFT). Given a set of data sampled at discrete even time intervals $\{f(t_k) = f_0, f_1, f_2, \ldots, f_k, \ldots, f_N\}$, the discrete time FFT is defined by the formula

$$T(J) = \sum_{I=1}^{N} f(I)e^{-2\pi i(I-1)(J-1)/N} \tag{4-7.2}$$

where I and J are integers.

Several points should be made here which may appear obvious. First, the signal $f(t)$ is time sampled at a fixed time interval τ_0; thus, information is

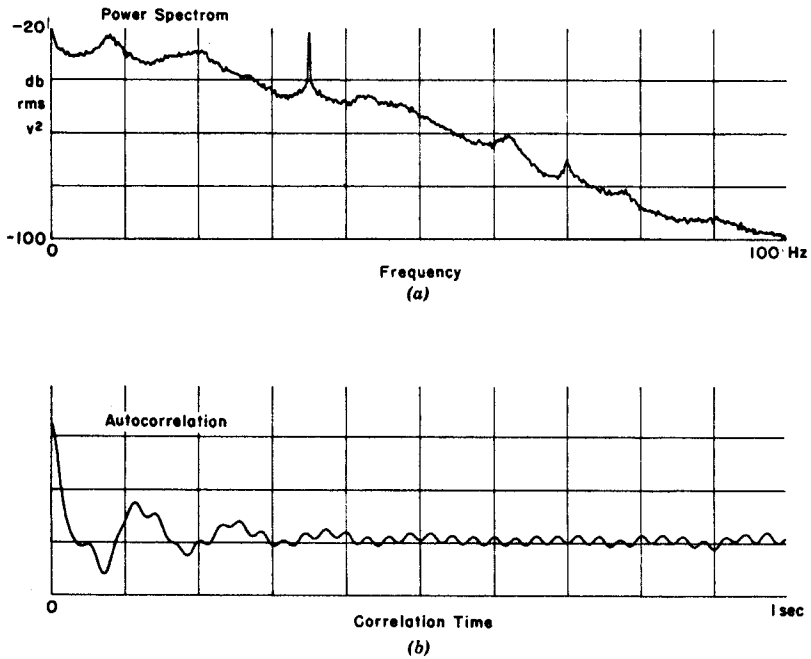

Figure 4-21 (*a*) Fourier spectrum of a chaotic signal. (*b*) Autocorrelation function of a chaotic signal.

lost for frequencies above $1/2\tau_0$. Second, only a finite set of points are used in the calculation, usually $N = 2^n$, and some built-in FFT electronics only do $N = 512$ or 1028 points. Thus, information is lost about very low frequencies below $1/N\tau_0$. Finally, the representation (4-7.2) having no information about $F(t)$ before $t = t_0$ or after $t = t_N$ essentially treats $f(t)$ as a periodic function. In general, this is not the case and since $f(t_0) \neq f(t_N)$, the Fourier representation treats this as a discontinuity which adds spurious information into $F(\omega)$. This is called *aliasing error* and methods exist to minimize its effect in $F(\omega)$. The reader using the FFT should be aware of this, however, when interpreting Fourier spectra about nonperiodic signals and should consult a signal processing reference for more information about FFTs.

Autocorrelation Function. Another signal processing tool that is related to the Fourier transform is the autocorrelation function given by

$$A(\tau) = \int_0^{\infty} x(t)x(t+\tau)\,dt$$

When a signal is chaotic, information about its past origins is lost. This means that $A(\tau) \to 0$ as $\tau \to \infty$, or the signal is only correlated with its recent past. This is illustrated in Figure 4-21*b* for the chaotic vibrations of a buckled beam. The Fourier spectrum shows a broad band of frequencies, while the autocorrelation function has a peak at the origin $\tau = 0$, and drops off rapidly with time.

(b) Fractal Dimension

I will not go into too many technical details about fractal dimensions since Chapter 6 is devoted entirely to this topic. However, the basic idea is to characterize the "strangeness" of the chaotic attractor. If one looks at a Poincaré map of a typical low-dimensional strange attractor, as in Figure 4-8, one sees sets of points arranged along parallel lines. This structure persists when one enlarges a small region of the attractor. As noted in Chapter 2, this structure of the strange attractor differs from periodic motions (just a finite set of Poincaré points) or quasiperiodic motion which in the Poincaré map becomes a closed curve. In the Poincaré map, one can say that the dimension of the periodic map is zero and the dimension of the quasiperiodic map is one. The idea of the fractal dimension calculation is to attach a measure of dimension to the Cantor-like set of points in the strange attractor. If the points uniformly covered some area on the plane, we might say its dimension was close to two. Because the chaotic map in Figure 4-8 has an infinite set of gaps, its dimension is between one and two —thus the word fractal dimension.

In general, the set of Poincaré points in a strange attractor does not cover an integer-dimensional subspace (in Figure 4-8 this subspace is a plane).

Another use for the fractal dimension calculation is to determine the lowest order phase space for which the motion can be described. For example, in the case of some preturbulent convective flows in a Rayleigh–Benard cell (see Figure 3-1), the fractal dimension of the chaotic attractor can be calculated from some measure of the motion $\{x(t_n) \equiv x_n\}$ (see Malraison et al., 1983). From $\{x_n\}$, pseudo-phase-spaces of different dimension can be constructed (see Section 4.4). Using a computer algorithm, the fractal dimension d was found to reach an asymptotic $d = 3.5$ when the dimension of the pseudo-phase-space was four or larger. This suggests that a low-order approximation of the Navier–Stokes equation may be used to model this motion.

The reader is referred to Chapter 6 for further details. Although there are questions about the ability to calculate fractal dimensions for attractors of dimensions greater than four or five, this technique has gained increasing

acceptance among experimentalists especially for low-dimensional chaotic attractors. If this trend continues, in the future, it is likely that electronic computing instruments will be available commercially that automatically calculate fractal dimension in the same way as FFTs are done at present.

(c) Lyapunov Exponents

Chaos in dynamics implies a sensitivity of the outcome of a dynamical process to changes in initial conditions. If one imagines a set of initial conditions within a sphere or radius ϵ in phase space, then for chaotic motions trajectories originating in the sphere will map the sphere into an ellipsoid whose major axis grows as $d = \epsilon e^{\lambda t}$, where $\lambda > 0$ is known as a *Lyapunov exponent*. (Lyapunov was a great Russian mathematician and mechanician 1857–1918.)

A number of experimenters in chaotic dynamics have developed algorithms to calculate the Lyapunov exponent μ. For regular motions $\lambda \leq 0$, but for chaotic motion $\lambda > 0$. Thus, *the sign of* λ *is a criterion for chaos*. The measurement involves the use of a computer to process the data. Algorithms have been developed to calculate λ from the measurement of a single dynamical variable $x(t)$ by constructing a pseudo-phase-space (e.g., see Wolf, 1984).

A more precise definition of Lyapunov exponents and techniques for measuring them is given in Chapter 5.

(d) Probability or Invariant Distributions

If a nonlinear dynamical system is in a chaotic state, precise prediction of the time history of the motion is impossible because small uncertainties in the initial conditions lead to divergent orbits in the phase space. If damping is present, we know that the chaotic orbit lies somewhere on the strange attractor. Failing specific knowledge about the whereabouts of the orbit, there is increasing interest in knowing the probability of finding the orbit somewhere on the attractor. One suggestion is to find a probability density in phase space to provide a statistical measure of the chaotic dynamics. There is some mathematical and experimental evidence that such a distribution does exist and that it does not vary with time.

To measure this distribution function, one time samples the motion at a number of points large enough to believe that the chaotic trajectory has visited most regions of the attractor. This minimum number can be determined by observing a Poincaré map to see when the attractor takes shape and when the Poincaré points fill in the different sections of the map. The

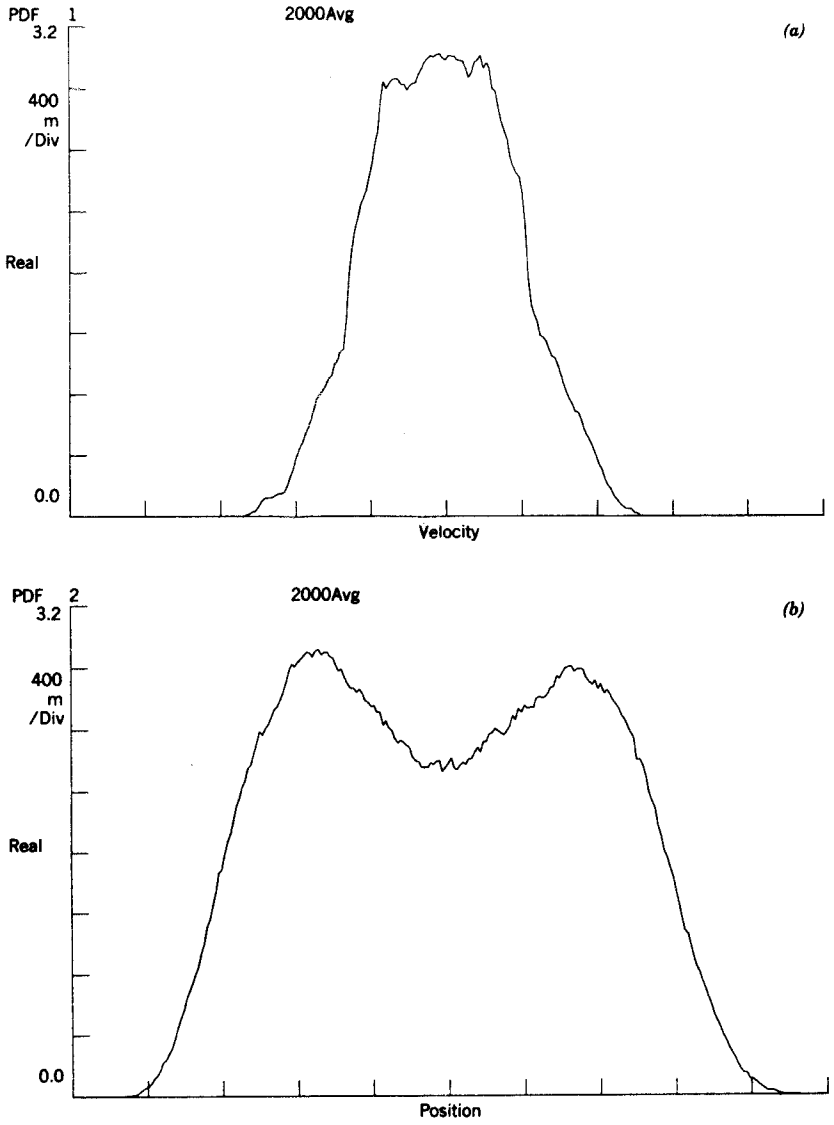

Figure 4-22 Experimental probability density function for chaotic vibration of a buckled beam averaged in time over many thousands of forcing periods. *Top*: Distribution of velocities of the beam tip; *Bottom*: Distribution of positions of the beam tip.

phase space is then partitioned into cells and the number of time-sampled points in each cell is counted using a computer.

An example of a probability density distribution for chaotic vibrations of the buckled beam problem is shown in Figure 4-22. Here we have projected the distribution onto the position axis and the velocity axis.

The distribution of velocities shows a shape similar to a classic Gaussian bell shaped curve (Figure 4-22*a*). The distribution of displacements on the other hand shows two peaks near the two potential wells (Figure 4-22*b*). This distribution is similar to that of a randomly excited two-well potential oscillator (Soong, 1973). It suggests that it might be possible to calculate probability density functions for deterministic chaotic systems using techniques from random vibration theory.

The usefulness of probability distribution for chaotic vibrations is similar to that for random vibrations (e.g., see Soong, 1973, or Lin, 1976). If the probability distribution can be determined for a chaotic system, one can calculate the mean square amplitude, mean zero crossing times, and probabilities of displacements, voltages, or stresses exceeding some critical value. However, much remains to be done on this subject both at the mathematical and experimental levels.

The use of probabilistic methods of analysis in chaotic vibrations has been developed by C. S. Hsu and coworkers at the University of California at Berkeley (Hsu, 1981, 1987; Hsu and Kim, 1985; Kreuzer, 1985 [now at Stuttgart]). This method, which divides the phase space into many cells, uses ideas from the theory of Markov processes. The method seems suited for the coming age of supercomputers and may become more widely known if it can be implemented in a parallel processing mode.

5

Criteria for Chaotic Vibrations

But you will ask, how could a uniform chaos coagulate at first irregularly in heterogeneous veins or masses to cause hills—Tell me the cause of this, and the answer will perhaps serve for the chaos.
Isaac Newton, *On Creation*—from a letter circa 1681

5.1 INTRODUCTION

In this chapter, we study how the parameters of a dynamical system determine whether the motion will be chaotic or regular. This is analogous to finding the critical velocity in viscous flow of fluids above which steady flow becomes turbulent. This velocity, when normalized by multiplying by a characteristic length and dividing by the kinematic viscosity of the fluid, is known as the critical *Reynolds number*, Re. A reliable theoretical value for the critical Re has eluded engineers and physicists for over a century and for most fluid problems experimental determination of $(\mathrm{Re})_{\mathrm{crit}}$ is necessary. In like manner, the determination of criteria for chaos in mechanical or electrical systems in most cases must be found by experiment or computer simulation. For such systems the search for critical parameters for deterministic chaos is a ripe subject for experimentalists and theoreticians alike.

Despite the paucity of experimentally verified theories for the onset of chaotic vibrations, there are some notable theoretical successes and some general theoretical guidelines.

We distinguish between two kinds of criteria for chaos in physical systems: a predictive rule and a diagnostic tool. A *predictive* rule for

chaotic vibrations is one that determines the set of input or control parameters that will lead to chaos. The ability to predict chaos in a physical system implies either that one has some approximate mathematical model of the system from which a criterion may be derived or that one has some empirical data based on many tests.

A *diagnostic* criterion for chaotic vibrations is a test that reveals if a particular system was or is in fact in a state of chaotic dynamics based on measurements or signal processing of data from the time history of the system.

We begin with a review of empirically determined criteria for specific physical systems and mathematical models which exhibit chaotic oscillations (Section 5.2). These criteria were determined by both physical and numerical experiments. We examine such cases for two reasons. First, it is of value for the novice in this field to explore a few particular chaotic systems in detail and to become familiar with the conditions under which chaos occurs. Such cases may give clues to when chaos occurs in more complex systems. Second, in the development of theoretical criteria, it is important to have some test case with which to compare theory with experiment.

In Section 5.3 we present a review of the principal, predictive models for determining when chaos occurs. These include the period-doubling criterion, homoclinic orbit criterion, and the overlap criterion of Chirikov for conservative chaos, as well as intermittency and transient chaos. We also review several ad hoc criteria that have been developed for specific classes of problems.

Finally, in Section 5.4 we discuss an important diagnostic tool, namely, the Lyapunov exponent. Another diagnostic concept, the fractal dimension, is described in Chapter 6.

5.2 EMPIRICAL CRITERIA FOR CHAOS

In the many introductory lectures the author has given on chaos, the following question has surfaced time and time again: *Are chaotic motions singular cases in real physical problems or do they occur for a wide range of parameters*? For engineers this question is very important. To design, one needs to predict system behavior. If the engineer chooses parameters that produce chaotic output, then he or she loses predictability. In the past, many designs in structural engineering, electrical circuits, and control systems were kept within the realm of linear system dynamics. However, the needs of modern technology have pushed devices into nonlinear regimes

(e.g., large deformations and deflections in structural mechanics) that increase the possibility of encountering chaotic dynamic phenomena.

To address the opening question, *are chaotic dynamics singular events in real systems*, we examine the range of parameters for which chaos occurs in seven different problems. A cursory scan of the figures accompanying each discussion will lead one to the conclusion that chaotic dynamics is not a singular class of motions and that *chaotic oscillations occur in many nonlinear systems for a wide range of parameter values*.

We examine the critical parameters for chaos in the following problems:

(a) Circuit with nonlinear inductor: Duffing's equation
(b) Particle in a two-well potential or buckling of an elastic beam: Duffing's equation
(c) Low-dimensional model for convection turbulence: Lorenz equations
(d) Vibrations of nonlinear coupled oscillators
(e) Rotating magnetic dipole: pendulum equation
(f) Circuit with nonlinear capacitance
(g) Surface waves on a fluid

(a) Forced Oscillations of a Nonlinear Inductor: Duffing's Equation

In Chapter 3 (Figure 3-13), we examined the chaotic dynamics of a circuit with a nonlinear inductor. Extensive analog and digital simulation for this system was performed by Y. Ueda (1979, 1980) of Kyoto University. The nondimensional equation, where x represents the flux in the inductor, takes the form

$$\ddot{x} + k\dot{x} + x^3 = B\cos t \tag{5-2.1}$$

The time has been nondimensionalized by the forcing frequency so that the entire dynamics is determined by the two parameters k and B and the initial conditions $(x(0), \dot{x}(0))$. Here k is a measure of the resistance of the circuit, while B is a measure of the driving voltage. Ueda found that by varying these two parameters one could obtain a wide variety of periodic, subharmonic, ultrasubharmonic as well as chaotic motions. The regions of chaotic behavior in the (k, B) plane are plotted in Figure 5-1. The regions of subharmonic and harmonic motions are quite complex and only a few are shown for illustration. The two different hatched areas indicate either regions of only chaos, or regions with both chaotic as well as periodic

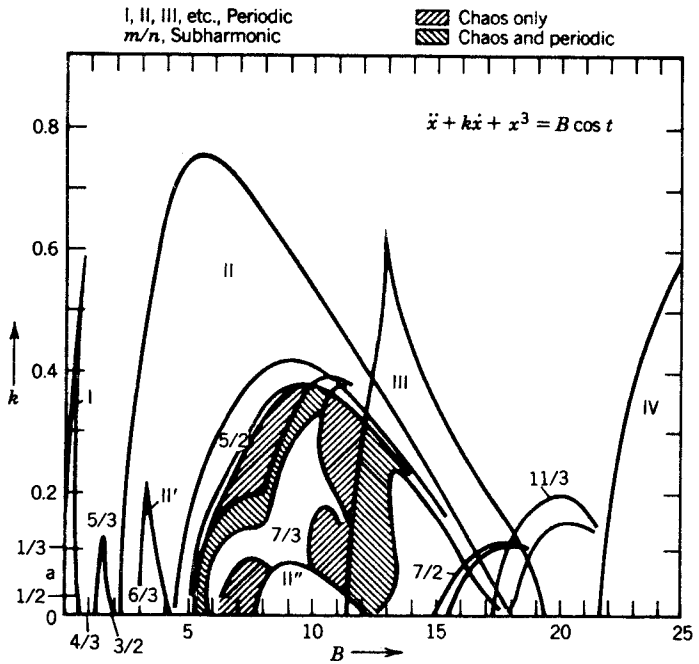

Figure 5-1 Chaos diagram showing regions of chaotic and periodic motions for a nonlinear circuit as functions of nondimensionalized damping and forcing amplitude [from Ueda (1980)].

motion depending on initial conditions. A theoretical criterion for this relatively simple equation has not been found to date.

(b) Forced Oscillations of a Particle in a Two-Well Potential: Duffing's Equation

This example was discussed in great detail in Chapters 2 and 3. It was first studied by Holmes (1979) and later in a series of papers by the author and coworkers. The mathematical equation describes the forced motion of a particle between two states of equilibrium, which can be described by a two-well potential

$$\ddot{x} + \delta\dot{x} - \tfrac{1}{2}x(1 - x^2) = f\cos\omega t \qquad (5\text{-}2.2)$$

This equation can represent a particle in a plasma, a defect in a solid, and, on a larger scale, the dynamics of a buckled elastic beam (see Chapter 3). The dynamics are controlled by three nondimensional groups (δ, f, ω),

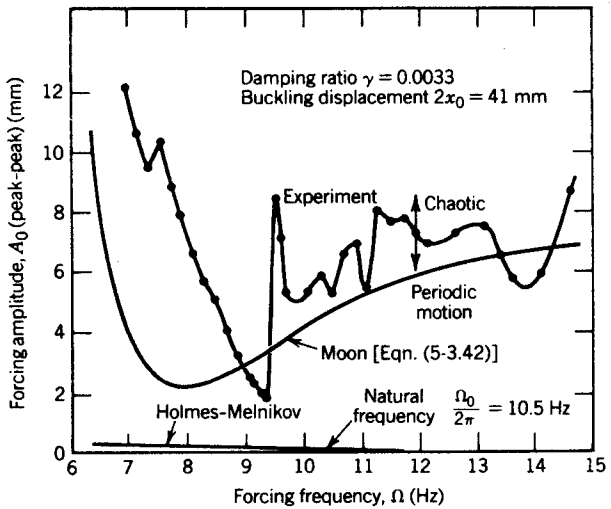

Figure 5-2 Experimental chaos diagram for vibrations of a buckled beam for different values of forcing frequency and amplitude [from Moon (1980b); reprinted with permission from *New Approaches to Nonlinear Problems in Dynamics*, ed. by P. S. Holmes; copyright 1980 by SIAM].

where δ represents nondimensional damping and ω is the driving frequency nondimensionalized by the small amplitude natural frequency of the system in one of the potential wells.

Regions of chaos from two studies are shown in Figures 5-2 and 5-3. The first represents experimental data for a buckled cantilevered beam (see Chapter 2). The ragged boundary is the experimental data, while the smooth curve represents a theoretical criterion (see Section 5.3). Recently, an upper boundary has been measured beyond which the motion again becomes periodic. The experimental criterion was determined by looking at Poincaré maps of the motion (see Chapters 2 and 4).

Results from numerical simulation of Eq. (5-2.2) are shown in Figure 5-3. The diagnostic tool used to determine if chaos were present was the Lyapunov exponent using a computer algorithm developed by Wolf et al. (1985) (see Section 5.4). This diagram shows that there are complex regions of chaotic vibrations in the plane (f, ω) for fixed damping δ. For very large forcing $f \gg 1$, one expects the behavior to emulate the previous problem studied by Ueda.

The theoretical boundary found by Holmes (1979) is discussed in the next section. It has special significance since below this boundary periodic motions are predictable, while above this boundary one loses the ability to exactly predict to which of the many periodic or chaotic modes the motion

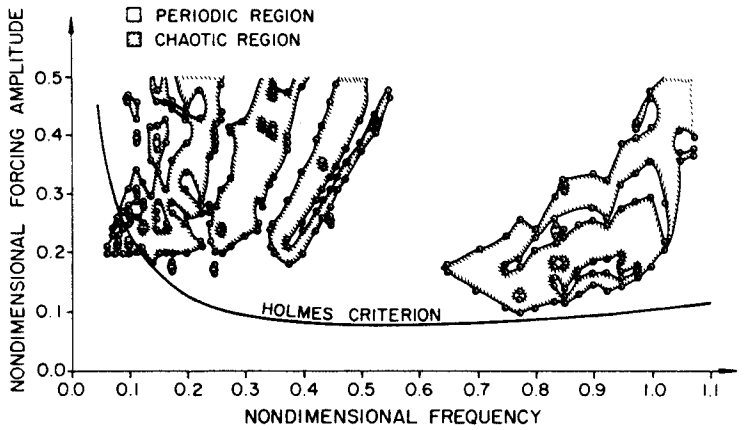

Figure 5-3 Chaos diagram for vibration of a mass in a double-well potential [Duffing's equation (5-2.2)]. The smooth boundary represents the homoclinic orbit criterion (Section 5.3).

will be attracted. Above the theoretical criteria (based on homoclinic orbits), the motion is very sensitive to initial conditions, even when it is periodic.

(c) Rayleigh–Benard Convection: Lorenz Equations

Aside from the logistic equation, the Lorenz model for convection turbulence (see Chapters 1 and 3) is perhaps the most studied system of equations that admit chaotic solutions. Yet most mathematicians have focused on a few sets of parameters. These equations take the form

$$\begin{aligned} \dot{x} &= \sigma(y - x) \\ \dot{y} &= rx - y - xz \\ \dot{z} &= xy - bz \end{aligned} \tag{5-2.3}$$

Sparrow (1982) in his book on the Lorenz attractor concentrates his analysis on the parameter values $\sigma = 10$, $b = \frac{8}{3}$, $r > 14$. However, he does speculate on the range of values for which stable chaotic motions might exist as reproduced in Figure 5-2. The vertical hatched region in Figure 5-4 represents a region of steady chaotic motion, while the horizontally hatched region represents a preturbulent region in which there may be chaotic transients. This region is bounded below by a criterion based on the

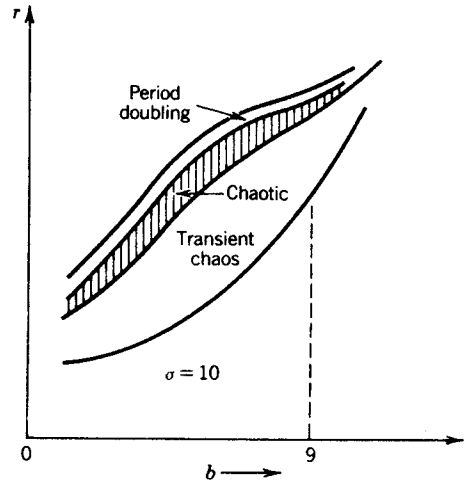

Figure 5-4 Chaos diagram for Lorenz's equations (5-2.3) for thermal convection dynamics.

existence of homoclinic orbits (see next section). A period-doubling region is also shown in the dotted region.

(d) Forced Vibrations of a Two-Degree-of-Freedom Oscillator in a Two-Well Potential

As extension of the one-degree-of-freedom particle in a two-well potential has been studied by the author for the experiment shown in Figure 5-5. This problem can be modeled by two coupled nonlinear oscillators (3-3.7),

$$\begin{aligned} \ddot{x} + \gamma\dot{x} + \frac{\partial V}{\partial x} &= 0 \\ \ddot{y} + \gamma\dot{y} + \frac{\partial V}{\partial y} &= f\cos\omega t \end{aligned} \tag{5-2.4}$$

where $V(x, y)$ represents the potential for the magnets and the elastic stiffness. The chaotic regime for the forcing amplitude and frequency are shown in Figure 5-5. Comparing this regime to that in either Figure 5-2 or 5-3, we see that the addition of the extra degree of freedom seems to have reduced the extent of the chaos region at least in the vicinity of the natural frequency of the mass in one of the potential wells.

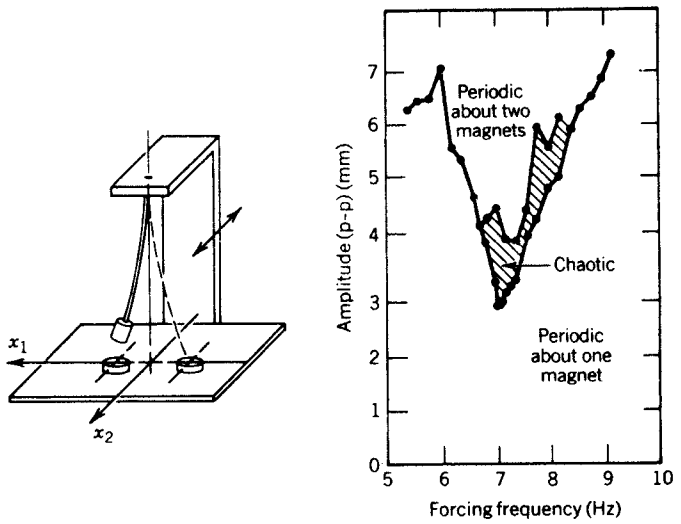

Figure 5-5 Regions of chaotic and periodic motions for two-dimensional motion of a mass in a double-well potential in the forcing amplitude–frequency plane [from Moon (1980b); reprinted with permission from *New Approaches to Nonlinear Problems* in *Dynamics*, ed. by P. S. Holmes; copyright 1980 by SIAM].

(e) Forced Motions of a Rotating Dipole in Magnetic Fields: The Pendulum Equation

In this experiment, a permanent magnet rotor is excited by crossed steady and time harmonic magnetic fields (see Moon et al., 1987), as shown in Figure 3-18. The nondimensionalized equation of motion for the rotation angle θ resembles that for the pendulum in a gravitational potential:

$$\ddot{\theta} + \gamma\dot{\theta} + \sin\theta = f\cos\theta\cos\omega t \qquad (5\text{-}2.5)$$

The regions of chaotic rotation in the f–ω plane, for fixed damping, are shown in Figure 5-6. This is one of the few published examples where both experimental and numerical simulation data are compared with a theoretical criterion for chaos. The theory is based on the homoclinic orbit criterion and is discussed in Section 5.4. As in the case of the two-well potential, chaotic motions are to be found in the vicinity of the natural frequency for small oscillations ($\omega = 1.0$ in Figure 5-6).

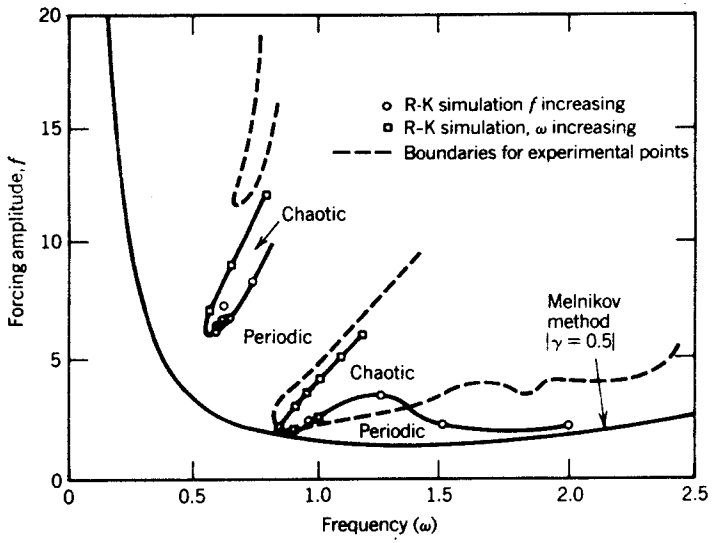

Figure 5-6 Experimental chaos diagram for forced motions of a rotor with nonlinear torque–angle property. Comparison with homoclinic orbit criterion calculated using the Melnikov method (Section 5.3) [From Moon et al. (1987) with permission of North-Holland Publishing Co., copyright 1987].

(f) Forced Oscillations of a Nonlinear *RLC* Circuit

There have been a number of experimental studies of chaotic oscillations in nonlinear circuits (e.g., see Chapter 3). One example is a *RLC* circuit with a diode. Shown in Figure 5-7 are the subharmonic and chaotic regimes in the driving voltage–frequency plane (Klinker et al., 1984). In this example, regions of period doubling are shown as precursors to the chaotic motions. However, in the midst of the hatched chaotic regime, a period 5 subharmonic was observed. Periodic islands in the center of chaotic domains are common observations in experiments on chaotic oscillations. (See a similar study by Bucko et al., 1984. See also Figure 3-33.).

(g) Harmonically Driven Surface Waves in a Fluid Cylinder

As a final example, we present experimentally determined harmonic and chaotic regions of the amplitude–frequency parameter space for surface waves in a cylinder filled with water from a paper by Cilberto and Gollub (1985). A 12.7 cm diameter cylinder with 1 cm deep water was harmonically

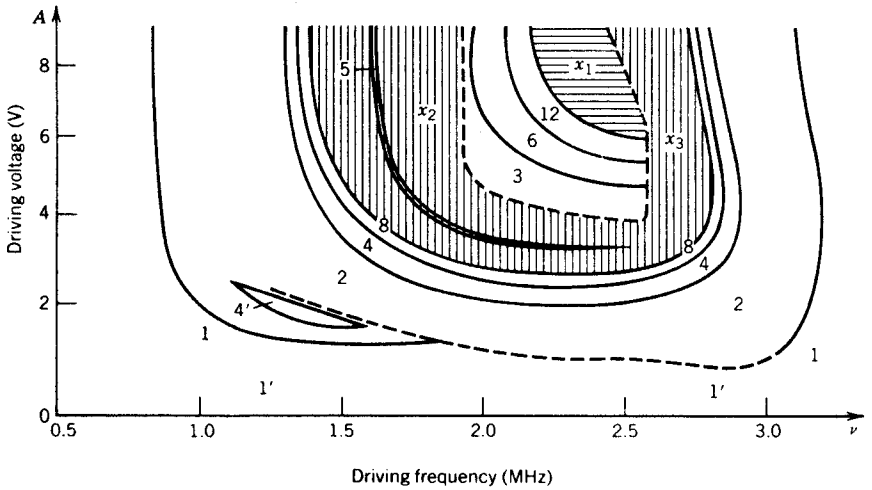

Figure 5-7 Experimentally determined chaos diagram for a driven *RLC* circuit with a varactor diode that acts as a nonlinear capacitor. The hatched regions are chaotic motions while the numbers indicate the order of the subharmonic. Dashed lines indicate a hysteretic transition [from Klinker et al. (1984) with permission of North-Holland Publishing Co., copyright 1984].

vibrated in a speaker cone (Figure 5-8). The amplitude of the transverse vibration above the flat surface of the fluid can be written in terms of Bessel functions where the linear mode shapes are given by

$$U_{nm} = J_n(k_{nm}r)\sin(n\theta + d_{nm})$$

Figure 5-8 shows the driving amplitude–frequency plane in a region where two modes can interact—$(n, m) = (4, 3)$ and $(7, 2)$. Below the lower boundary, the surface remains flat. A small region of chaotic regimes intersect. Presumably, other chaotic regimes exist where other modes (n, m) interact.

In summary, these examples show that, given periodic forcing input to a physical system, large regions of periodic or subharmonic motions do exist and presumably are predictable using classical methods of nonlinear analysis. However, these examples also show that *chaos is not a singular happening*; that is, it can exist for wide ranges in the parameters of the problem. Also, and perhaps this is most important, there are regions where both

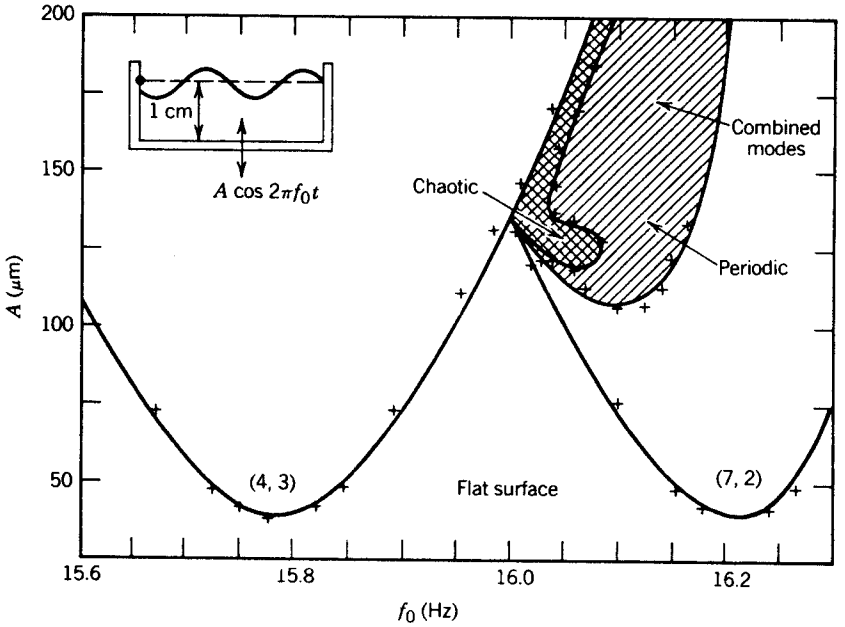

Figure 5-8 Experimental chaos diagram for surface waves in a cylinder filled with water. The diagram shows where two linear modes interact [from Ciliberto and Gollub (1985)].

periodic and chaotic motions can exist and the precise motion that will result may be unpredictable.

5.3 THEORETICAL PREDICTIVE CRITERIA

The search for theoretical criteria to determine under what set of conditions a given dynamical system will become chaotic has tended to be ad hoc. The strategy thus far has been for theorists to find criteria for specific mathematical models and then use these models as analogs or paradigms to infer when more general or complex physical systems will become unpredictable. An example is the period-doubling bifurcation sequence discussed by May (1976) and Feigenbaum (1978) for the quadratic map (e.g., see Chapter 1). Although these results were generalized for a wider class of one-dimensional maps using a technique called renormalization theory, the period-doubling criterion is not always observed for higher-dimensional maps. In mechanical and electrical vibrations, a Poincaré section of the solution in phase space often leads to maps of two or higher dimensions. Nonetheless,

the period-doubling scenario is one possible route to chaos. In more complicated physical systems, an understanding of the May–Feigenbaum model can be very useful in determining when and why chaotic motions occur.

In this section, we briefly review a few of the principal theories of chaos and explore how they lead to criteria that may be used to predict or diagnose chaotic behavior in real systems. These theories include the following:

(a) Period doubling
(b) Homoclinic orbits and horseshoe maps
(c) Intermittency and transient chaos
(d) Overlap criteria for conservative chaos
(e) Ad hoc theories for multiwell potential problems

(a) Period-Doubling Criterion

This criterion is applicable to dynamical systems whose behavior can be described exactly or approximately by a first-order difference equation, known in the new jargon as a one-dimensional map:

$$x_{n+1} = \lambda x_n(1 - x_n) \tag{5-3.1}$$

The dynamics of this equation were studied by May (1976), Feigenbaum (1978, 1980), and others. They discovered solutions whose period doubles as the parameter λ is varied (the period in this case is the number of integers p for x_{n+p} to return to the value x_n). One of the important properties of Eq. (5-3.1) that Feigenbaum discovered was that the sequence of critical parameters $\{\lambda_m\}$ at which the period of the orbit doubles satisfies the relation

$$\lim_{m\to\infty} \frac{\lambda_{m+1} - \lambda_m}{\lambda_m - \lambda_{m-1}} = \frac{1}{\delta}, \qquad \delta = 4.6692\cdots \tag{5-3.2}$$

This important discovery gave experimenters a specific criterion to determine if a system was about to become chaotic by simply observing the prechaotic periodic behavior. It has been applied to physical systems involving fluid, electrical, and laser experiments. Although these problems are often modeled mathematically by continuous differential equations, the Poincaré map can reduce the dynamics to a set of difference equations. For

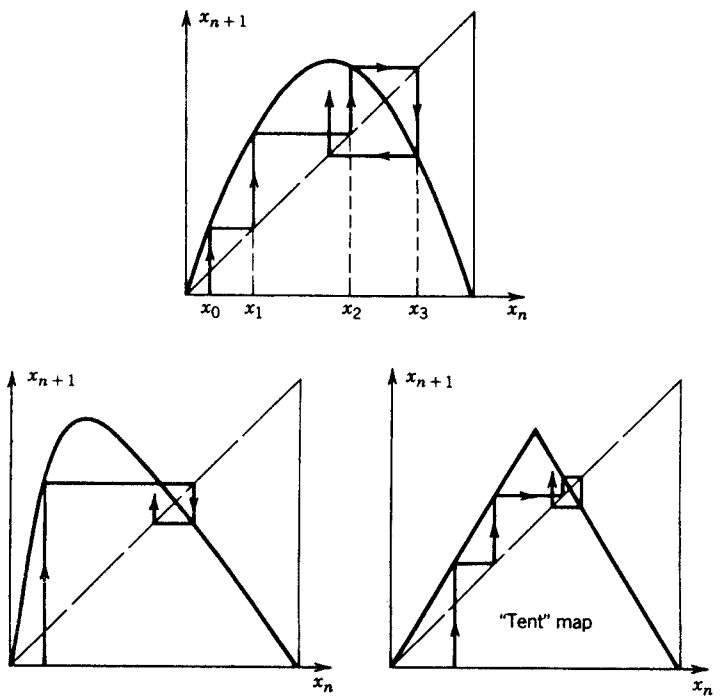

Figure 5-9 One hump noninvertible difference equations (maps) which exhibit period doubling.

many physical problems, the essential dynamics can be modeled further as a one-dimensional map.

$$x_{n+1} = f(x_n) \tag{5-3.3}$$

The importance of Feigenbaum's work is that he showed how period-doubling behavior was typical of one-dimensional maps that have a hump or zero tangent as shown in Figure 5-9 [i.e., the map is *noninvertible* or there exists two values of x_n which when put into $f(x_n)$ give the same value of x_{n+1}]. He also demonstrated that if the mapping function depends on some parameter Λ, that is, $f(x_n; \Lambda)$, then the sequence of critical values of this parameter at which the orbit's period doubles $\{\Lambda_m\}$ satisfies the same relation (5-3.2) as that for the quadratic map. Thus, the period-doubling phenomenon has been called *universal* and δ has been called a universal constant (now known quite naturally as the *Feigenbaum number*).

The author must raise a flag of caution here. The term "universal" is used in the context of one-dimensional maps (5-3.3). There are many chaotic phenomena which are described by two- or higher-dimensional maps (e.g., see the buckled beam problem in Chapter 2). In these cases, period doubling may indeed be one route to chaos, but there are many other bifurcation sequences that result in chaos beside period doubling (see Holmes, 1984).

The reader wishing a very detailed mathematical discussion of the quadratic map and period doubling should see either Lichtenberg and Lieberman (1983) or Guckenheimer and Holmes (1983). For the reader who desires a taste of the mathematics of period doubling, a distilled version of the treatment by Lichtenberg and Lieberman, especially as it pertains to the critical parameter λ_∞ at which the motion becomes chaotic, is presented next.

Renormalization and the Period-Doubling Criterion. There are two ideas that are important in understanding the period-doubling phenomenon. The first is the concept of *bifurcation* of solutions, and the second is the idea of *renormalization*. The concept of bifurcation is illustrated in Figure 5-10. The term bifurcate is used to denote the case where the qualitative behavior of the system suddenly changes as some parameter is varied. For example, in Figure 5-12 a steady periodic solution x_0 becomes unstable at a parameter value of λ, and the amplitude now oscillates between two values x_2^+ and x_2^-, completing a cycle in twice the time of the previous solution. Further changes in λ make x_2^+ and x_2^- unstable and the solution branches to a new cycle with period 4. In the case of the quadratic map (5-3.1), these solution bifurcations continue ad infinitum as λ is increased (or decreased). However, the critical values of λ approach an accumulation value, that is, $\lim_{i\to\infty}|\lambda_i| = |\lambda_\infty| < \infty$, beyond which the system can exhibit a chaotic, nonperiodic solution. Thus, if λ is some nondimensional function of physical variables (e.g., a Reynolds number in fluid mechanics), $\lambda = \lambda_\infty$ becomes a useful criterion to predict when chaos is likely to occur.

A readable description of renormalization as it applies to period doubling may be found in Feigenbaum (1980). The technique recognizes the fact that a cascade of bifurcations exists and that it might be possible to map each bifurcation into the previous one by a change in scale of the physical variable x and a transformation of the control parameter. To illustrate this technique, we outline an approximate scheme for the quadratic map (see also Lichtenberg and Lieberman, 1983).

One form of the quadratic map is given by

$$x_{n+1} = f(x_n)$$

where $f(x) = \lambda x(1 - x)$. Period 1 cycles are just constant values of x given

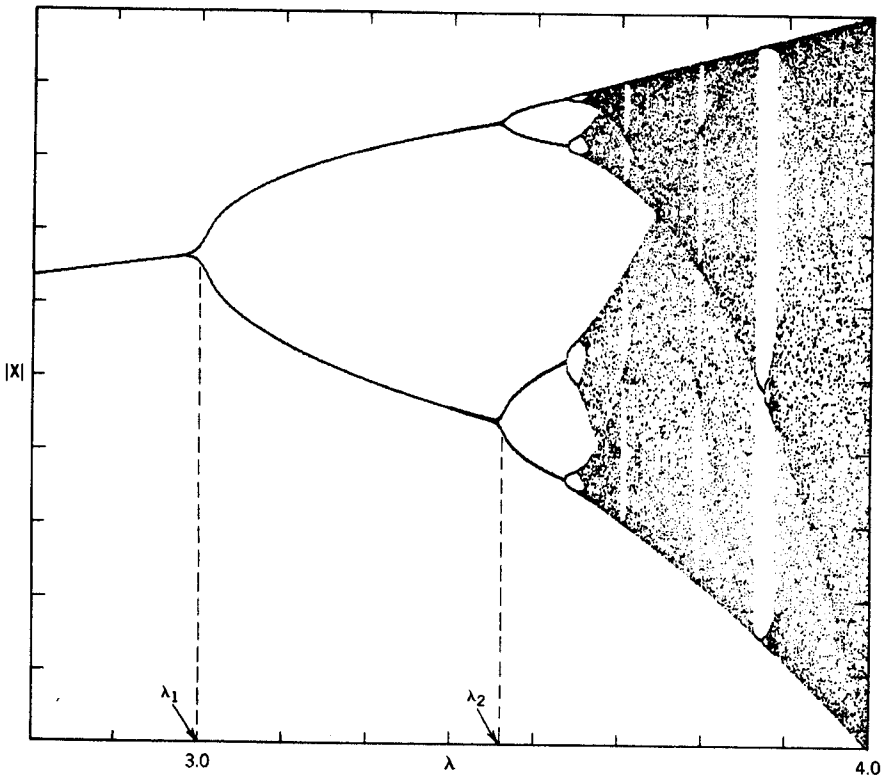

Figure 5-10 Bifurcation diagram for the quadratic map (5-3.3). Steady-state behavior as a function of the control parameter showing period-doubling phenomenon.

by fixed points of the mapping, that is, $x_n = f(x_n)$, or

$$x_0 = \lambda x_0(1 - x_0) \tag{5-3.4}$$

which gives $x_0 = 0$, $x_0 = (\lambda - 1)/\lambda$. Now a fixed point, or equilibrium point can be stable or unstable. That is, iteration of x can move toward or away from x_0. The stability of the map depends on the slope of $f(x)$ at x_0; that is,

$$\left|\frac{df(x_0)}{dx}\right| < 1 \quad \text{implies stability}$$
$$\left|\frac{df(x_0)}{dx}\right| > 1 \quad \text{implies instability} \tag{5-3.5}$$

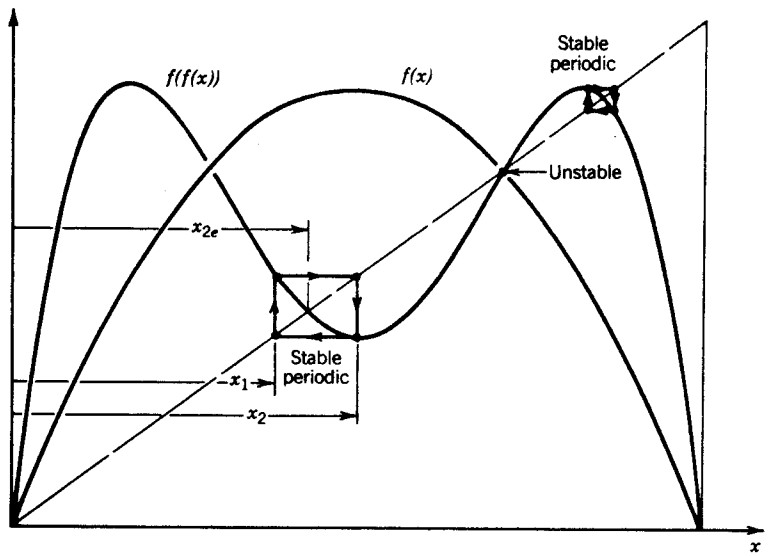

Figure 5-11 First and second iteration functions for the quadratic map (5-3.3) [see also Eq. (5-3.6)].

Since the slope $f' = \lambda(1 - 2x)$ depends on λ, x_0 becomes unstable at $\lambda_1 = \pm 1/|1 - 2x_0|$. Beyond this value, the stable periodic motion has period 2. The fixed points of the period 2 motion are given by

$$x_2 = f(f(x_2)) \quad \text{or} \quad x_2 = \lambda^2 x_2(1 - x_2)[1 - \lambda x_2(1 - x_2)] \tag{5-3.6}$$

The function $f(f(x))$ is shown in Figure 5-11.

Again there are stable and unstable solutions. Suppose the x_0 solution bifurcates and the solution alternates between x^+ and x^- as shown in Figure 5-12. We then have

$$x^+ = \lambda x^-(1 - x^-) \quad \text{and} \quad x^- = \lambda x^+(1 - x^+) \tag{5-3.7}$$

To determine the next critical value $\lambda = \lambda_2$ at which a period 4 orbit emerges, we change coordinates by writing

$$x_n = x^{\pm} + \eta_n \tag{5-3.8}$$

Putting Eq. (5-3.8) into (5-3.7), we get

$$\begin{aligned} \eta_{n+1} &= \lambda\eta_n[(1 - 2x^+) - \eta_n] \\ \eta_{n+2} &= \lambda\eta_{n+1}[(1 - 2x^-) - \eta_{n+1}] \end{aligned} \tag{5-3.9}$$

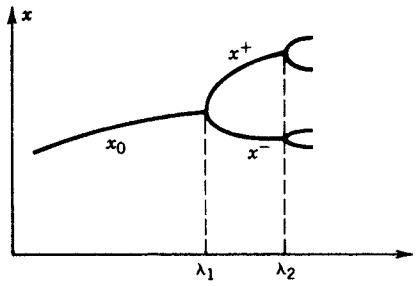

Figure 5-12 Diagram showing two branches of a bifurcation diagram near a period-doubling point.

We next solve for η_{n+2} in terms of η_n, keeping only terms to order η_n^2 (this is obviously an approximation), to obtain

$$\eta_{n+2} = \lambda^2\eta_n[A - B\eta_n] \tag{5-3.10}$$

where A and B depend on x^+, x^-, and λ. Next, we rescale η and define a new parameter $\bar{\lambda}$ using

$$\bar{x} = \alpha\eta, \qquad \bar{\lambda} = \lambda^2 A, \qquad \alpha = B/A$$

$$\bar{x}_{n+2} = \bar{\lambda}\bar{x}_n(1 - \bar{x}_n)$$

This has the same form as our original equation (5-3.2). Thus, when the solution bifurcates to period 4 at $\lambda = \lambda_2$, the critical value of $\bar{\lambda} = \lambda_1$. We therefore obtain an equation

$$\lambda_1 = \lambda_2^2 A(\lambda_2) \tag{5-3.11}$$

Starting from the point $x_0 = 0$, there is a bifurcation sequence for $\lambda < 0$. For this case Lichtenberg and Lieberman show that (5-3.11) is given by

$$\lambda_1 = -\lambda_2^2 + 2\lambda_2 + 4 \tag{5-3.12}$$

It can be shown that $\lambda_1 = -1$, so that $\lambda_2 = (1 - \sqrt{6}) = -1.4494$. If one is bold enough to propose that the recurrence relation (5-3.12) holds at higher-order bifurcations, then

$$\lambda_\kappa = -\lambda_{\kappa+1}^2 + 2\lambda_{\kappa+1} + 4 \tag{5-3.13}$$

At the critical value for chaos,

$$\begin{aligned} \lambda_\infty &= -\lambda_\infty^2 + 2\lambda_\infty + 4 \\ &= (1 - \sqrt{17})/2 = -1.562 \end{aligned} \tag{5-3.14}$$

One can also show that another bifurcation sequence occurs for $\lambda > 0$ (Figure 5-10) where the critical value is given by,

$$\lambda = \hat{\lambda}_\infty = 2 - \lambda_\infty = 3.56 \qquad (5\text{-}3.15)$$

The exact value is close to $\lambda_\infty = 3.56994$. Thus, the rescaling approximation scheme is not too bad.

This line of analysis also leads to the relation

$$\lambda_\kappa \simeq \lambda_\infty + a\delta^{-\kappa} \qquad (5\text{-}3.16)$$

which results in the scaling law (5-3.2). Thus, knowing that two successive bifurcation values can give one an estimate of the chaos criterion λ_∞, we obtain

$$\lambda_\infty \simeq \frac{1}{(\delta - 1)}[\delta\lambda_{\kappa+1} - \lambda_\kappa] \qquad (5\text{-}3.17)$$

A final word before we leave this section: The fact that λ may exceed the critical value ($|\lambda| > |\lambda_\infty|$) does not imply that chaotic solutions will occur. They certainly are possible. But there are also many *periodic windows* in the range of parameters greater than the critical value in which periodic motions as well as chaotic solutions can occur.

We do not have space to do complete justice to the rich complexities in the dynamics of the quadratic map. It is certainly one of the major paradigms for understanding chaos and the interested reader is encouraged to study this problem in the aforementioned references. (See also Appendix B for computer experiments.)

(b) Homoclinic Orbits and Horseshoe Maps

One theoretical technique that has led to specific criteria for chaotic vibrations is a method based on the search for horseshoe maps and homoclinic orbits in mathematical models of dynamical systems. This strategy and a mathematical technique, called the Melnikov method, has led to Reynolds-numberlike criteria for chaos relating the parameters in the system. In two cases, these criteria have been verified by numerical and physical experiments. Keeping with the tenor of this book, we do not derive or go into too much of the mathematical theory of this method, but we do try to convey the rationale behind it and guide the reader to the literature for a more detailed discussion of the method. We illustrate the Melnikov method with two applications: the vibrations of a buckled beam and the rotary dynamics of a magnetic dipole motor.

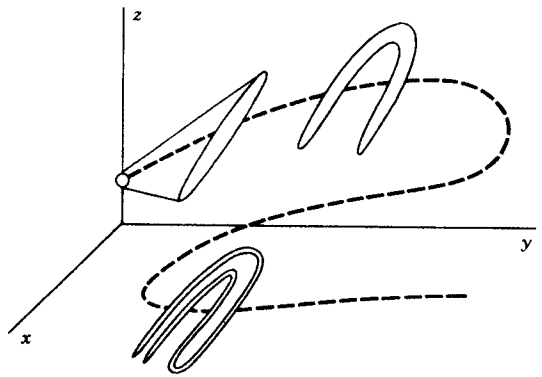

Figure 5-13 Evolution of an initial condition sphere.

The homoclinic orbit criterion is a mathematical technique for obtaining a predictive relation between the nondimensional groups in the physical system. It gives one a necessary but not sufficient condition for chaos. It may also give a necessary and sufficient condition for predictability in a dynamical system (see Chapter 6, Section 6.5, Fractal Basin Boundaries). Stripped of its complex, somewhat arcane mathematical infrastructure, it is essentially a method to prove whether a model in the form of partial or ordinary differential equations has the properties of a horseshoe or a baker's-type map.

The horseshoe map view of chaos (see also Chapter 1) looks at a collection of initial condition orbits in some ball in phase space. If a system has a horseshoe map behavior, this initial volume of phase space is mapped under the dynamics of the system onto a new shape in which the original ball is stretched and folded (Figure 5-13). After many iterations, this folding and stretching produces a fractal-like structure and the precise information as to which orbit originated where is lost. More and more precision is required to relate an initial condition to the state of the system at a later time. For a finite precision problem (as most numerical or laboratory experiments are), predictability is not possible.

One path to an understanding of the homoclinic orbit criterion (see the flow chart in Figure 5-14) is to go through the following questions:

1. What are homoclinic orbits?
2. How do homoclinic orbits arise in mathematical models of physical systems?
3. How are they related to horseshoe maps?
4. Finally, how does the Melnikov method lead to a criterion for chaos?

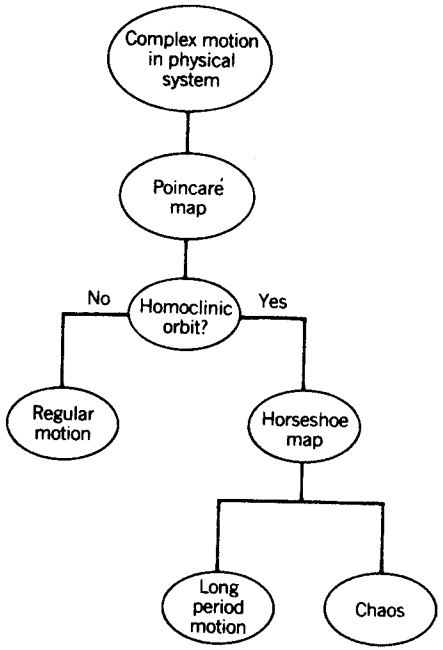

Figure 5-14 Diagram showing the relation between homoclinic orbits, horseshoes, and chaos in physical systems.

Homoclinic Orbits. A good discussion of homoclinic orbits may be found in the books by Lichtenberg and Lieberman (1983) and Guckenheimer and Holmes (1983). We have learned earlier that although many dynamics problems can be viewed as a continuous curve in some phase space (x versus $v = \dot{x}$) or solution space (x versus t), the mysteries of nonlinear dynamics and chaos are often deciphered by looking at a digital sampling of the motion such as a Poincaré map. We have also seen that the Poincaré map, although a sequence of points in some n-dimensional space, can lie along certain continuous curves. These curves are called *manifolds*. A discussion of homoclinic orbits refers to a sequence of points. This sequence of points is called an orbit. For example, for a period 3 orbit, the sequence of points will sequentially visit three states in the phase plane as in Figure 5-15*a*. On the other hand, a *quasiperiodic orbit* will involve a sequence of points that move on some closed curve, as in Figure 5-15*b*. Quasiperiodic vibrations are common in the motion of two coupled oscillators with two incommensurate frequencies.

In the dynamics of mappings, one can have critical points at which orbits move away from or toward. One example is a saddle point at which there are two manifold curves on which orbits approach the point and two curves

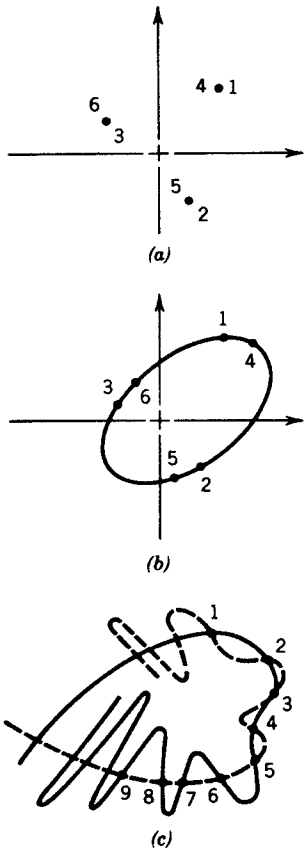

Figure 5-15 (*a*) Periodic orbit in a Poincaré map. (*b*) Quasiperiodic orbit. (*c*) Homoclinic orbit.

on which the sequence of Poincaré points move away from the point, as illustrated in Figure 5-15. Such a point is similar to a *saddle point* in nonlinear differential equations.

To illustrate a homoclinic orbit, we consider the dynamics of the forced damped pendulum. First, recall that for the unforced damped pendulum, the unstable branches of the saddle point swirl around the equilibrium point in a vortexlike motion in the θ–$\dot{\theta}$ phase plane as shown in Figure 5-16.

Although it is not obvious, the Poincaré map synchronized with the forcing frequency also has a saddle point in the neighborhood of $\theta = \pm n\pi$ (n odd), as shown in Figure 5-17 for the case of the forced pendulum. For small forcing, the stable and unstable branches of the saddle do not touch each other. However, as the force is increased, these two manifolds inter-

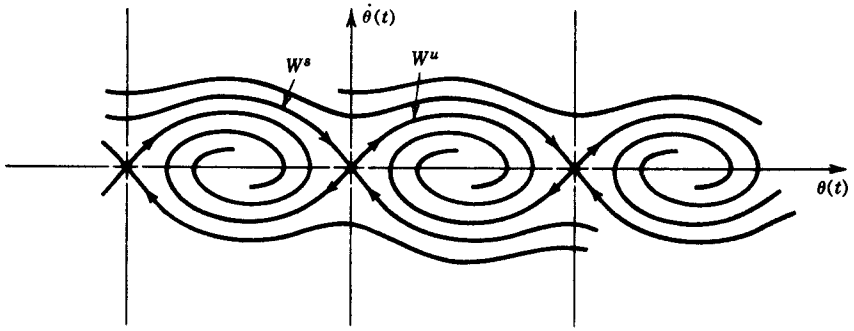

Figure 5-16 Stable and unstable manifolds for the motion of an unforced, damped pendulum.

sect. It can be shown that *if they intersect once*, they will *intersect an infinite number of times*. The points of intersection of stable and unstable manifolds are called *homoclinic points*. A Poincaré point near one of these points will be mapped into all the rest of the intersection points. This is called a *homoclinic orbit* (Figure 5-15*c*). Now why are these orbits important for chaos?

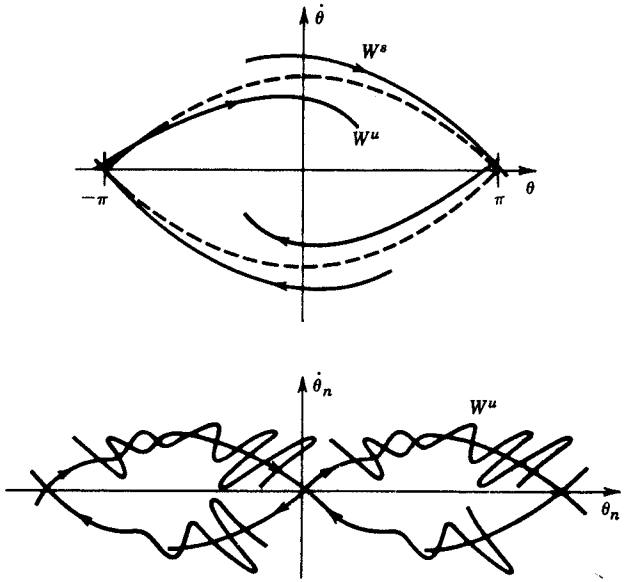

Figure 5-17 Sketch of stable and unstable manifolds of the Poincaré map for the harmonically forced, damped pendulum.

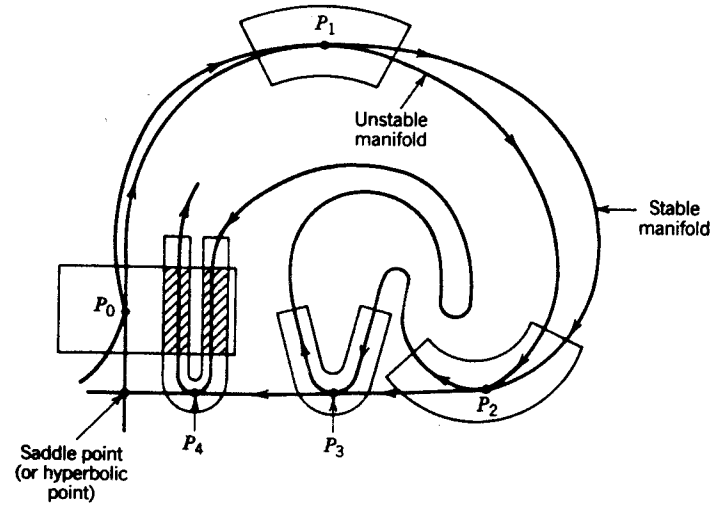

Figure 5-18 The development of a folded horseshoe-type map for points in the vicinity of a homoclinic orbit.

The intersection of the stable and unstable manifolds of the Poincaré map leads to a horseshoe-type map in the vicinity of each homoclinic point. As we saw in Chapter 1, horseshoe-type maps lead to unpredictability and unpredictability or sensitivity to initial conditions is a hallmark of chaos.

To see why homoclinic orbits lead to horseshoe maps, we recall that for a dissipative system areas get mapped into smaller areas. However, near the unstable manifold, the areas are also stretched. Since the total area must decrease, the area must also contract more than it stretches. Areas near the homoclinic points also get folded, as shown in Figure 5-18.

A dynamic process can be thought of as a transformation of phase space; that is, a volume of points representing different possible initial conditions is transformed into a distorted volume at a later time. Regular flow results when the transformed volume has a conventional shaped volume. Chaotic flows result when the volume is stretched, contracted, and folded as in the baker's transformation or *horseshoe* map.

The Melnikov Method. The Melnikov function is used to measure the distance between unstable and stable manifolds when that distance is small [see Guckenheimer and Holmes (1983) for a mathematical discussion of the Melnikov method]. It has been applied to problems where the dissipation is small and the equations for the manifolds of the zero dissipation problem are known. For example, suppose we consider the forced motion of a

nonlinear oscillator where (q, p) are the generalized coordinate and momentum variables. We assume that both the damping and forcing are small and that we can write the equations of motion in the form

$$\dot{q} = \frac{\partial H}{\partial p} + \epsilon g_1$$
$$\dot{p} = -\frac{\partial H}{\partial q} + \epsilon g_2 \tag{5-3.18}$$

where $\mathbf{g} = \mathbf{g}(p, q, t) = (g_1, g_2)$, ϵ is a small parameter, and $H(q, p)$ is the Hamiltonian for the undamped, unforced problems ($\epsilon = 0$). We also assume that $\mathbf{g}(t)$ is periodic so that

$$\mathbf{g}(t + T) = \mathbf{g}(t) \tag{5-3.19}$$

and that the motion takes place in a three-dimensional phase space $(q, p, \omega t)$, where ωt is the phase of the periodic force and is modulo the period T.

In many nonlinear problems a saddle point exists in the unperturbed Hamiltonian problem [$\epsilon = 0$ in Eq. (5-3.18)], such as for the pendulum or the double-well potential Duffing's equation, (5.22). When $\epsilon \neq 0$, one can take a Poincaré section of the three-dimensional torus flow synchronized with the phase ωt. It has been shown (see Guckenheimer and Holmes, 1983) that the Poincaré map also has a saddle point with stable and unstable manifolds, W^s and W^u, shown in Figure 5-19.

The Melnikov function provides a measure of the separation between W^s and W^u as a function of the phase of the Poincaré map ωt. This function is given by the integral

$$M(t_0) = \int_{-\infty}^{\infty} \mathbf{g}^* \cdot \nabla \mathbf{H}(q^*, p^*)\, dt \tag{5-3.20}$$

where $\mathbf{g}^* = \mathbf{g}(q^*, p^*, t + t_0)$ and $q^*(t)$ and $p^*(t)$ are the solutions for the unperturbed homoclinic orbit originating at the saddle point of the Hamiltonian problem. The variable t_0 is a measure of the distance along the original unperturbed homoclinic trajectory in the phase plane. We consider two examples.

Magnetic Pendulum. A convenient experimental model of a pendulum may be found in the rotary dynamics of a magnetic dipole in crossed steady and time periodic magnetic fields as shown in Figure 3-18 (See also Moon et al., 1987).

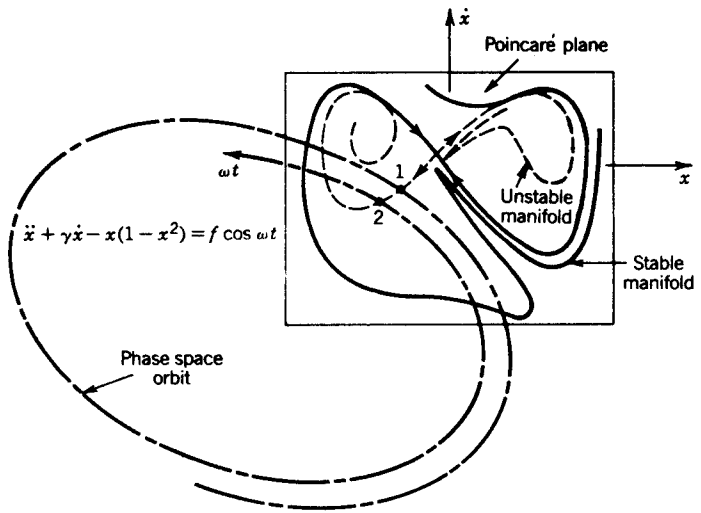

Figure 5-19 Saddle point of a Poincaré map and its associated stable and unstable manifolds before a homoclinic orbit develops.

The equation of motion when normalized is given by

$$\ddot{\theta} + \gamma\dot{\theta} + \sin\theta = f_1 \cos\theta \cos\omega t + f_0 \tag{5-3.21}$$

The $\sin\theta$ term is produced by the steady magnetic field, and the f_1 term is produced by the dynamic field. We have also included linear damping and a constant torque f_0. Keeping with the assumptions of the theory, we assume that one can write $\gamma = \epsilon\bar{\gamma}$, $f_0 = \epsilon\bar{f}_0$, and $f_1 = \epsilon\bar{f}_1$, where $0 \ll \epsilon < 1$ and $\bar{\gamma}$, $\bar{f}_0$, and $\bar{f}_1$ are of order one.

The Hamiltonian for the undamped, unforced problem is given by

$$H = \tfrac{1}{2}v^2 + (1 - \cos\theta)$$

where $q \equiv \theta$ and $p \equiv v = \dot{\theta}$. The energy H is constant ($H = 2$) on the homoclinic orbit emanating from the saddle point ($\theta = v = 0$). The unperturbed homoclinic orbit is given by

$$\theta^* = 2\tan^{-1}(\sinh t)$$
$$v^* = 2\,\mathrm{sech}\, t \tag{5-3.22}$$

In Eq. (5-3.18), $g_1 = 0$ and $g_2 = f_0 + f_1\cos\theta\cos\omega t$. The resulting integral

can be carried out exactly using contour integration (e.g., see Guckenheimer and Holmes for a similar example). The result gives

$$M(t_0) = -8\bar{\gamma} + 2\pi\bar{f}_0 + 2\pi\bar{f}_1\omega^2 \operatorname{sech}\left(\frac{\pi\omega}{2}\right)\cos\omega t_0 \qquad (5\text{-}3.23)$$

The two perturbed manifolds will touch transversely when $M(t_0)$ has a simple zero, or when

$$f_1 > \left|\frac{4\gamma}{\pi} - f_0\right| \frac{\cosh(\pi\omega/2)}{\omega^2} \qquad (5\text{-}3.24)$$

where we have canceled the ϵ factors. When $f_0 = 0$, the critical value of the forcing torque is given by

$$f_{1c} = \frac{4\gamma}{\pi\omega^2}\cosh\left(\frac{\pi\omega}{2}\right) \qquad (5\text{-}3.25)$$

This function is plotted in Figure 5-6 along with experimental and numerical simulation data. The criterion (5-3.25) gives a remarkably good lower bound on the regions of chaos in the forcing amplitude–frequency plane.

Two-Well Potential Problem. Forced motion of a particle in a two-well potential has numerous applications such as postbuckling behavior of a buckled elastic beam (Moon and Holmes, 1979) or certain plasma dynamics (Mahaffey, 1976). Damped periodically forced oscillations can be described by a Duffing-type equation

$$\ddot{x} + \gamma\dot{x} - x + x^3 = f\cos\omega t \qquad (5\text{-}3.26)$$

The Hamiltonian for the unperturbed problem is

$$H(x, v) = \tfrac{1}{2}\left(v^2 - x^2 + \tfrac{1}{2}x^4\right)$$

For $H = 0$, there are two homoclinic orbits originating and terminating at the saddle point at the origin. The variables x^* and v^* take on values along the right half plane curve given by

$$x^* = \sqrt{2}\operatorname{sech} t \quad \text{and} \quad v^* = -\sqrt{2}\operatorname{sech} t \tanh t$$

In this problem, $g_1 = 0$ and $g_2 = \bar{f}\cos\omega t - \bar{\gamma}v$, where $\gamma = \epsilon\bar{\gamma}$ and $f = \epsilon\bar{f}$ as in the previous example. The Melnikov function (5-3.20) then takes the

form

$$M(t_0) = -\sqrt{2}f\int_{-\infty}^{\infty} \operatorname{sech} t \tanh t \cos\omega(t + t_0)\, dt - 2\gamma\int_{-\infty}^{\infty} \operatorname{sech}^2 t \tanh^2 t\, dt$$

which can be integrated exactly using methods of contour integration. The solution was originally found by Holmes (1979) but an error crept into his paper. The correct analysis is in Guckenheimer and Holmes (1983):

$$M(t_0) = -\frac{4\gamma}{3} - \sqrt{2}f\pi\omega \operatorname{sech}\left(\frac{\pi\omega}{2}\right)\sin\omega t_0 \qquad (5\text{-}3.27)$$

For a simple zero we require

$$f > \frac{4\gamma}{3}\frac{\cosh(\pi\omega/2)}{\sqrt{2}\,\pi\omega} \qquad (5\text{-}3.28)$$

This lower bound on the chaotic region in (f, ω, γ) space has been verified in experiments by Moon (1980a) (see also Figures 5-2, 5-3).

(c) Intermittent and Transient Chaos

Thus far we have discussed what one might call "steady-state" chaotic vibration. Two other forms of unpredictable, irregular motions are intermittency and transient chaos. In the former, bursts of chaotic or noisy motion occur between periods of regular motion (see Figure 5-20). Such behavior was even observed by Reynolds in pipe flow preturbulence experiments in 1883 (see Sreenivasan, 1986). Transient chaos is also observed in some systems as a precursor to steady-state chaos. For certain initial conditions, the system may behave in a randomlike way, with the trajectory moving in phase space as if it were on a strange attractor. However, after some time,

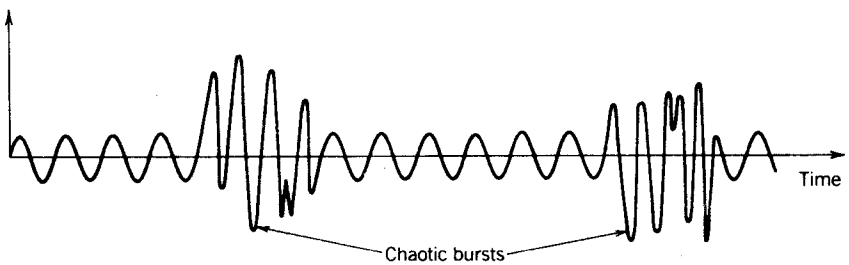

Figure 5-20 Sketch of intermittent chaotic motion.

the motion settles onto a regular attractor such as a periodic vibration. Scaling properties of nonlinear motion can sometimes be used to determine experimentally a critical parameter for these two types of chaotic motion. In the case of intermittency, where the dynamic system is close to a periodic motion but experiences short bursts of chaotic transients, an explanation of this behavior has been posited by Manneville and Pomeau (1980) in terms of one-dimensional maps or difference equations.

From numerical experiments on maps, the mean time duration of the periodic motion between chaotic bursts $\langle \tau \rangle$ has been found to be

$$\langle \tau \rangle \sim \frac{1}{|\lambda - \lambda_c|^{1/2}} \tag{5-3.29}$$

where λ is a control parameter (e.g., fluid velocity, forcing amplitude, or voltage) and λ_c is the value at which a chaotic motion occurs. As $\lambda - \lambda_c$ increases, the chaotic time interval increases and the periodic interval decreases. Thus, one might call this *creeping chaos*.

To measure λ_c experimentally, one must measure two average times $\langle \tau \rangle_1$ and $\langle \tau \rangle_2$ at corresponding values of the control parameter, that is, λ_1 and λ_2. This should determine the proportionality constant in Eq. (5-3.29) as well as λ_c. Having obtained a candidate value for λ_c, however, one should then measure other values of $(\langle \tau \rangle, \lambda)$ to validate the scaling relation (5-3.29).

The case of transient chaos has been studied by Grebogi et al. (1983a, b, 1985b) of the University of Maryland in a series of papers describing numerical experiments on two-dimensional maps. In one study (1983), they investigate a two-dimensional extension of the one-dimensional quadratic difference equation called the Henon map (see also Section 1.3):

$$x_{n+1} = 1 - \alpha x_n^2 + y_n$$

$$y_{n+1} = -J x_n$$

J is the determinant of the Jacobian matrix which controls the amount of area contraction of the map. In the Maryland group's research on transient chaos, the case of $J = -0.3$ with the parameter α varied was investigated. For example, for $\alpha > \alpha_0 = 1.062371838$, a period-6 orbit gave birth to a six-piece strange attractor that exists in the region

$$\alpha_0 < \alpha < \alpha_c = 1.080744879$$

For $\alpha > \alpha_c$, the orbit under the iteration of the Henon map was found to wander around the ghost of the strange attractor in the x–y plane, sometimes for over 10^3 iterations, before settling onto a period-4 motion.

They also discovered that the average time for the transient chaos $\langle \tau \rangle$ followed a scaling law

$$\langle \tau \rangle \sim (\alpha - \alpha_c)^{-1/2} \tag{5-3.30}$$

The average was found by choosing 10^2 initial conditions for each choice of α. The initial conditions were chosen in the original basin of attraction of the defunct strange attractor. These transients can be very long. For example, in the case of the Henon map, Grebogi and coworkers found $\langle \tau \rangle \approx 10^4$ for $\alpha - \alpha_c = 5 \times 10^{-7}$ and $\langle \tau \rangle \approx 10^3$ for $\alpha - \alpha_c = 10^{-5}$.

This same research group has also found maps that exhibit *supertransient chaos* in which the transient lifetime scales as (see Grebogi et al., 1985b)

$$\langle \tau \rangle \geq k_1 \exp\left[k_2 (\alpha - \alpha_c)^{-1/2}\right] \tag{5-3.31}$$

These results suggest that some transients could live beyond the practical life of any experiment. The mathematics relating to these studies again involves homoclinic intersections of stable and unstable manifolds in maps. The Maryland group refers to such homoclinic tangencies as *crises*. A full discussion of the mathematics concerning transient chaos is beyond the scope of this book and the reader is referred to the original work of the Maryland group cited above.

Unfortunately, few if any physical examples or experiments have been associated with the study of transient chaos thus far. But it would appear to be a fertile subject for further study.

(d) Chirikov's Overlap Criterion for Conservative Chaos

The study of chaotic motions in conservative systems (no damping) predates the current interest in chaotic dissipative systems. Since the practical application of conservative dynamical systems is limited to areas such as planetary mechanics, plasma physics, and accelerator physics, engineers have not followed this field as closely as other advances in nonlinear dynamics.

In this section, we focus on the bouncing ball chaos described in Chapter 3 (Figure 3-5). However, the resulting difference equations are relevant to the behavior of coupled nonlinear oscillators (e.g., see Lichtenberg and Lieberman, 1983) as well as the behavior of electrons in electromagnetic fields. The equations for the impact of a mass, under gravity, on a vibrating

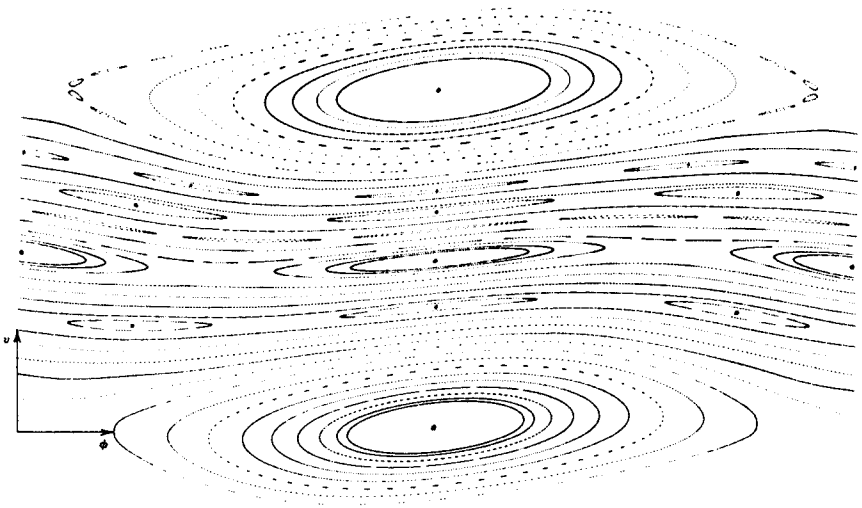

(a)

Figure 5-21 (a) Poincaré map for elastic motion of a ball on a vibrating table (standard map) for the parameter $K = 0.6$ in Eq. (5-3.32) showing periodic and quasiperiodic orbits.

table are given by (3-2.9) with a change of variables these become

$$\begin{aligned} v_{n+1} &= v_n + K \sin \varphi_n \\ \varphi_{n+1} &= \varphi_n + v_{n+1} \end{aligned} \tag{5-3.32}$$

where v_n is the velocity before impact and φ_n is the time of impact normalized by the frequency of the table (i.e., $\varphi = \omega t$ modulo 2π). K is proportional to the amplitude of the vibrating table in Figure 3-5. These equations differ from those in (3-2.9) by the assumption that there is no energy loss on impact. This implies that regions of initial conditions in the phase space (v, φ) preserve their areas under multiple iteration of the map (5-3.32).

Orbits in the (v, φ) plane for different initial conditions are shown in Figure 5-21 for two different values of K.

Consider the case of $K = 0.6$. The dots at $v = 0, 2\pi$ correspond to period 1 orbits; that is,

$$\begin{aligned} v_1 &= v_1 + K \sin \varphi_1 \\ \varphi_1 &= \varphi_1 + v_1 \end{aligned}$$

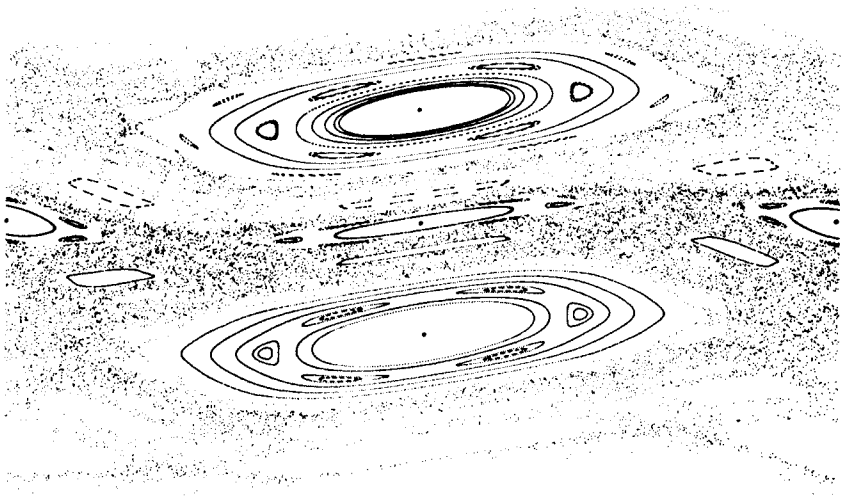

(b)

Figure 5-21 (b) The case of $K = 1.2$ showing the appearance of stochastic orbits.

whose solution is given by $\varphi_1 = 0, \pi$, $v_1 = 0$ (both mod 2π). The solution near $\varphi = \pi$ is stable for $|2 - K| < 2$. The solution near $\varphi = 0, 2\pi$, however, can be shown to be unstable for $|2 + K| < 2$ and can represent saddle points of the map.

Near $v = \pi$ one can see a period 2 orbit given by the solution to

$$\begin{aligned} v_2 &= v_1 + K \sin \varphi_1, \qquad \varphi_2 = \varphi_1 + v_2 \\ v_1 &= v_2 + K \sin \varphi_2, \qquad \varphi_1 = \varphi_2 + v_1 \end{aligned}$$

Again one can show that there are both stable and unstable period 2 points. One can also show that the stable points exists as long as $K < 2$.

The rest of the continuous looking orbits in Figure 5-21 represent quasiperiodic solutions where the ball impact frequency is incommensurate with the driving period. Finally, a third type of motion is present in Figure 5-21 ($K = 1.2$). Here we see a diffuse set of dots near where saddle points and the saddle separatrices used to exist. This diffuse set of points represents *conservative chaos*. For $K < 1$, it is localized around the saddle points. However, for $K \approx 1$, this wandering orbit becomes global in nature.

The reader should note that in Figure 5-21 ($K = 0.6$) one can obtain all types of motion by simply choosing different initial conditions (since there is no damping, there are no attractors).

A criterion for global chaos in this system was proposed by the Soviet

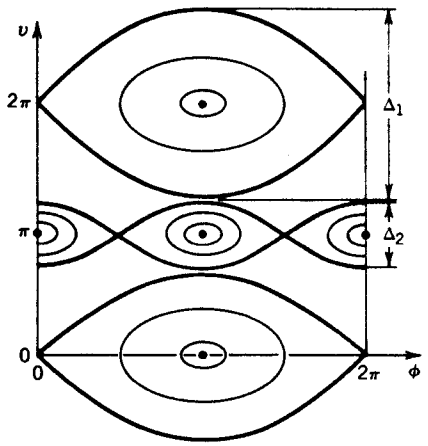

Figure 5-22 Sketch of period-1 and period-2 orbits and concomitant quasiperiodic orbits for the standard map used in the derivation of Chirikov's criterion.

physicist Chirikov (1979). He observed that as K is increased, the vertical distance between the separatrices associated with both period-1 and period-2 motion decreased. If chaos did not intervene, these separatrices would overlap (Figure 5-22)—thus the name *overlap criterion*.

If one performs a small-K analysis of the standard map (5-3.32) near one of these periodic resonances, the size of each separatrix region is found to be

$$\Delta_1 = 4K^{1/2}$$
$$\Delta_2 = K \tag{5-3.33}$$

Each analysis ignores the effect of the other resonance. The condition for overlap is that $\Delta_1 + \Delta_2 = 2\pi$, or

$$4K_c^{1/2} + K_c = 2\pi \tag{5-3.34}$$

The solution to this equation is $K_c = 1.46$. This value overestimates the critical value of $K = K_c$ for global chaos which is found numerically to be around $K_c \approx 1.0$. The reader is referred to Lichtenberg and Lieberman (1983) for further details concerning the overlap criterion.

The more practical minded reader might ask: *What happens when we have a small amount of damping present*? For that case, some of the multiperiod subharmonics become attractors and the ellipses surrounding these attractors become spirals that limit the periodic motions. *What of the conservative chaos*? Initial conditions in regions where there was conservative chaos become long chaotic transients which wander around phase space before settling into a periodic motion. *And what about real chaotic motions*? When damping is present, one needs a much larger force, $K > 6$, for which a fractal-like strange attractor appears (see Figure 3-5). Thus, the overlap criterion discussed above is only useful for strictly conservative, Hamiltonian systems.

(e) Multiwell Potential Criteria

In this section, we describe an ad hoc criterion for chaotic oscillations in problems with multiple potential energy wells. Such problems include the buckled beam (Chapter 2) and a magnetic dipole motor with multiple poles. In solid-state physics, interstitial atoms in a regular lattice can have more than one equilibrium position. Often the forces that create such problems can be derived from a potential. Let $\{q_i\}$ be a set of generalized coordinates and $V(q_i)$ be the potential associated with the conservative part of the force such that $-\partial V/\partial q_i$ is the generalized force associated with the q_i degree of freedom. For one degree of freedom, a special case might have the following equation of motion:

$$\ddot{q} + \gamma\dot{q} + \frac{\partial V}{\partial q} = f\cos\omega t \tag{5-3.35}$$

where linear damping and periodic forcing have been added. $V(q_i)$ has as many local minima as stable equilibrium positions, as shown in Figure 5-23.

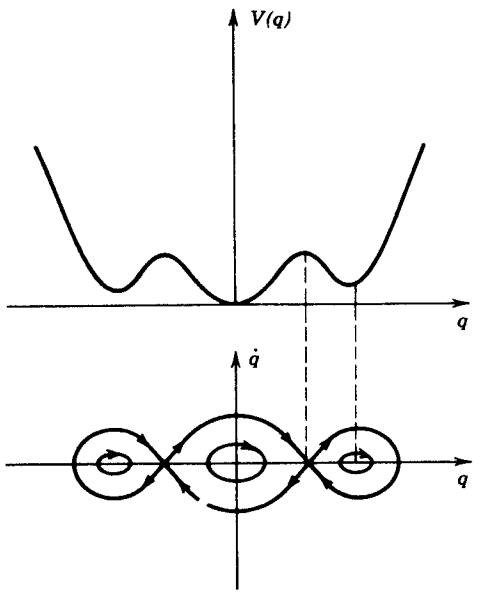

Figure 5-23 Multiwell potential energy function and associated phase plane.

For small periodic forcing, the system oscillates periodically in one potential well. But for larger forcing, the motion "spills over" into other wells and chaos often results. This criterion then seeks to determine *what value of the forcing amplitude will cause the periodic motion in one well to jump into another well.*

To illustrate the method, consider the particle in a two-well symmetric potential (i.e., the buckled beam problem of Chapter 2):

$$\ddot{q} + \gamma\dot{q} - \tfrac{1}{2}q(1 - q^2) = f\cos\omega t \qquad (5\text{-}3.36)$$

Since we are seeking a criterion that governs the transition from periodic to chaotic motion, we use standard perturbation theory to find a relation between the amplitude of forced motion $\langle q^2\rangle$ (where $\langle\ \rangle$ indicates a time average) and the parameters γ, f, and ω. We then try to find a *critical* value of $\langle q^2\rangle \equiv A_c$ independent of the forcing amplitude; that is,

$$\langle q^2\rangle = g(\gamma, \omega, f) = A_c(\omega) \qquad (5\text{-}3.37)$$

The left-hand equality in Eq. (5-3.37) is found using classical perturbation theory, while the right-hand equality is based on a heuristic postulate.

To carry out this program for the two-well potential, we must write Eq. (5-3.36) in coordinates centered about one of the equilibrium positions:

$$\eta = q - 1$$

To obtain a perturbation parameter, we write $\eta = \mu X$, so that the equation of motion takes the form

$$\ddot{X} + \gamma\dot{X} + X\left(1 + \tfrac{3}{2}\mu X + \tfrac{1}{2}\mu^2X^2\right) = \frac{f}{\mu}\cos(\omega t + \phi_0) \qquad (5\text{-}3.38)$$

The phase angle ϕ_0 is adjusted so that the first-order motion is proportional to $\cos\omega t$. The resulting periodic motion for small f is assumed to take the form

$$X = C_0\cos\omega t + \mu(C_1 + C_2\cos\omega t) + \mu^2X_1(t) \qquad (5\text{-}3.39)$$

Using either Duffing's method or Lindstedt's perturbation method (e.g., see Stoker, 1950), the resulting amplitude force relation can be found to be

$$(\mu C_0)^2\left\{\left[(1 - \omega^2) - \tfrac{3}{2}(\mu C_0)^2\right]^2 + \gamma^2\omega^2\right\} = f^2 \qquad (5\text{-}3.40)$$

Based on numerical experiments, we postulate the existence of a *critical velocity*. We propose that chaos is imminent when the maximum velocity of the motion is near the maximum velocity on the separatrix for the phase plane of the undamped, unforced oscillator. In terms of the original variables, this criterion becomes (see Figure 5-24)

$$\mu C_0 = \frac{\alpha}{2\omega} \qquad (5\text{-}3.41)$$

where α is close to unity. Substituting Eq. (5-3.41) into (5-3.40), we obtain a lower bound on the criterion for chaotic oscillations:

$$f_c = \frac{\alpha}{2\omega}\left\{\left[(1 - \omega^2) - \frac{3\alpha^2}{8\omega^2}\right]^2 + \gamma^2\omega^2\right\}^{1/2} \qquad (5\text{-}3.42)$$

This expression has been checked against experiments by the author (Moon, 1980a) and a factor of $\alpha \approx 0.86$ seemed to give excellent agreement with experimental chaos boundaries as shown in an earlier figure (Figure 5-2). For low damping, this criterion gives a much better bound than the homoclinic orbit criterion using the Melnikov function.

As illustrated in Figure 5-24, this criterion is similar to the Chirikov overlap criterion—namely, that chaos results when a regular motion becomes too large.

The method outlined in this section has also been used on a three-well potential problem and has been tested successfully in experiments on a vibrating beam with three equilibria by Li (1985).

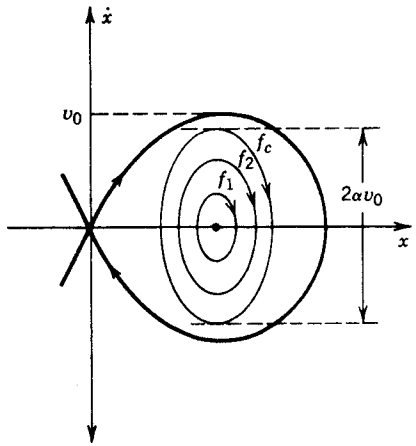

Figure 5-24 Overlap criteria for a multiwell problem using semiclassical analytic methods.

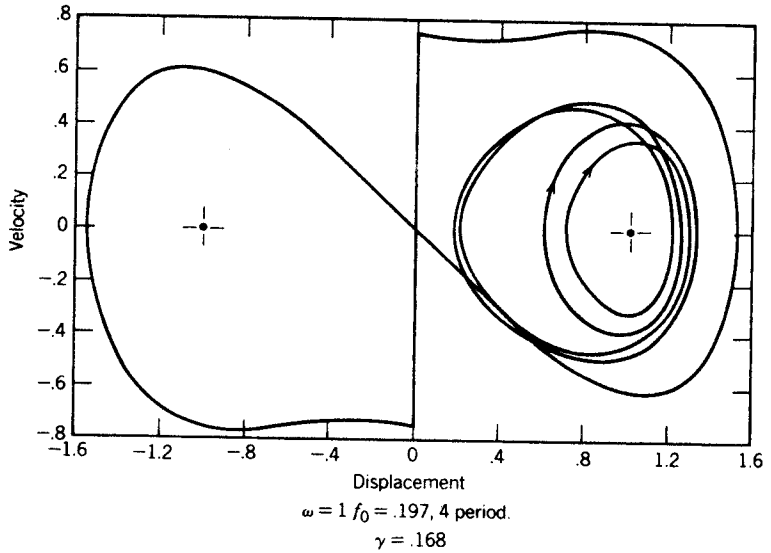

Figure 5-25 Basins of attraction for different initial conditions for the unforced, two-well potential oscillator [from Dowell and Pezeshki (1986) with permission of the American Society of Mechanical Engineers, copyright 1985].

Dowell and Pezeshki (1986) have posited another heuristic criterion for the two-well potential problem (5-3.36). Instead of comparing the size of periodic orbits with the undamped, unforced problem, they compare the prechaotic, periodic, subharmonic orbits for the driven oscillator with the boundary of the basin of attraction for the *damped*, unforced problem (Figure 5-25). This boundary represents the set of initial conditions $(A(0), \dot{A}(0))$ for which the orbit goes to the left or right equilibrium point without crossing $A = 0$. They also observe, through numerical simulation, that the driven motion becomes chaotic when the force level of f_0 is larger than the value for which a periodic orbit touches the basin boundary. (See Chapter 6 for a discussion of basin boundaries.)

Criteria Derived from Classical Perturbation Analysis. The novitiate to the field of nonlinear dynamics may be misled by the current interest in chaos to conclude that the field lay dormant in the prechaos era. However, a large literature exists describing mathematical perturbation methods for calculating primary and subharmonic resonances, as well as the stability characteristics of solutions to nonlinear systems (e.g., see Nehfeh and Mook, 1979). Thus, it is no surprise that studies are beginning to emerge that attempt to use the more classical analyses in the effort to find criteria for chaotic motion. For example, Nayfeh and Khdeir (1986) use perturbation techniques to predict the occurrence of period-doubling or period-tripling bifurcations as precursors to chaotic oscillations of ships in regular sea waves.

In another study Szemplinska-Stupnicka and Bajkowski (1986) have studied the Duffing oscillator of Ueda (3-2.25). They find subharmonic solutions using perturbation techniques and link the onset of chaos to the loss of stability of the subharmonics using classical stability analysis. They use analog computer experiments to check their results. They conclude that for the Duffing–Ueda attractor (3-2.35), the chaotic motion is a transition zone between the subharmonic and resonant harmonic solutions.

Although the author believes that the fundamental nature of chaotic motion is more closely related to such mathematical paradigms as horseshoe maps, fractals, and homoclinic orbits, the use of semiclassical methods of perturbation analysis may provide more practical analytic chaos criteria for certain classes of nonlinear systems.

6.3 FRACTAL DIMENSION OF STRANGE ATTRACTORS

There are two principal applications of fractal mathematics to nonlinear dynamics: characterization of strange attractors and measurement of fractal boundaries in initial condition and parameter space. In this section, we discuss the use of the fractal dimension in both numerical and experimental measurements of motions associated with strange attractors.

As yet, there are no instruments, electronic or otherwise, that will produce an output proportional to the fractal dimension, although electro-optical methods may achieve this end in the future (see Section 6.5). To date, in both numerical and experimental measurements, the fractal dimension and Lyapunov exponents are found by discretizing the signals at uniform time intervals and processing the data with a computer. There are

three basic methods:

(a) Time discretization of phase space variables
(b) Calculation of fractal dimension of Poincaré maps
(c) Construction of pseudo-phase-space using single variable measurements (sometimes called the embedding space method)

In both the first and third methods, the variables are measured and stored at uniform time intervals $\{\mathbf{x}(t_0 + n\tau)\}$, where n is a set of integers. The time interval τ is chosen to be a fraction of the principal forcing period or characteristic orbit time. If the Poincaré map in (b) is based on a time signal, τ is just the period of the time-based Poincaré map. However, if the Poincaré map is based on other phase space variables, the data are collected at variable times depending on the specific type of Poincaré map (see Chapter 4).

There are three principal definitions of fractal dimension used today: averaged pointwise dimension, correlation dimension, and Lyapunov dimension. In most of the current experience with actual calculation of fractal dimension, between 2000 and 20,000 points are used, although several recent papers claim to have reliable algorithms based on as little as 500 points (e.g., see Abraham et al., 1986). Direct algorithms for calculating fractal dimension based on N_0 points generally take N_0^2 operations so that superminicomputers or mainframe computers are often used. However, clever use of basic machine operations can reduce the number of operations to order $N_0 \ln N_0$ and significantly speed up calculation (e.g., see Grassberger and Proccacia, 1983).

(a) Discretization of Phase Space Variables

Suppose we know or suspect a chaotic system to have an attractor in three-dimensional phase space based on the physical variables $\{x(t), y(t), z(t)\}$. For example, in the case of the forced motion of a beam or particle in a two-well potential (see Chapter 2) x = position, $v = \dot{x}$ is the velocity, and $z = \omega t$ is the phase of the periodic driving force. In this method, time samples of $(x(t), y(t), z(t))$ are obtained at a rate that is smaller than the driving force period. To each time interval there corresponds a point $\mathbf{x}_n = (x(n\tau), y(n\tau), z(n\tau))$ in phase space.

To calculate an averaged pointwise dimension, one chooses a number of random points $\mathbf{x}_n$. About each point one calculates the distances from $\mathbf{x}_n$ to the nearest points surrounding $\mathbf{x}_n$. (Note that these points are not the

nearest in time, but in distance.) One does not need to use a Euclidean measure of distance. For example, the sum of absolute values of the components of $(\mathbf{x}_n - \mathbf{x}_m)$ could be used, that is,

$$s_{nm} = |x(n\tau) - x(m\tau)| + |y(n\tau) - y(m\tau)| + |z(n\tau) - z(m\tau)| \quad (6\text{-}3.1)$$

Then the number of points within a ball, cube, or other geometric shape of order ϵ is counted and a probability measure is found as a function of ϵ.

$$P_n(\epsilon) = \frac{1}{N_0} \sum_{m=1} H(\epsilon - S_{nm}) \quad (6\text{-}3.2)$$

where N_0 is the total number of sampled points and H is the Heaviside step function: $H(r) = 1$ if $r > 0$; $H(r) = 0$ if $r < 0$. The averaged pointwise dimension, following Eq. (6-2.3), is then

$$d_n = \lim_{\epsilon \to 0} \frac{\log P_n(\epsilon)}{\log \epsilon}$$
$$d \equiv \frac{1}{M} \sum_{n=1}^{M} d_n \quad (6\text{-}3.3)$$

where the limit defining d_n exists. For some attractors, the function P_n versus ϵ is not a power law but has steps or abrupt changes in slope. One can then calculate a modified average pointwise dimension by first averaging P_n. For example, let

$$\hat{C}(\epsilon) = \frac{1}{M} \sum_{n=1}^{M} P_n(\epsilon)$$
$$d = \lim_{\epsilon \to 0} \frac{\log \hat{C}(\epsilon)}{\log \epsilon} \quad (6\text{-}3.4)$$

This is similar to the correlation dimension discussed in the previous section.

The example of the two-well potential (5-2.2) is shown in Figure 6-8*a*, *b* using the correlation dimension. This dimension is computed from numerically generated data using the equation $\dot{x} = y$, $\dot{y} = -sy - \frac{1}{2}x(1 - x^2) + f\cos z$, $\dot{z} = \omega$ for values of δ, f, ω in the chaotic regime. Figure 6-8*a* shows the logarithm of the correlation function while Figure 6-8*b* shows the local slope versus the logarithm of the size of the test volume. The slope for the

intermediate values of ϵ is around 2.5. This is consistent with the fact that the attractor lives in a three-dimensional space (x, y, z).

In practice, $N_0 \approx 3\text{–}10^3 \times 10^4$ points and $M \approx .20N_0$. One should experiment with the choice of M by starting with a small value and increasing it until d reaches some limit.

The choice of ϵ also requires some judgment. The upper limit of ϵ is much smaller than the maximum size of the attractor yet large enough to capture the large-scale structure in the vicinity of the point $\mathbf{x}_n$. The smallest value of ϵ must be such that the associated sphere or cube contains at least one sample point. For example, in a three-dimensional phase space, if the mean global scale of the attractor is L, the average point density is

$$\rho \approx \frac{N_0 6}{\pi L^3}$$

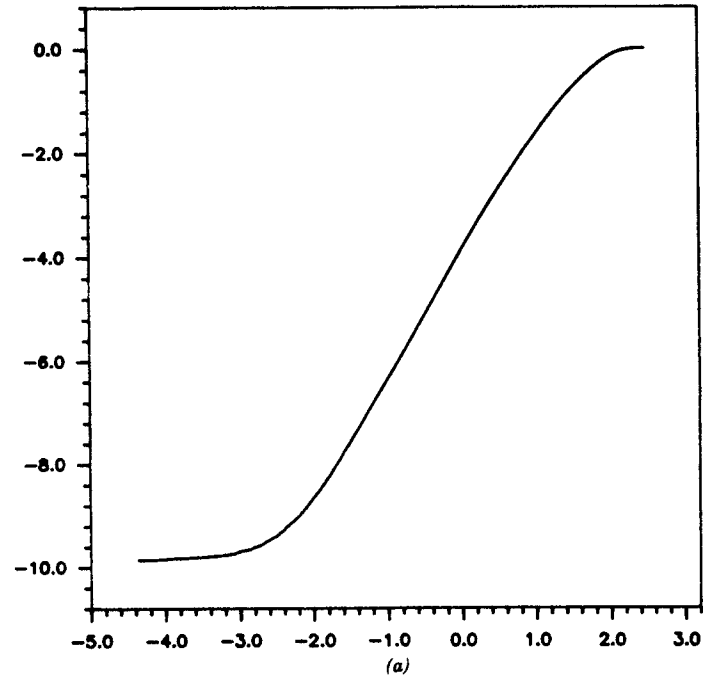

Figure 6-8 (*a*) $\log C$ versus $\log \epsilon$ for chaotic motion in a two-well potential (3-3.6). Data obtained from numerical integration.

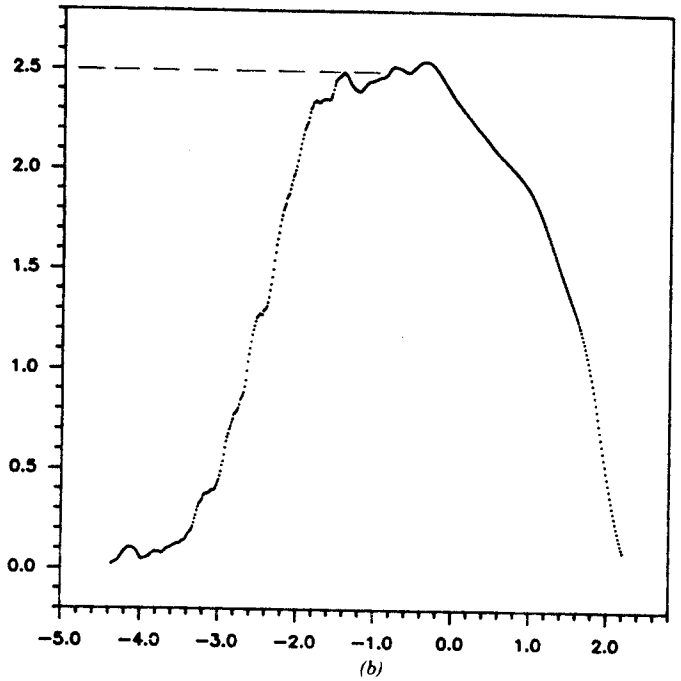

Figure 6-8 (*b*) Local slope of (*a*) showing fractal dimension in linear region of (*a*) of around 2.5.

so that the volume associated with ϵ should be greater than ρ^{-1} or

$$\epsilon > \frac{L}{2N_0^{1/3}} \tag{6-3.5}$$

Another constraint on the minimum size of ϵ is the "real noise" or uncertainty in the measurements of the state variables (x, y, z). In an actual experiment, there is a sphere of uncertainty surrounding each measured point in phase space. When ϵ becomes smaller than the radius of this sphere, the theory of fractal dimension discussed above comes into question since for smaller ϵ one cannot expect a self-similar structure.

(b) Fractal Dimension of Poincaré Maps

In systems driven by a periodic excitation, as in the Duffing–Ueda strange attractor (3-2.25) or the two-well potential strange attractor (3-3.6), time or the phase $\phi = \omega t$ becomes a natural phase space variable. In most cases,

this time variable will lie in the attractor subspace and time can be considered as one of the contributions to the dimension of the attractor. In the case of a periodically forced, nonlinear, second-order oscillator, the Poincaré map based on periodic time samples produces a distribution of points in the plane. To calculate the fractal dimension of the complete attractor, it is sometimes convenient to calculate the fractal dimension of the Poincaré map $0 < D < 2$. If D is independent of the phase of the Poincaré map (remember $0 \leq \omega t \leq 2\pi$), the dimension of the complete attractor is just

$$d = 1 + D \tag{6-3.6}$$

As an example, we present numerical and experimental data for the two-well potential or Duffing–Holmes strange attractor (Chapter 2):

$$\ddot{x} + \gamma\dot{x} - \tfrac{1}{2}x(1 - x^2) = f\cos\omega t \tag{6-3.7}$$

In this example, we are interested in two questions:

1. Does the fractal dimension of the strange attractor vary with the phase of the Poincaré map?
2. How does the fractal dimension vary with the damping γ?

The fractal dimension was calculated for a set of experimental Poincaré maps and are listed in Table 6-2. This table shows an almost constant value around the attractor. Thus, the assumption $d = 1 + D$ in Eq. (6-3.6) appears to be a good one.

TABLE 6-2 Dimension of Experimental Poincaré Map versus Phase for Vibration of a Buckled Beam[a]

ϕ	$D(1,4)$[b]	$D(1,7)$[c]
0	1.741	1.628
45	1.751	1.627
90	1.742	1.638
135	1.748	1.637
180	1.730	1.637

[a] Nondimensional damping, $\gamma = 0.013$; forcing frequency, 8.5 Hz; natural frequency about buckled state, 9.3 Hz; from Moon and Li (1985a).
[b] Based on four smallest log r points in log C versus log r.
[c] Based on seven smallest log r points in log C versus log r.

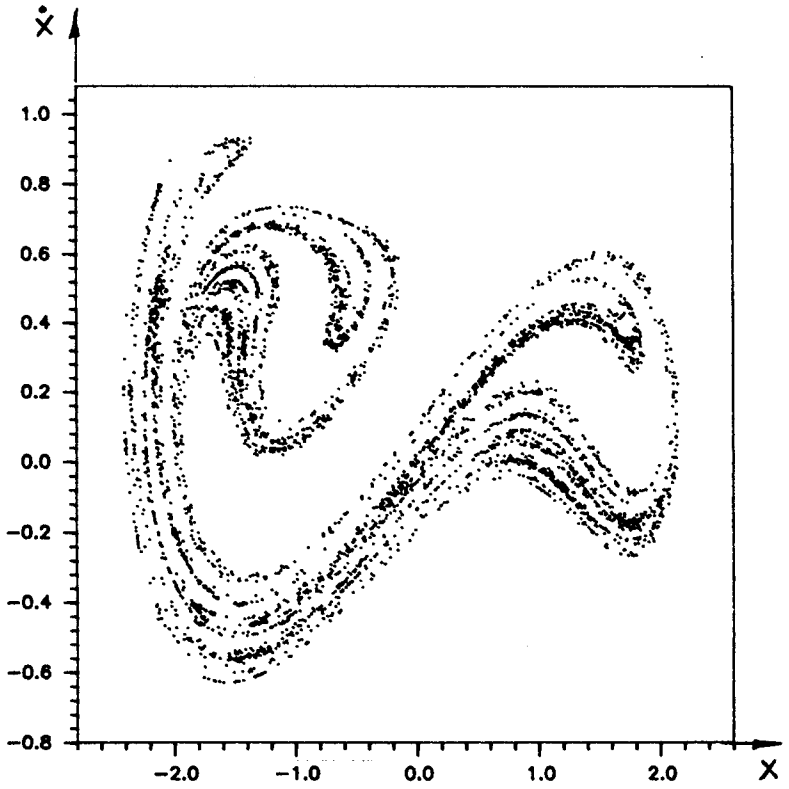

Figure 6-9 Fractal distribution of points from a Poincaré map for the two-well potential problem (3-2.10), using the same data as in Figure 6-8.

A numerically generated Poincaré map for the case of a particle in a two-well potential under periodic excitation is shown in Figure 6-9. The correlation function (Figure 6-10*a* $C(\epsilon)$ vs ϵ is shown plotted in a log-log scale and shows a linear dependence as assumed in the theory.

The data in Figure 6-10 was the same as that used in Figure 6-8. From Figure 6-10*b*, $D \simeq 1.5$ or $d = 2.5$, which agrees with that calculated directly from the attractor in the phase space $(x, \dot{x}, \omega t)$ as in Figure 6-8.

The effect of damping on the fractal dimension of the two-well potential strange attractor was determined from Runge–Kutta numerical simulation. This dependence is shown in Figure 6-11. The data show that low damping yields an attractor that fills phase space ($D = 2$, $d = 3$) as would a Hamiltonian (zero damping) system. As damping is increased, however, the Poincaré map looks one dimensional and the attractor has a dimension close to $d = 2$, as in the case of the Lorenz equations.

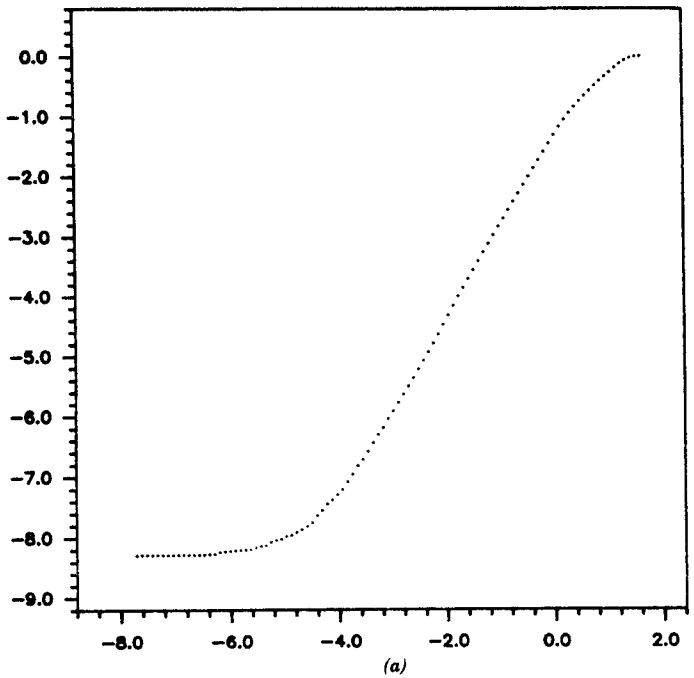

Figure 6-10 (*a*) $\log C$ versus $\log \epsilon$ for the set of points in the Poincaré map in Figure 6-9.

The fractal dimension of a chaotic circuit (diode, inductor, and resistor in series driven with an oscillator) has been measured by Linsay (1985) using a Poincaré map. He measures the current at a sampling time equal to the period of the oscillator and constructs a three-dimensional pseudo-phase-space using $(I(t), I(t + \tau), I(t + 2\tau))$ (see next section). He obtains a fractal dimension of the Poincaré map of $D = 1.58$ and infers a dimension of the attractor of 2.58.

(c) Dimension Calculation from Single Time Series Measurement

The methods discussed above assume that (1) one knows the dimension of the phase space wherein the attractor lies and (2) one has the ability to measure all the state variables. However, in many experiments, the time history of only one state variable may be available or possible. Also, in continuous systems involving fluid or solid continua, the number of degrees of freedom or minimum number of significant modes contributing to the chaotic dynamics may not be known a priori. In fact, one of the important

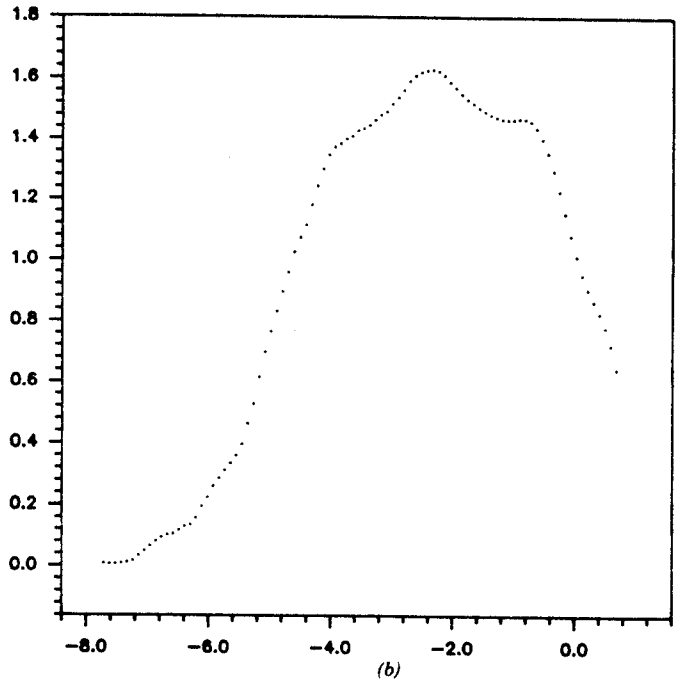

Figure 6-10 (*b*) Local slope of (*a*) showing a fractal dimension in the linear region of (*a*) of around 1.5.

applications of fractal mathematics is to allow one to determine the smallest number of first-order differential equations that may capture the qualitative features of the dynamics of continuous systems. This has already had some success in thermofluid problems such as Rayleigh–Benard convection (see Malraison et al., 1983).

In early theories of turbulence (e.g., Landau, 1944), it was thought that chaotic flow was the result of the interaction of a very large or infinite set of modes or degrees of freedom in the fluid. At the present time, it is believed that the chaos associated with the transition to turbulence can be modeled by a finite set of ordinary differential equations.

Thus, suppose that the number of first-order equations required to simulate the dynamics of a dissipative system is N. Then the fractal dimension of the attractor would be $d < N$. Then if we were to determine d by some means, we would then determine the minimum N.

Not knowing N, we cannot know how many physical variables $(x(t), y(t), z(t), \ldots)$ to measure. Instead, we construct a pseudo-phase-space, or embedding space, using time-delayed measurements of one physi-

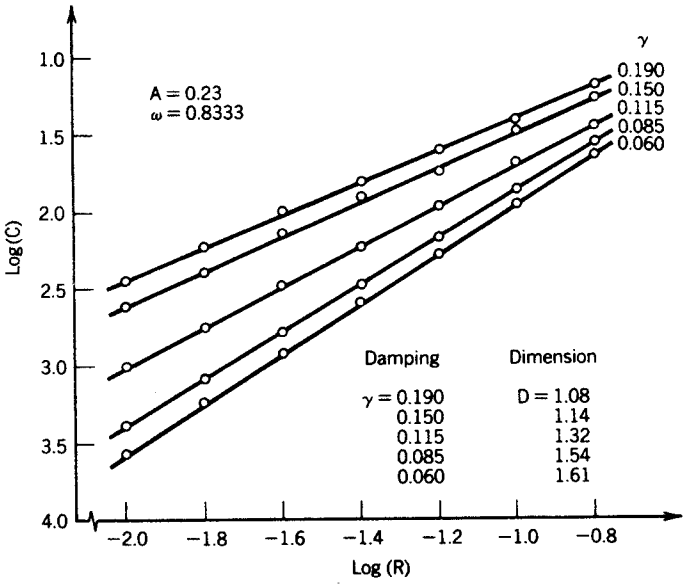

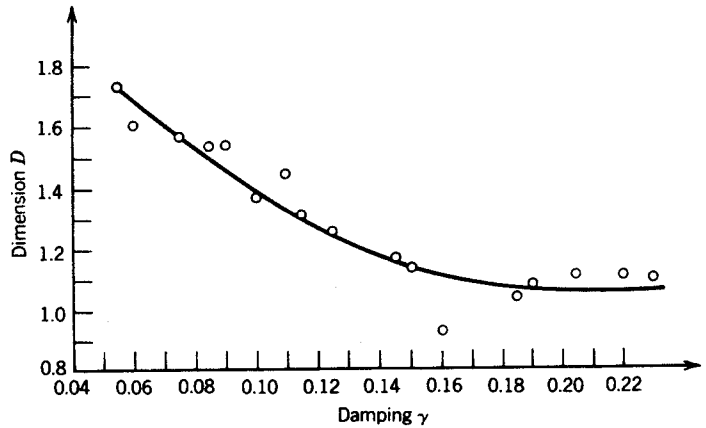

Figure 6-11 Dependence of fractal dimension on the damping for the two-well potential oscillator (3-2.10).

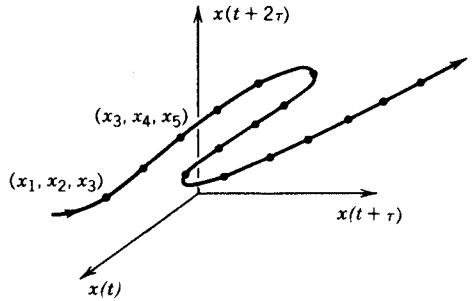

Figure 6-12 Sketch of an orbit in a three-dimensional pseudo-phase-space constructed from a single time series measurement.

cal variable, say $(x(t), x(t+\tau), x(t+2\tau), \ldots)$ (see Chapter 4 and also Packard et al., 1980). For example, three-dimensional pseudo-phase-space vectors are calculated using three successive components of the digitized $x(t)$ (Figure 6-12), that is,

$$\mathbf{x}_n = \{x(t_0 + n\tau), x(t_0 + (n+1)\tau), x(t_0 + (n+2)\tau)\} \quad (6\text{-}3.8)$$

With these position vectors, one can use the correlation function (6-2.6) or averaged probability function (6-2.3) to calculate a fractal dimension.

To determine the minimum N, one constructs higher-dimensional pseudo-phase-spaces based on the time-sampled $x(t)$ measurements until the value of the fractal dimension reaches an asymptote, say, $d = M + \mu$, where $\mu < 1$. Then the minimum phase space dimension for this chaotic attractor is $N = M + 1$.

In reconstructing a dynamical attractor from the time history measurements of a single variable, the question arises of how many dimensions are required in the embedding space in order to capture all the topological features of the original attractor. A mathematician named Takens has proved several theorems about this question. If the original phase space attractor lives in an $N =$ dimensional space, then in general one must reconstruct an embedding space (our pseudo-phase-space) of $2N + 1$ dimensions.

To illustrate these ideas we have applied the embedding space method to find the dimension of the two-welled potential (or buckled beam) attractor (5-2.2). Earlier we saw that this attractor lives in a three-dimensional phase space $(x, \dot{x}, \omega t)$ and has a fractal dimension of $d = 2.5$ (Figure 6-8). Using the same data we also saw that we could calculate d from the Poincaré map (Figures 6-9, 6-10). Using the same numerical data from a Runge–Kutta

integration, we reconstructed the motion in a pseudo-phase-space using digitized values of $x(t)$ and embedding space dimensions of $m = 2 - 8$. The graphs in Figure 6-13*a*, *b* show the correlation function as well as the calculated dimension of the attractor in each embedding space.

One can see in Figure 6-13*b* that the dimension reaches an asymptote of $d = 2.5$ after $M \sim 4 - 5$, which is in agreement with Taken's theorem.

As an example using experimental data, we describe the work of a group at the French research laboratory at Saclay (e.g., see Malraison et al., 1983; Bergé et al., 1985). They measured the fractal dimension of a convective fluid cell under a thermal gradient (Rayleigh–Benard convection, see Chapter 3). They calculated the fractal dimension using an averaged pointwise dimension (6-2.3) for different sizes of pseudo-phase-spaces. As shown in Figure 6-14, the fractal dimension saturated at a value of $d = 2.8$ when the embedding dimension of the phase space reached 5 or greater. They used 15,000 points and averaged $P_n(\epsilon)$ over 100 random points.

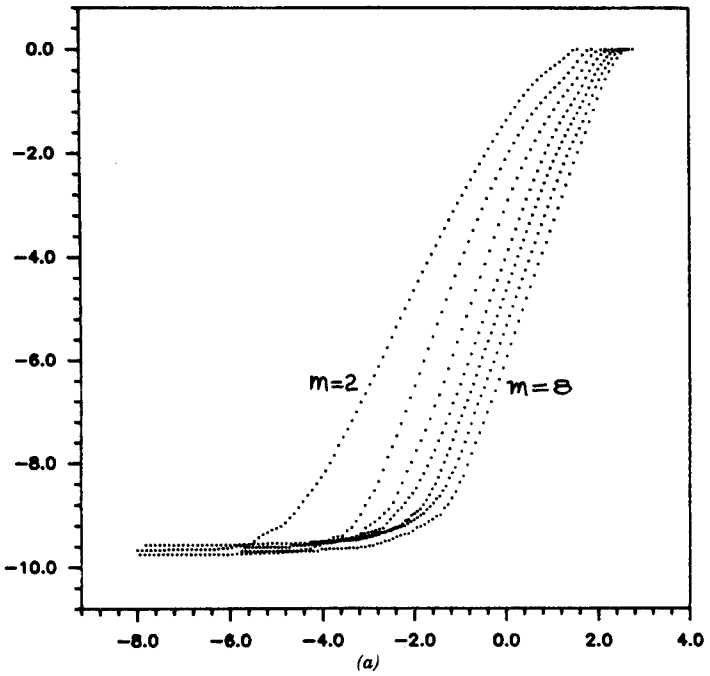

Figure 6-13 (*a*) log C versus log ϵ for the two-well potential problem for different dimension embedding spaces. Time history data identical to that in Figures 6-8 and 6-10.

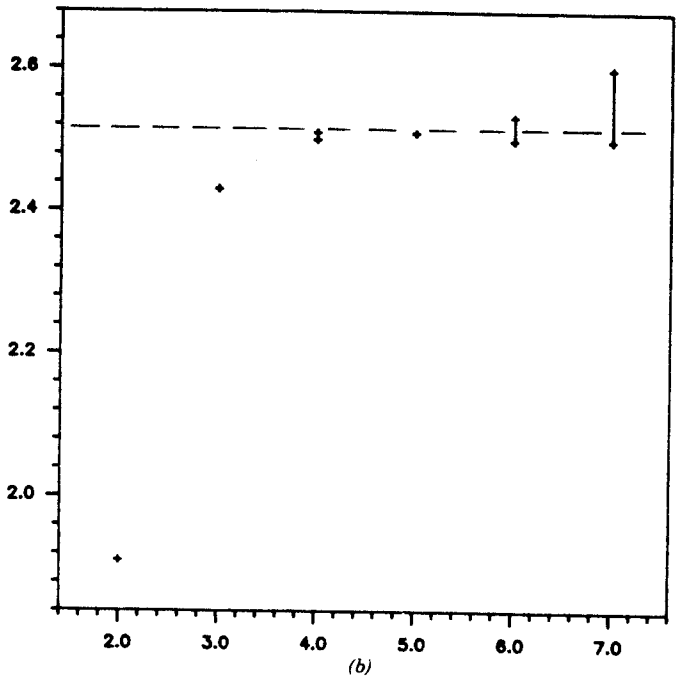

Figure 6-13 (*b*) Fractal dimensions of attractor versus the dimension of the embedding space.

However, they also found regimes of chaotic flow where no clear slope of $\log C(\epsilon)$ versus $\log \epsilon$ existed.

Similar results for the flow between two cylinders (Taylor–Couette flow) has been reported by a group from the Soviet Union (L'vov et al., 1981). They claim to measure the information dimension. Figure 6-15 shows the value of the slope of $\log C(\epsilon)$ versus $\log \epsilon$ as a function of ϵ. This is characteristic of these measurements. The slope values at small ϵ reflect instrumentation noise, while the values at large ϵ are those for which the size of the covering sphere or hypercube reaches the scale of the attractor.

Using such techniques, one can determine how the fractal dimension changes as some control parameter in the experiment is varied. For example, in the case of Taylor–Couette flow (see Figure 3-37), Swinney and coworkers have measures the change in d as a function of the Reynolds number (Figure 6-16; see Swinney, 1985).

In another fluid experiment, Ciliberto and Gollub (1985) have studied chaotic excitation of surface waves in a fluid. The surface wave chaos was excited by a 16 Hz vertical amplitude frequency; 2048 points were sampled with a sampling time of 1.5 s or around 300 orbits. Using the embedding

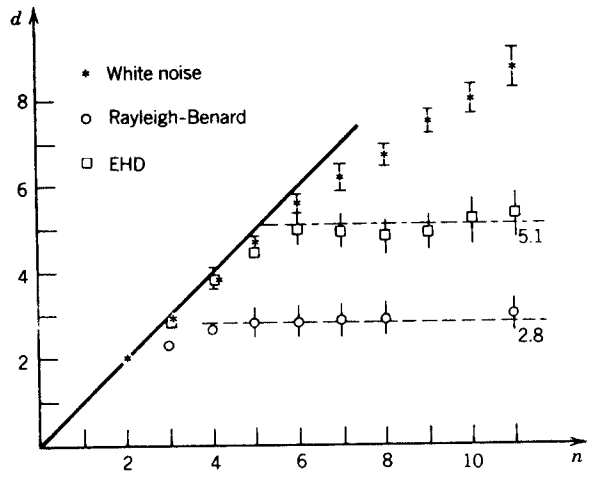

Figure 6-14 Fractal dimension versus dimension of embedding pseudo-phase-space for measurements of electrohydrodynamic fluid flow, Rayleigh–Benard flow (Chapter 3), and white noise [From Malraison et al, 1983).

space technique, they measured both the correlation dimension ($d_c = 2.20 \pm 0.04$) and the information dimension ($d_I = 2.22 \pm 0.04$), both of which reached asymptotic values when the embedding space dimension was 4 or greater. (See also Figure 5-8.)

Holzfuss and Mayer-Kress (1986) have examined the probable errors in estimating dimensions from a time series data set. The three methods studied involved the correlation dimension, averaged pointwise dimension, and the averaged radius method of Termonia and Alexandrowicz (1983). They tested each on a set of 20,000 points from a quasiperiodic motion on a 5 torus, which consists of a time history with 5 incommensurate frequencies. Using the pseudo-phase-space method for embedding dimensions of 2–20, they found that the averaged pointwise dimension had the smallest standard deviation of the three. The average was taken over 20% of the reference points, and curves that did not show scaling behavior over a significant portion of the range of r were rejected.

6.4 OPTICAL MEASUREMENT OF FRACTAL DIMENSION

All the methods for calculating the fractal dimension of strange attractors discussed above require the use of a powerful digital micro or minicomputer. From an experimental point of view, however, it is natural to ask

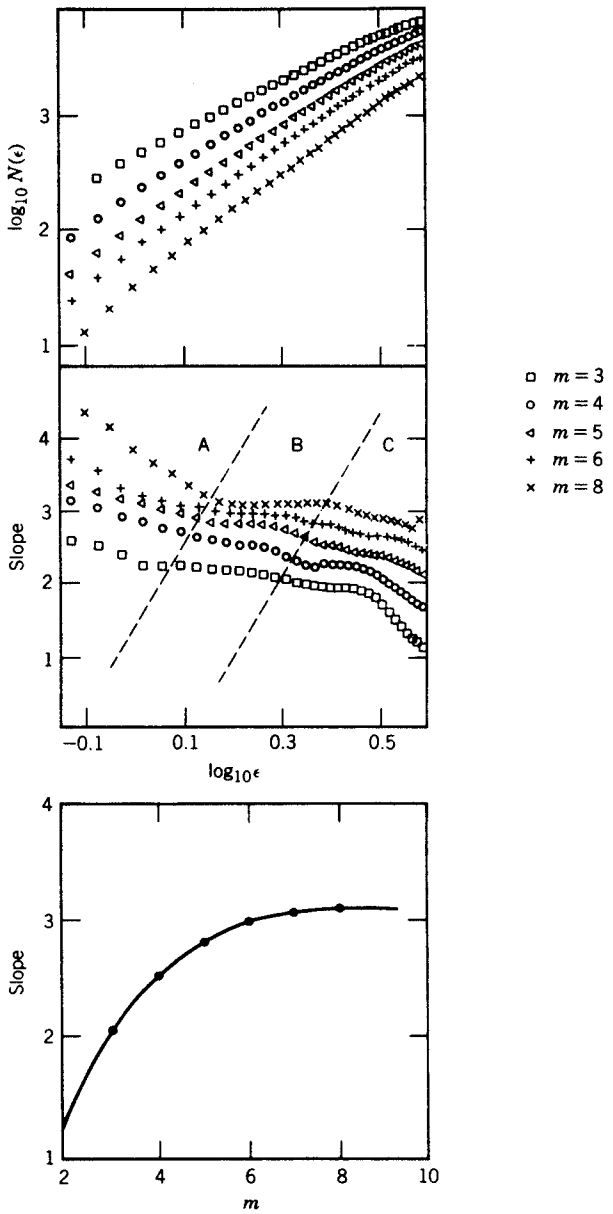

Figure 6-15 Calculation of fractal dimension for chaotic flow of fluid between two rotating cylinders: Taylor–Couette flow (see Chapter 3) [from L'vov et al. (1981) with permission of Elsevier Science Publishers, copyright 1981].

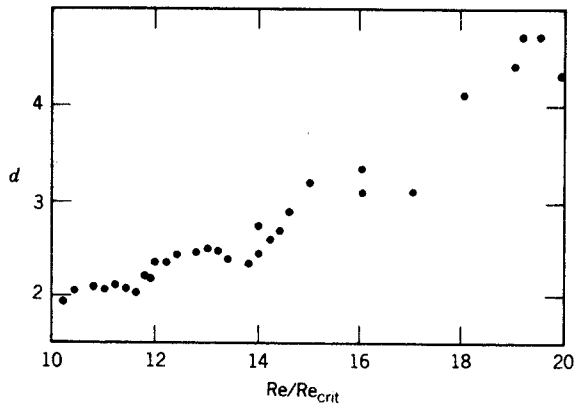

Figure 6-16 Dependence of information dimension on the Reynolds number for flow in a Taylor–Couette system [from Swinney (1985) with permission of Elsevier Science Publishers, copyright 1985].

whether the fractal properties in dynamical systems can be measured directly using *analog devices* in the same way that other dynamical properties such as velocity or acceleration are measured. For general, multi-degree-of-freedom systems, the answer is not known; but for simple nonlinear problems, the fractal dimension of a two-dimensional Poincaré map can be measured using optical techniques (Lee and Moon, 1986). This method is based on an optical interpretation of the correlation function (6-2.5).

A diagram illustrating this method is shown in Figure 6-17. We recall that the correlation function involves counting the number of points in a cube or ball surrounding each point in the fractal set of points. The optical method uses a parallel processing feature to perform all the sums at once. Light coming from one film creates a disk of light on another film. If each film is an identical copy of the Poincaré map of the strange attractor, the total light emanating from the second film is proportional to the correlation function. By changing the distance between the two films in Figure 6-17, the radius of the small circle changes and one can obtain the correlation sum as a function of the radius r. A plot of $\log C(r)$ versus $\log r$ then yields the fractal dimension of the Poincaré map D.

If the map is a time triggered Poincaré map, the dimension of the attractor is $1 + D$.

An Optical Parallel Processor for the Correlation Function

A sketch of the experimental setup is shown in Figure 6-18, displaying the optical path of light in this method. The method makes use of two

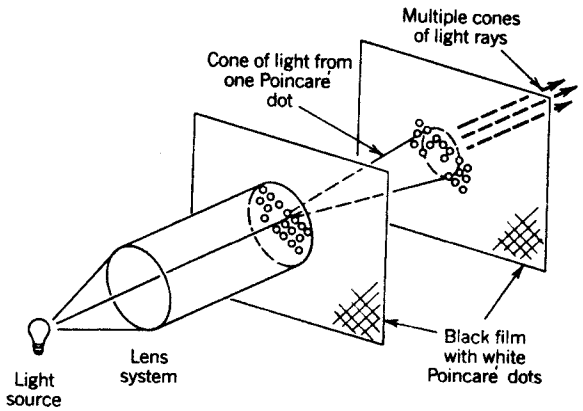

Figure 6-17 Diagram illustrating the parallel processing feature of optically measuring the correlation function and fractal dimension of a planar distribution of points.

properties of classical optics. First, if light is passed through a small aperture of diameter D in the region of Fraunhofer diffraction (if λ is the wavelength, $D \gg \lambda$), then light will cast a circle of radius r, with uniform intensity, on a plane located at a distance L from the aperture. This radius is given by $r = 1.22L\lambda/D$. In our method, the aperture originates from a small dot on the negative of a planar Poincaré map and the small circle of

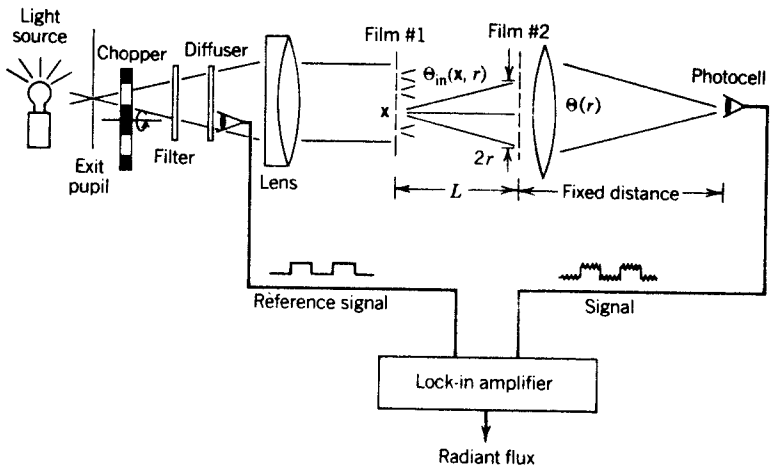

Figure 6-18 Experimental setup of the optical method for measuring fractal dimension [from Lee and Moon (1986) with permission of Elsevier Science Publishers, copyright 1986].

light falls on an identical copy of this negative located at a distance L (Figure 6-18). Second, for incoherent light, the amount of light that emanates from the second negative is proportional to the number of small dots or circles within the circle of illumination. The total amount of light passing through both films is thus proportional to the correlation function $C(r)$. To calculate or vary r, we simply measure or vary L, the distance between the two negatives.

To make these ideas more concrete, let $\Phi(\mathbf{x}, r)$ be the radiant flux behind film #2 due to the flux $\Phi_{in}(\mathbf{x})$ entering the circular aperture at x on film #1:

$$\Phi(\mathbf{x}, r) = n(x, r)A\frac{\Phi_{in}(\mathbf{x})}{\pi r^2} \tag{6-4.1}$$

where $n(\mathbf{x}, r) = \sum_j H(r - |\mathbf{x} - \mathbf{x}_j|)$ is the number of apertures located within the circle of light illuminated by the flux in the aperture at x, and A is the area of the aperture of a point on film #1. One can see that Φ depends on both n and r explicitly. However, we would like a measure of n alone. Using the linear relation between r and L, we define an adjusted radiant flux $\Phi^* = (r/r_0)^2\Phi$, where r is the radius of the illuminated area when $L = L_0$ (L_0 is a convenient reference distance). Summing over all points in film #1,

$$\sum_{k=1}^{N} \Phi^*(\mathbf{x}, r) = \left(\frac{r}{r_0}\right)^2 \sum \Phi(\mathbf{x}, r) = \frac{A}{\pi r_0^2} \sum \Phi_{in}(\mathbf{x}) n(r) \tag{6-4.2}$$

When the incident light intensity is uniform over film #1, we find

$$\left(\frac{L}{L_0}\right)^2 \sum_{k=1}^{N} \Phi_0(\mathbf{x}_k, r) \approx \sum_{k=1}^{N} n(r) \approx C(r) \tag{6-4.3}$$

The maps can be obtained from either numerical solution of a third-order system of equations or from experimental data. The light passing through film #2 was focused onto a photocell for the light flux measurement. A light filter (orange-amber color filter) was used at the light source to optimize the photocell response around 6328 Å. The dot size on the negatives was less than 0.2 mm so that $D/\lambda \simeq 300$, which satisfies the Fraunhofer diffraction criterion.

The output voltage from the photocell contained a lot of noise. To extract the signal from the noise, a mechanical light chopper and a lock-in

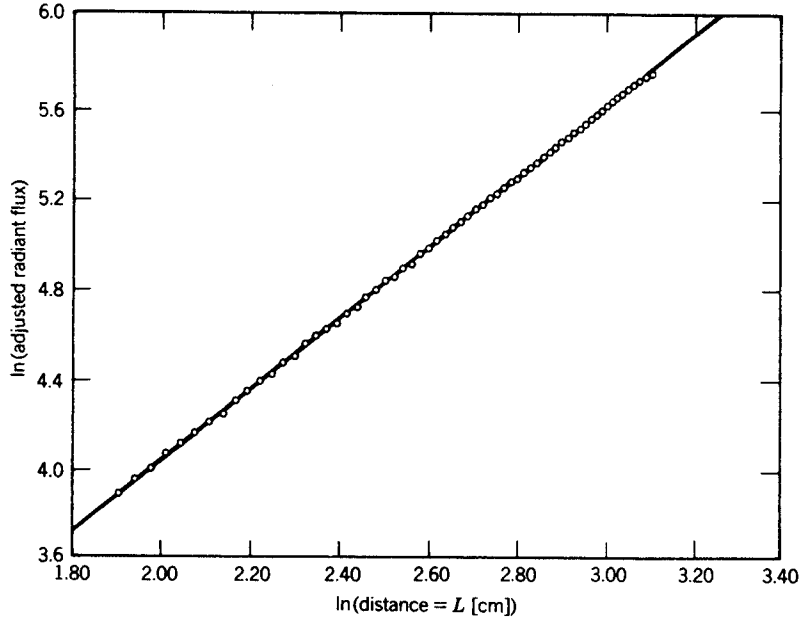

Figure 6-19 Radiant flux versus distance between two films of Poincaré maps on a log–log scale for data from the vibration of a buckled beam [from Lee and Moon (1986) with permission of Elsevier Science Publishers, copyright 1986].

amplifier were used in the signal processing. The chopper was operated at approximately 100 Hz to avoid power line noise.

The radiant flux behind film #2 was measured at the photocell as a function of the distance between films, and the adjusted radiant flux (6-4.2) versus L was plotted on a log–log scale as shown in Figure 6-19. Theoretically, the slope of this curve should give the fractal dimension (6-2.5).

Calculations of fractal dimensions using the correlation function $C(r)$ have shown that there is an optimum range of r to measure the slope. For small r, one encounters the noise error in generating the original map (increasing slope); for large r, one reaches the size of the attractor itself which results in a saturation of $C(r)$ (leading to decreasing slope). A plot of the slope as a function of r is shown in Figure 6-20. One can see that the slope reaches a plateau for a certain range of r or film distance L. This plateau value was chosen as the fractal dimension. The data were obtained from a Runge–Kutta simulation of the forced, two-well potential equation (6-3.7). The 4000 points were generated by taking a Poincaré map synchro-

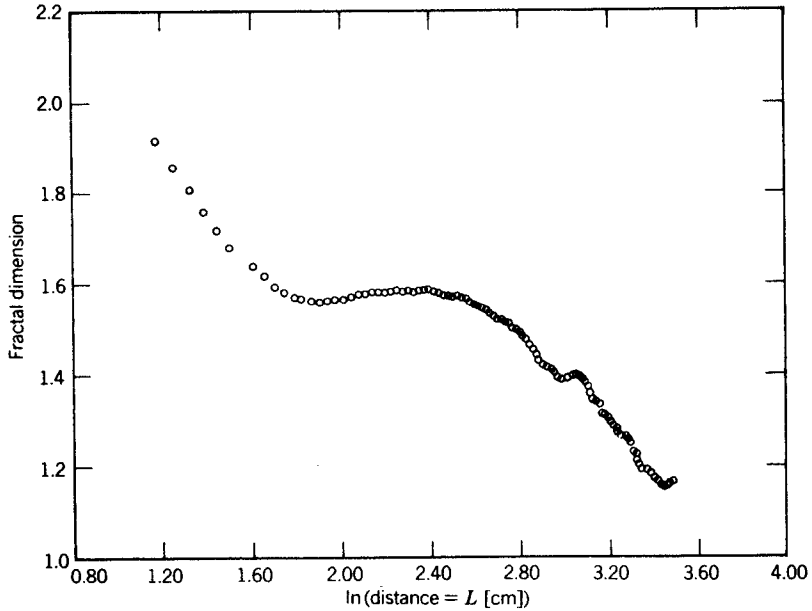

Figure 6-20 Slope versus distance between films L or radius r for data similar to that in Figure 6-19 [from Lee and Moon (1986) with permission of Elsevier Science Publishers, copyright 1986].

nous with the driving frequency. The adjusted radiant flux output was measured at approximately 200 values of L. However, only the linear section of $\log C$ versus $\log L$ is plotted in Figure 6-19. The slopes in Figure 6-20 were based in 30 points/local averages of the slope of the $\log C(r)$ curve.

A comparison of the optically measured fractal dimension with those calculated from the numerical data of Moon and Li (1985a) is shown in Table 6-3 for several values of the damping. The results, as one can see, are remarkably good.

A comparison of the optical and numerical methods for experimental Poincaré maps for the buckled beam is also shown in Table 6-3. In this set of tests, the phase of the Poincaré map trigger was changed. The optical measurement of fractal dimension confirms the results of the numerical method, namely, that the dimension is independent of the phase of the map. This implies that the dimension of the strange attractor itself is $1 + D$, where D is the planar map dimension.

TABLE 6-3 Optically Measured Fractal Dimension for Computer-Simulated and Experimental Poincaré Maps

Numerical Poincaré Map [Eq. (6-3.7)]			
Damping	Calculated[a]		Measured
0.075	1.565[b]		1.558
0.105	1.393		1.417
0.135	1.202		1.162
Experimental Poincaré Map			
Phase Angle	Calculated[a]		Measured
0°	1.741[b]	1.628[c]	1.678
45°	1.751	1.627	1.671
90°	1.742	1.638	1.631
135°	1.748	1.637	1.676
180°	1.730	1.637	1.635

[a] Moon and Li (1985a).
[b] Based on four smallest log r points in log C versus log r.
[c] Based on seven smallest log r points in log C versus log r.

REFERENCES

Abraham, R. H., and Shaw, C. D. (1983). *Dynamics: The Geometry of Behavior*, Aerial Press, Santa Cruz, CA.

Abraham, N. B., Albano, A. M., Das, B., DeGuzman, G., Yang, S., Gioggia, R. S., Puccioni, G. P., and Tredicce, J. R. (1986). "Calculating the Dimension of Attractors From Small Data Sets," *Phys. Lett.* **114A**(5), 217–221.

Arnold, V. I. (1978). *Ordinary Differential Equations*, MIT Press, Cambridge, MA.

Babitsky, V. I., Landa, P. S., Ol'khovoi, A. F., and Perminov, S. M. (1982). "Stochastic Behavior of Auto-Oscillating Systems with Inertial Self-Excitation," *Z. angew. Math. Mech.* **66**(2), 73–81.

Baillieul, J., and Brockett, R. W., and Washburn, R. B. (1980). "Chaotic Motion in Nonlinear Feedback Systems," *IEEE Trans. on Circuits and Systems* **CAS-27**, (11), 990–997.

Baker, N. H., Moore, P. W., and Spiegel, E. A. (1971). "Aperiodic Behavior of a Nonlinear Oscillator," *Q. J. Mech. Appl. Math.*, **24**(4), 391–422.

Bau, H. H., and Torrance, K. E. (1981). "On the Stability and Flow Reversal of an Asymmetrically Heated Open Convection Loop," *J. Fluid Mech.* **106**, 412–433.

Benettin, G., Galgani, L., Giogilli, A., and Strelcyn, J. M. (1980). "Lyapunov Characteristic Exponents for Smooth Dynamical Systems and for Hamiltonian Systems; A Method for Computing All of Them. Part 2: Numerical Application," *Meccanica* **15**, 21–30.

Bergé, P. (1982). "Study of the Phase Space Diagrams Through Experimental Poincaré Sections in Prechaotic and Chaotic Regimes," *Phys. Scr.* **T1**, 71–72.

Bergé, P., Dubois, M., Manneville, P., and Pomeau, P. (1980). "Intermittency in Rayleigh–Benard Convection," *J. Phys. (Paris) Lett.* **41**(15), L341–L345.

Bergé, P., Pomeau, Y., and Vidal, Ch. (1985). *L'Ordre dans le Chaos*, Hermann, Paris.

Brandstater, A., Swift, J., Swinney, H. L., Wolf, A., Farmer, J. O., Jen, E., and Crutchfield, J. P. (1983). "Low-Dimensional Chaos in a Hydrodynamics System," *Phys. Rev. Lett.* **51**(6), 1442–1445.

Brandstater, A., Swift, J., Swinney, H. L., and Wolf, A. (1984). "A Strange Attractor in a Couette–Taylor Experiment," in *Turbulence and Chaotic Phenomena in Fluids*, Proceedings of the IUTAM Symposium (Kyoto), T. Tatsumi (ed.), North-Holland, Amsterdam.

Brillouin, L. (1964), *Scientific Uncertainty and Information*, Academic Press, N.Y.

Brockett, R. W. (1982). "On Conditions Leading to Chaos in Feedback Systems," *IEEE Proc. 21st Conf. Decision Control*, 932–936.

Brorson, S. D., Dewey, D., and Linsay, P. S. (1983). "The Self-Replicating Attractor of a Driven Semiconductor Oscillator," *Phys. Rev. A. Rapid Comm.*

Bryant, P., and Jeffries, C. (1984a). "Bifurcations of a Forced Magnetic Oscillator Near Points of Resonance," *Phys. Rev. Lett.* **53**(3), 250–253.

Bryant, P., and Jeffries, C. (1984b). "Experimental Study of Driven Nonlinear Oscillator Exhibiting Hopf Bifurcations, Strong Resonances, Homoclinic Bifurcations and Chaotic Behavior," Lawrence Berkeley Laboratory report, LBL-16949, January.

Bucko, M. F., Douglass, D. H., and Frutch, H. H. (1984). "Bounded Regions of Chaotic Behavior in the Control Parameter Space of a Driven Non-linear Resonator," *Phys. Lett.* **104**(8), 388–390.

Campbell, D. K., and Rose, H. A. (eds.) (1982). "Order in Chaos," *Proceedings of a Conference Held at Los Alamos National Lab*, May, North-Holland, Amsterdam.

Chirikov, B. V. (1979). "A Universal Instability of Many-Dimensioanl Oscillator Systems," *Phys. Rep.* **52**, 265.

Ciliberto, S., and Gollub, J. P. (1985). "Chaotic Mode Competition in Parametri-[illegible]"

Croquette, V., and Poitou, C. (1981). "Cascade of Period Doubling Bifurcations and Large Stochasticity in the Motions of a Compass," *J. Phys. (Paris) Lett.* **42**, L537–L539.

Crutchfield, J. P., and Packard, N. H. (1982). "Symbolic Dynamics of One-Dimensional Maps: Entropies, Finite Precursor, and Noise," *Int. J. Theor. Phys.* **21**(6/7), 433–465.

Cvitanovic, P., and Predrag, P. (1984). *Universality in Chaos*, Heyden, Philadelphia, PA.

Dowell, E. H. (1975). *Aeroelasticity of Plates and Shells*, Noordhoff International, Groningen.

Dowell, E. H. (1982). "Flutter of a Buckled Plate as an Example of Chaotic Motion of a Deterministic Autonomous System," *J. Sound Vib.* **85**(3), 333–344.

Dowell, E. H. (1984). "Observation and Evolution of Chaos for an Autonomous System," *J. Appl. Mech.*, paper no. 84-WA/APM-15.

Dowell, E. H., and Pezeshki, C. (1986). "On the Understanding of Chaos in Duffing's Equation Including a Comparison with Experiment," *J. Appl. Mech.* **53**(1), 5–9.

Dubois, M., Bergé, P., and Croquette, V. (1982). "Study of Nonsteady Convective Regimes Using Poincaré Sections," *J. Phys. (Paris) Lett.* **43**, L295–L298.

Eckmann, J. P. (1981). "Roads to Turbulence in Dissipative Dynamical Systems," *Rev. Mod. Phys.* **53**(4), part 1, 643–654.

Evenson, D. A. (1967). *Nonlinear Flexural Vibrations of Thin-Walled Circular Cylinders*. NASA Technical Note, NASA TN D-4090, August.

Everson, R. M. (1986). "Chaotic Dynamics of a Bouncing Ball," *Physica* **19D**, 355–383.

Farmer, J. D., Ott, E., and Yorke, J. A. (1983). "The Dimension of Chaotic Attractors," *Physica* **7D**, 153–170.

Feigenbaum, M. J. (1978). "Qualitative Universality for a Class of Nonlinear Transformations," *J. Stat. Phys.* **19**(1), 25–52.

Feigenbaum, M. J. (1980). "Universal Behavior in Nonlinear Systems," *Los Alamos Sci.* (Summer), 4–27.

Fung, Y. C. (1958). "On Two-dimensional Panel Flutter," *J. Aero/Space Sci.* **25**(3), 145–159.

Glass, L., Guevau, X., and Shrier, A. (1983). "Bifurcation and Chaos in Periodically Stimulated Cardiac Oscillator", *Physica* **7D** (1983), 89–101.

[illegible] A. L., Bhargava, V., West, B. J., and Mandell, A. J. (1986). "Some [illegible] on the Question: Is Ventricular Fibrillation 'Chaos'?," *Physica*

Gollub, J. P., and Benson, S. V. (1980). "Many Routes to Turbulent Convection," *J. Fluid Mech.* **100**(3), 449–470.

Gollub, J. P., Brunner, T. O., and Danly, B. G. (1978). "Periodicity and Chaos in Coupled Nonlinear Oscillators," *Science* **200**, 48–50.

Gollub, J. P., Romer, E. J., and Socalar, J. E. (1980). "Trajectory Divergence for Coupled Relaxation Oscillators: Measurements and Models," *J. Stat. Phys.* **23**(3), 321–333.

Golnaraghi, M., and Moon, F. C. (1985). "Chaotic Dynamics of a Nonlinear Servo Device," *24th IEEE Conf. on Decision and Control*, December 1985, Cornell University Report, Department of Theoretical and Applied Mechanics, July 1985.

Gorman, M., Widmann, P. J., and Robbins, K. A. (1984). "Chaotic Flow Regimes in a Convection Loop," *Phys. Rev. Lett.* **52**(25), 2241–2244.

Grassberger, P., and Proccacia, I. (1983). "Characterization of Strange Attractors," *Phys. Rev. Lett.* **50**, 346–349.

Grassberger, P. and Proccacia, I. (1984). "Dimensions and Entropies of Strange Attractors from a Fluctating Dynamics Approach," *Physica* **13D**, 34–54.

Grebogi, C., Ott, E., and Yorke, J. A. (1983a). "Crises, Sudden Changes in Chaotic Attractors and Transient Chaos," *Physica* **7D**, 181–200.

Grebogi, C., Ott, E., and Yorke, J. A. (1983b). "Fractal Basin Boundaries, Long Lived Chaotic Transients and Unstable–Unstable Pair Bifurcation," *Phys. Rev. Lett.* **50**(13), 935–938.

Grebogi, C., Ott, E., Pelikan, S., and Yorke, J. A. (1984). "Strange Attractors that Are Not Chaotic," *Physica* **13D**, 261–268.

Grebogi, C., Ott, E., and Yorke, J. A. (1985a). "Attractors on an *N*-Torus: Quasiperiodicity Versus Chaos," *Physica* **15D**, 354–373.

Grebogi, C., Ott, E., and Yorke, J. A. (1985b). "Superpersistent Chaotic Transients," *Ergod. Theor. Dynam. Syst.* **5**, 341–372.

Grebogi, C., McDonald, S. W., Ott, E., and Yorke, J. A., (1985c). "Exterior Dimension of Fat Fractals," *Phys. Lett.* **110A**(1), 1–4.

Grebogi, C., Ott, E., and Yorke, J. A. (1986). "Metamorphoses of Basin Boundaries in Nonlinear Dynamical Systems," *Phys. Rev. Lett.* **56**(10), 1011–1014.

Guckenheimer, J. (1982). "Noise in Chaotic Systems," *Nature* **298**, 358.

Guckenheimer, J., and Holmes, P. J. (1983). *Nonlinear Oscillations, Dynamical Systems and Bifurcations of Vector Fields*, Springer-Verlag, New York.

Gwinn, E. G., and Westervelt, R. M. (1985). "Intermittent Chaos and Low-Frequency Noise in the Driven Damped Pendulum," *Phys. Rev. Lett.* **54**(15), 1613–1616.

Hao, B.-L. (1984). *Chaos*, World Scientific Publishers, Singapore.

Harrison, R. G. and Biswas, D. J. (1986). "Chaos in Light," *Nature* 321, **22**, May, 394–401.

Hart, J. E. (1984). "A New Analysis of the Closed Loop Thermosyphon," *Int. J. Heat Mass Transfer* **27**(1), 125–136.

Haucke, H. and Ecke, R. E. (1987). "Mode-Locking and Chaos in Rayleigh-Benard Convection," *Physica D* (in press), Los Alamos National Lab. Report LA-UR-86-1257.

Hayashi, C. (1953). *Forced Oscillations in Nonlinear Systems*, Nippon Printing and Publishing Co., Osaka, Japan.

Hayashi, H., Ishizuka, S., Ohta, M., and Hirakawa, J. (1982). "Chaotic Behavior in the 'Onchidium' Giant Neuron under Sinusoidal Stimulation," *Phys. Lett.* **88A**(8), 5 April, 435–438.

Helleman, R. H. G. (1980a). "Self-Generated Chaotic Behavior in Nonlinear Mechanics," *Fund. Probl. Stat. Mech.* **5**, 165–233.

Helleman, R. H. G. (ed.) (1980b). "Nonlinear Dynamics," *Ann. N.Y. Acad. Sci.* **357**.

Hendriks, F. (1983). "Bounce and Chaotic Motion in Print Hammers," *IBM J. Res. Dev.* **27**(3), 273–280.

Henon, M. (1976). "A Two-Dimensional Map with a Strange Attractor," *Commun. Math. Phys.* **50**, 69.

Henon, M. (1982). "On the Numerical Computation of Poincaré Map," *Physica* **5D**, 412–414.

Henon, M., and Heiles, C. (1964). "The Applicability of the Third Integral of Motion: Some Numerical Experiments," *Astron. J.* **69**(1), 73–79.

Henon, M., and Wisdom, J. (1983). "The Benettin–Strelcyn Oval Billiard Revisited," *Physica* **8D**, 157–169.

Hockett, K., and Holmes, P. J. (1985). "Josephson Junction, Annulus Maps, Birkhoff Attractors, Horseshoes and Rotation Sets," Center for Applied Math Report Cornell University.

Holmes, P. J. (1979). "A Nonlinear Oscillator With a Strange Attractor," *Philos. Trans. R. Soc. London A* **292**, 419–448.

Holmes, P. J. (ed.) (1981). *New Approaches to Nonlinear Problems in Dynamics*, SIAM, Philadelphia, PA.

Holmes, P. J. (1982). "The Dynamics of Repeated Impacts With a Sinusoidally Vibrating Table," *J. Sound Vib.* **84**, 173–189.

Holmes, P. J. (1984b). "Bifurcation Sequences in Horseshoe Maps: Infinitely Many Routes to Chaos," *Phys. Lett. A* **104**(6, 7), 299–302.

Holmes, P. J. (1985). "Dynamics of a Nonlinear Oscillator with Feedback Control," *J. of Dynamics Systems, Measurements and Control* **107**, 159–165.

Holmes, P. J. (1986). "Chaotic Motions in a Weakly Nonlinear Model for Surface Waves," *J. Fluid Mech.* **162**, 365–388.

Holmes, P. J., and Moon, F. C. (1983). "Strange Attractors and Chaos in Nonlinear Mechanics," *J. Appl. Mech.* **50**, 1021–1032.

Holzfuss, J. and Mayer-Kress, G. (1986). "An Approach to Error-Estimation in the Application of Dimension Algorithms," *Dimensions and Entropies in Chaotic Systems*, G. Mayer-Kress (ed.), Springer-Verlag, Berlin.

Hudson, J. L., Mankin, J. C., and Rossler, O. E. (1984). "Chaos in Continuous Stirred Chemical Reaction," in *Stochastic Phenomena and Chaotic Behavior in Complex Systems*, P. Schuster (ed.), Springer-Verlag, Berlin, pp. 98–105.

Hunt, E. R., and Rollins, R. W. (1984). "Exactly Solvable Model of a Physical System Exhibiting Multidimensional Chaotic Behavior," *Phys. Rev. A* **29**(2), 1000–1002.

Hsu, C. S. (1981). "A Generalized Theory of Cell-to-Cell Mapping for Nonlinear Dynamical Systems," *J. Appl. Mech.* **48**, 634–642.

Hsu, C. S. (1987). *Cell to Cell Mapping*, Springer-Verlag.

Hsu, C. S., and Kim, M. C. (1985). "Statistics for Strange Attractors by Generalized Cell Mapping," *J. Stat. Phys.*

Iansiti, M., Hu, Q., Westervelt, R. M., and Tinkham, M. (1985). "Noise and Chaos in a Fractal Basin Boundary Regime of a Josephson Junction," *Phys. Rev. Lett.* **55**(7), August 12, 746–749.

Iooss, G., and Joseph, D. D. (1980). *Elementary Stability and Bifurcation Theory*, Springer-Verlag, New York.

Isomaki, H. M., von Boehm, J., and Raty, R. (1985). "Devil's Attractors and Chaos of a Driven Impact Oscillator," *Phys. Lett.* **107A**(8), 343–346.

Kadanoff, L. P. (1983). "Roads to Chaos," *Phys. Today* (Dec.), 46–53.

Kaplan, J., and Yorke, J. A. (1978). *Springer Lecture Notes in Mathematics*, No. 730, p. 228.

Keolian, R., Turkevich, L. A., Putterman, S. J., Rudnick, I., and Rudnick, J. A. (1981). "Subharmonic Sequences in the Faraday Experiment: Departures from Period Doubling," *Phys. Rev. Lett.* **47**(16), 1133–1511.

Klinker, T., Meyer-Ilse, X., and Lauterborn, W. (1984). "Period Doubling and Chaotic Behavior in a Driven Toda Oscillator," *Phys. Lett. A* **101**(8), 371–375.

Kobayashi, S. (1962). "Two-dimensional Panel Flutter 1. Simply Supported Panel," *Trans. Japan Society Aeronautical Space Sciences* **5**(8), 90–102.

Kostelich, E. J., and Yorke, J. A. (1985). "Lorenz Cross Sections and Dimension of the Double Rotor Attractor," *Dimensions and Entropies in Chaotic Systems*, G. Mayer-Kress (ed.), Springer-Verlag, Berlin, pp. 62–66.

Kostelich, E. J., Grebogi, C., Ott, E., and Yorke, J. A. (1987). "The Double Rotor Chaotic Attractor," to appear in *Physica D*.

Kreuzer, E. J. (1985). "Analysis of Chaotic Systems Using the Cell Mapping Approach," *Ingenieur-Archiv* **55**, 285–294.

Kuhn, T. (1962), *The Structure of Scientific Revolutions*, The University of Chicago Press, Chicago.

Landau, L. D. (1944). "On the Problem of Turbulence," *Akad. Nauk, Doklady* **44**, 339, Russian original reprinted in *Chaos* Hao, Bai-Lin (ed.) 107, World Scientific Publishers, Singapore.

Landauer, R. (1977). "Poor Man's Chaos," Internal Memo IBM Corp.

Lauterborn, W. (1981). "Subharmonic Route to Chaos in Acoustics," *Phys. Rev. Lett.* **47**(20), 1445–1448.

Lauterborn, W., and Cramer, E. (1981). "Subharmonic Route to Chaos Observed in Acoustics," *Phys. Rev. Lett.* **47**(20), 1145.

Lee, C.-K., and Moon, F. C. (1986). "An Optical Technique for Measuring Fractal Dimensions of Planar Poincaré Maps," *Phys. Lett. A* **114**(5), 222–226.

Leipnik, R. B. and Newton, T. A. (1981). "Double Strange Attractors in Rigid Body Motion with Linear Feedback Control," *Phys. Lett.* **86A**(2), 2, November, 63–67.

Levin, P. W., and Koch, B. P. (1981). "Chaotic Behavior of a Parametrically Excited Damped Pendulum," *Phys. Lett. A* **86**(2), 71–74.

Li, G. X. (1984). *Chaotic Vibrations of a Nonlinear System with Five Equilibrium States*, M.S. Thesis, Cornell University, Ithaca, N.Y., August.

Li, G. X. (1987). Doctoral dissertation, Department of Theoretical and Applied Mechanics, Cornell University, Ithaca, NY.

Libchaber, A. (1982). "Convections and Turbulence in Liquid Helium I," *Physica* **109 & 110B**, 1583–1589.

Libchaber, A. and Maurer (1978). *J. Phys. Lett.* **39**, 369.

Libchaber, A., Fauve, S., and Laroche, C. (1982). "Two-Parameter Study of the Routes to Chaos," in *Order in Chaos*, X. Campbell and X. Rose (eds.), North-Holland, Amsterdam.

Lichtenberg, A. J., and Lieberman, M. A. (1983). *Regular and Stochastic Motion*, Springer-Verlag, New York.

Lieberman, M. A., and Tsang, K. Y. (1985). "Transient Chaos in Dissipatively Perturbed Near-Integrable Hamiltonian Systems," *Phys. Rev. Lett.* **55**(9), 26, August, 908–911.

Lin, Y. K. (1976). *Probabilistic Theory of Structural Dynamics*, Krieger, Huntington, NY.

Linsay, P. A. (1981). "Period Doubling and Chaotic Behavior in a Driven, Anharmonic Oscillator," *Phys. Rev. Lett.* **47**(19), 1349–1352.

Linsay, P. S. (1985). The Structure of Chaotic Behavior in a PN Junction Oscillator, MIT, Department of Physics Report.

Lorenz, E. N. (1963). "Deterministic Non-Periodic Flow," *J. Atmos. Sci.* **20**, 130–141.

Lorenz, E. N. (1984). "The Local Structure of a Chaotic Attractor in Four Dimensions," *Physica* **13D**, 90–104.

Love, A. E. H. (1922). *A Treatise on the Mathematical Theory of Elasticity*, 4th Ed., Dover, New York.

L'vov, V. S., Predtechensky, A. A., and Chernykh, A. I. (1981). "Bifurcation and chaos in a system of Taylor vortices: a natural and numerical experiment," *Soviet Physics JETP* **53**, 562.

McDonald, S. W., Grebogi, C., Ott, E., and Yorke, J. A. (1985). "Fractal Basin Boundaries," *Physica* **17D**, 125–153.

McLaughlin, J. B. (1981). "Period-Doubling Bifurcations and Chaotic Motion for a Parametrically Forced Pendulum," *J. Stat. Phys.* **24**(2), 375–388.

Maganza, C. Caussé, and Laloë, F. (1986). "Bifurcations, Period Doubling and Chaos in Clarinetlike Systems," *Europhys. Lett.* **1**(6), 295–302.

Mahaffey, R. A. (1976). *Phys. Fluids* **19** 1387–1391.

Malraison, G., Atten, P., Bergé, P., and Dubois, M. (1983). "Dimension of Strange Attractors: An Experimental Determination of the Chaotic Regime of Two Convective Systems," *J. Phys. Lett.* **44**, 897–902.

Mandelbrot, B. B. (1977). *Fractals, Form, Chance, and Dimension*, W. H. Freeman, San Francisco, CA.

Manneville, P., and Pomeau, Y. (1980). "Different Ways to Turbulence in Dissipative Dynamical Systems," *Physica* **1D**, 219–226.

Marzec, C. J., and Spiegel, E. A. (1980). "Ordinary Differential Equations with Strange Attractors," *SIAM J. Appl. Math.* **38**(3), 403–421.

Matsumoto, T. (1984). "A Chaotic Attractor from Chua's Circuit," *IEEE. Trans. Circuits Syst.* **CAS-31**(12), 1055–1058.

Matsumoto, T., Chua, I. O., and Tanaka, S. (1984). "Simplest Chaotic Nonautonomous Circuit," *Phys. Rev. A.* **30**(2), 1155–1157.

Matsumoto, T., Chua, L. O., and Komuro, M. (1985). "The Double Scroll," *IEEE Trans. Circuits Syst.* **CAS-32**(8), 798–818.

May, R. M. (1976). "Simple Mathematical Models with Very Complicated Dynamics," *Nature* **261**, 459–467.

Mayer-Kress, G. (1985). "Introductory Remarks," in *Dimensions and Entropies in Chaotic Systems*, G. Mayer-Kress (ed.), Springer-Verlag, Berlin.

Miles, J. (1984a). "Resonant Motion of Spherical Pendulum," *Physica* **11D**, 309–323.

Miles, J. (1984b). "Resonantly Forced Motion of Two Quadratically Coupled Oscillators," *Physica* **13D**, 247–260.

Miles, J. (1984c). "Resonant, Nonplanar Motion of a Stretched String," *J. Acoust. Soc. Am.* **75**(5), 1505–1510.

Minorsky, N. (1962). *Nonlinear Oscillations*, Van Nostrand, Princeton, NJ.

Moon, F. C. (1980a). "Experiments on Chaotic Motions of a Forced Nonlinear Oscillator: Strange Attractors," *ASME J. Appl. Mech.* **47**, 638–644.

Moon, F. C. (1980b). "Experimental Models for Strange Attractor Vibration in Elastic Systems," in *New Approaches to Nonlinear Problems in Dynamics*, P. J. Holmes (ed.), pp. 487–495.

Moon, F. C. (1984a). *Magneto-Solid Mechanics*, Wiley, New York.

Moon, F. C. (1984b), "Fractal Boundary for Chaos in a Two State Mechanical Oscillator," *Phys. Rev. Lett.* **53**(60), 962–964.

Moon, F. C. (1986). "New Research Directions for Chaotic Phenomena in Solid Mechanics," in *Perspectives in Nonlinear Dynamics*, R. Cawley and M. Shlesinger (eds.), World Scientific Publishers, Singapore.

Moon, F. C., and Holmes, P. J. (1979). "A Magnetoelastic Strange Attractor," *J. Sound Vib.* **65**(2), 275–296; "A Magnetoelastic Strange Attractor," *J. Sound Vib.* **69**(2), 339.

Moon, F. C., and Holmes, W. T. (1985). "Double Poincaré Sections of a Quasi-Periodically Forced, Chaotic Attractor," *Phys. Lett. A* **111**(4), 157–160.

Moon, F. C., and Li, G.-X. (1985a). "The Fractal Dimension of the Two-Well Potential Strange Attractor," *Physica* **17D**, 99–108.

Moon, F. C., and Li, G.-X. (1985b). "Fractal Basin Boundaries and Homoclinic Orbits for Periodic Motion in a Two-Well Potential," *Phys. Rev. Lett.* **55**(14), 1439–1442.

Moon, F. C., and Shaw, S. W. (1983). "Chaotic Vibration of a Beam with Nonlinear Boundary Conditions," *J. Nonlinear Mech.* **18**, 465–477.

Moon, F. C., Cusumano, J., and Holmes, P. J. (1987). "Evidence for Homoclinic Orbits as a Precursor to Chaos in a Magnetic Pendulum," *Physica* **D** (in press).

Moore, D. W., and Spiegel, E. A. (1966). "A Thermally Excited Non-linear Oscillator," *Astrophys. J.* **143**(3), 871–887.

Nayfeh, A. H., and Mook, D. T. (1979). *Nonlinear Oscillations*, Wiley, New York.

Nayfeh, A. H. and Khdeir, A. A. (1986). "Nonlinear Rolling of Ships in Regular Beam Seas," *Int. Shipbuilding Prog.* **33**, No. 379, 40–49.

Newhouse, S., Ruelle, D., and Takens, F. (1978). "Occurrence of Strange Axiom A Attractors Near Quasiperiodic Flows on T^m, $m \geq 3$," *Commun. Math. Phys.* **64**, 35–40.

Ott, E. (1981). "Strange Attractors and Chaotic Motions of Dynamical Systems," *Rev. Mod. Phys.* **53**(4), Part 1, 655–671.

Packard, N. H., Crutchfield, J. P., Farmer, J. D., and Shaw, R. S. (1980). "Geometry from a Time Series," *Phys. Rev. Lett.* **45**, 712.

Peitgen, H. -O., and Richter, P. H. (1986). *The Beauty of Fractals*, Springer-Verlag, Berlin.

Pezeshki, C., and Dowell, E. H. (1987). "An Examination of Initial Condition Maps for the Sinusoidally Excited Buckled Beam Modeled by Duffing's Equation," *J. Sound and Vibration* (in press).

Poddar, B., Moon, F. C., and Mukherjee, S. (1986). "Chaotic Motion of an Elastic–Plastic Beam," *J. Appl. Mech.* (in press).

Poincaré, H. (1921). *The Foundation of Science*: *Science and Method*, English Translation, The Science Press, N.Y.

Pomeau, Y., and Manneville, P. (1980). "Intermittent Transition to Turbulence in Dissipative Dynamical Systems," *Commun. Math. Phys.* **74**, 189–197.

Prigogine, I. and Stengers, I. (1984). *Order Out of Chaos*, Bantam Books, Toronto.

Rand, D., Ostlund, S., Sethna, J., and Siggia, E. D. (1982). "Universal Transition From Quasiperiodicity to Chaos in Dissipative Systems," *Phys. Rev. Lett.* **49**(2), 387–390.

Richter, P. H., and Scholz, H.-J. (1984). "Chaos in Classical Mechanics: The Double Pendulum," in *Stochastic Phenomena and Chaotic Behavior in Complex Systems*, P. Schuster (ed.), Springer-Verlag, Berlin, pp. 86–97.

Robbins, K. A. (1977). "A New Approach to Subcritical Instability and Turbulent Transitions in a Simple Dynamo," *Math. Proc. Camb. Philos. Soc.* **82**, 309–325.

Rollins, R. W., and Hunt, E. R. (1982). "Exactly Solvable Model of a Physical System Exhibition Universal Chaotic Behavior," *Phys. Rev. Lett.* **49**(18), 1295–1298.

Rössler, O. E. (1976a). "Chemical Turbulence: Chaos in a Small Reaction-Diffusion System," *Z. Naturforsch. a* **31**, 1168–1172.

Rössler, O. E. (1976b). "An Equation for Continuous Chaos," *Phys. Lett. A* **57**, 397.

Roux, T. C., Simoyi, R. H., and Swinney, H. L. (1983). "Observation of a Strange Attractor," *Physica* **8D**, 257–266.

Russel, D. A., Hanson, J. D., and Ott, E. (1980). "Dimension of Strange Attractors," *Phys. Rev. Lett.* **45**(14), 1175–1178.

Saltzman, B. (1962). "Finite Amplitude Free Convection as an Initial Value Problem—I," *J. Atmos. Sci.* **19**, 329–341.

Schreiber, I., Kubicek, M., and Marak, M. (1980). "On Coupled Cells," in *New Approaches to Nonlinear Problems in Dynamics*, P. J. Holmes (ed.), SIAM, Philadelphia, PA, pp. 496–508.

Schuster, H. G. (1984). *Deterministic Chaos*, Physik-Verlag GmbH, Weinheim (F.R.G.).

Shaw, R. (1981). "Strange Attractors, Chaotic Behavior and Information Flow," *Z. Naturforsch. A* **36**, 80–112.

Shaw, R. (1984). *The Dripping Faucet as a Model Chaotic System*, Aerial Press, Santa Cruz, CA.

Shaw, S. W. (1985). "The Dynamics of a Harmonically Excited System Having Rigid Amplitude Constraints, Parts 1, 2," *J. Applied Mechanics* **52**(2), 453–464.

Shaw, S., and Holmes, P. J. (1983). "A Periodically Forced Piecewise Linear Oscillator," *J. Sound Vib.* **90**(1), 129–155.

Shimada, I., and Nagashima, T. (1979). "A Numerical Approach to Ergodic Problem of Dissipative Dynamical Systems," *Prog. of Theoretical Phys.* **61**(6), 1605–1616.

Simoyi, R. H., Wolf, A., and Swinney, H. L. (1982). "One-Dimensional Dynamics in a Multi-Component Chemical Reaction," *Phys. Rev. Lett.* **49**, 245.

Soong, T. T. (1973). *Random Differential Equations in Science and Engineering*, Academic Press, New York.

Sparrow, C. T. (1981). "Chaos in a Three-Dimensional Single Loop Feedback System With a Piecewise Linear Feedback Function," *J. Math. Anal. Appl.* **83**, 275–291.

Sparrow, C. (1982). *The Lorenz Equations: Bifurcations, Chaos, and Strange Attractors*, Springer-Verlag, New York.

Sreenivasan, K. R. (1986). "Chaos in Open Flow Systems," in *Dimension and Entropies*, in *Chaotic Systems*, G. Mayer-Kress (ed.), Springer-Verlag, New York.

Stoker, J. J. (1950). *Nonlinear Vibrations*, Interscience, New York.

Swinney, H. L. (1983). "Observations of Order and Chaos in Nonlinear Systems," in *Order and Chaos*, Campbell and Rose (eds.), North-Holland, Amsterdam, pp. 3–15.

Swinney, H. L. (1985). "Observations of Complex Dynamics and Chaos," in *Fundamental Problems in Statistical Mechanics VI*, E. G. D. Cohen (ed.), Elsevier Science Publishers, New York, pp. 253–289.

Swinney, H. L., and Gollub, J. P. (1978). "The Transition of Turbulence," *Physics Today*, **31**(8), 41 (August).

Symonds, P. S., and Yu, T. X. (1985). "Counterintuitive Behavior in a Problem or Elastic–Plastic Beam Dynamics," *J. Appl. Mech.* **52**, 517–522.

Szczygielski, W., and Schweitzer, G. (1985). "Dynamics of a High-Speed Rotor Touching a Boundary," *IUTAM/IFT$_0$MM Symposium on the Dynamics of Multibody Systems*, CISM, Udine, Italy.

Szemplinska-Stupnicka, W., and Bajkowski, J. (1986). "The $\frac{1}{2}$ subharmonic Resonance and its Transition to Chaotic Motion in a Non-Linear Oscillator," *Int. J. Non-Linear Mechanics* (in press).

Tatsumi, T., (ed.) (1984). *Turbulence and Chaotic Phenomena in Fluids*, North-Holland, Amsterdam.

Termonia, Y., and Alexandrowicz, Z. (1983). *Phys. Rev. Lett.* **51**(14), 1265.

Testa, J., Perez, J., and Jeffries, C. (1982). "Evidence for Universal Chaotic Behavior in a Driven Nonlinear Oscillator," *Phys. Rev. Lett.* **48**, 714.

Thomson, W. T. (1965), *Vibration Theory*, Prentice Hall, Englewood Cliffs, New Jersey.

Thompson, J. M. T. (1983). "Complex Dynamics of Compliant Off-Shore Structures," *Proc. R. Soc. Land.* **A387**, 407–427.

Thompson, J. M. T., and Ghaffari, R. (1982). "Chaos After Period-Doubling Bifurcations in the Resonance of an Impact Oscillator," *Phys. Lett. A* **91**(1), 5–8.

Thompson, J. M. T., and Stewart, H. B. (1986). *Nonlinear Dynamics and Chaos*, Wiley, Chichester.

Tousi, S., and Bajaj, A. K. (1985). "Period-Doubling Bifurcations and Modulated Motions in Forced Mechanical Systems," *J. Appl. Mech.* **52**(2), 446–452.

Tseng, W.-Y., and Dugundji, J. (1971). "Nonlinear Vibrations of a Buckled Beam Under Harmonic Excitation," *J. Appl. Mech.* **38**, 467–476.

Tufillaro, N. B. and Albano, A. M. (1986). "Chaotic Dynamics of a Bouncing Ball," *Am. J. Phys.* **54**(10), 939–944.

Ueda, Y. (1979). "Randomly Transitional Phenomena in the System Governed by Duffing's Equation," *J. Stat. Phys.* **20**, 181–196.

Ueda, Y. (1980). "Steady Motions Exhibited By Duffing's Equation: a Picture Book of Regular and Chaotic Motions," *New Approaches to Nonlinear Problems in Dynamics*, P. J. Holmes (ed.) SIAM, Philadelphia, PA.

Ueda, Y., and Akamatsu, N. (1981). "Chaotically Transitional Phenomena in the Forced Negative Resistance Oscillator," *Proc. IEEE ISCA8 '80.* Also *IEEE Trans. Circuits Syst.* **CAS-28**(3), March.

Ueda, Y., Doumoto, H., and Nobumoto, K. (1978). "An Example of Random Oscillations in Three-Order Self-Restoring System," *Proceedings of the Electric and Electronic Communication Joint Meeting*, Kansai District, Japan, October.

Ueda, Y., Nakajima, H., Hikihara, T., and Stewart, H. B. (1986). *Forced Two-Well Potential Duffing Oscillator.*

Van Buskirk, R., and Jeffries, C. (1985a). "Observation of Chaotic Dynamics of Coupled Nonlinear Oscillators," *Phys. Rev. A* **31**(5), 3332–3357.

Van der Pol, B., and Van der Mark, J. (1927). "Frequency Demultiplication," *Nature* **120** (3019), 363–364.

Van Dyke, M. (1982). *An Album of Fluid Motion*, Parabolic Press, City.

Viet, O., Westfreid, X., and Guyon, E. (1983). "Art cinetique et chaos mëchanique," *Eur. J. Phys.* **4**, 74–76.

Virgin, L. N. (1986). "The Nonlinear Rolling Response of a Vessel Including Chaotic Motions Leading to Capsize in Regular Seas," *Applied Ocean Research.*

Wisdom, J., Peale, S. J. and Mignard, F. (1984). "The Chaotic Rotation of Hyperion," *Icarus*, **58**, 137–152.

Wolf, A. (1984). "Quantifying Chaos with Lyapunov Exponents," *Nonlinear Sci. Theory Appl.* Ed. A. V. Holden, Manchester Univ. Press.

Wolf, A., Swift, J. B., Swinney, H. L., and Vasano, J. A. (1985). "Determining Lyapunov Exponents from a Time Series," *Physica* **16D**, 285–317.

Wolfram, S. (1984). "Universality and Complexity in Cellular Automata," *Physica* **10D**, 1–35.

Wolfram, S. (1986). *Theory and Applications of Cellular Automata*, World Scientific Publ., Singapore.

Yorke, J. A., Yorke, E. D., and Maller-Paret, J. (1985). "Lorenz-like Chaos in Partial Differential Equations for a Heated Fluid Loop," University of Maryland Report.

Zaslavsky, G. M. (1978). "The Simplest Case of a Strange Attractor," *Phys. Lett. A* **69**(3), 145–147.

Zaslavsky, G. M., and Chirikov, B. V. (1972). "Stochastic Instability of Nonlinear Oscillations," *Sov. Phys. Usp.* **14**(5), 549–672.

Zhu, Z-X. (1983). "Experiment on the Chaotic Phenomena of an Upside Down Pendulum," Report of Laboratory of General Mechanics, Beijing University.

Chaotic Vibrations

An Introduction for Applied Scientists and Engineers

FRANCIS C. MOON
Theoretical and Applied Mechanics
Cornell University
Ithaca, New York

A WILEY-INTERSCIENCE PUBLICATION
JOHN WILEY & SONS
NEW YORK CHICHESTER BRISBANE TORONTO SINGAPORE